Targeting epigenetic dysregulation in Acute Myeloid Leukemia via BET protein inhibition: Mechanisms of resistance and contributions towards the anti-tumor response

By

Kyle A. Romine

A DISSERTATION

Presented to the Department of Cancer Biology and the Oregon Health & Science University School of Medicine

In partial fulfillment of the requirements for the degree of

Doctor of Philosophy

January 2022

School of Medicine

School of Medicine

Oregon Health & Science University

CERTIFICATE OF APPROVAL

This is to certify that the PhD dissertation of

Kyle Romine

has been approved

Jeffrey W. Tyner

Evan F. Lind

Mara Sherman

Julia Maxson

Pepper Schedin

Acknowledgments

It takes a village to raise a graduate student and I would like to thank the village that raised me. First I would like to thank both my mentors, Jeff and Evan, for not only agreeing to train me but also to allow me to work on a major project from each lab despite being in slightly distant fields. I feel that I have had such a rounded training here because of it. Jeff, you have taught me so much about the finer details of science and honed my molecular and cellular biology techniques but you also taught me a lot about how to take a step back and see the bigger picture. I would have never gotten that paper out without your advice and your teaching of how to craft an interesting scientific story. Evan, you have taught me the ins and outs of the complexities of immunology and how to ask/answer difficult scientific questions. I have a newfound appreciation for cancer immunology and how to use mouse models to tackle some of the most difficult scientific questions. I think you have forgotten more immunology than I know still but I feel confident in the foundation you helped me build to carry on in this field. To both of you I also thank you for your kindness. Both of you were exceptionally understanding when times were tough. Not having that all too common pressure from imaginary deadlines that many are given made grad school manageable for me.

To my other DAC members Pepper Schedin and Mara Sherman, thank you both for your help throughout my time at OHSU. I know that, given our differences in field of study, keeping up with my research was extra work but the feedback you were able to give was extremely helpful and I am very grateful. To that end you have both taught me the art of presenting my research in a more broadly applicable way.

I also want to acknowledge the many informal mentors who went above and beyond to help me be successful at OHSU either through experimental design, career advice, grant writing, post doc hunting, and just generally being awesome people. Thank

you Julia Maxson, Amy Moran, Yoko Kosaka, Daniel Bottomly, Tamilla Nechiporuk, Ted Braun, and Haijiao Zhang.

I was very fortunate to have made so many friends at OHSU and they have made this experience one that I will always think fondly of for the rest of my life. First to my closest friend Jake Van Winkle, thank you for everything. As much as I hated that our wives made us watch The Bachelor every week it was all worth it for the time we got to spend together. Next, to my KCRB squad Breanna, Isabel, Bree, Kaelan, Matt, Sarah, and Pat– you guys are just the best. I know we will be in touch and I can't wait to see where all our careers take us. You have all helped me in so many aspects and I will forever be grateful.

Finally, I want to thank my wife Alexis Romine, my parents, and my brother Josh. Alexis you have supported me so much through this process and I will forever be grateful. I had many late nights/weekends in the lab but you always helped pick up the slack around home during these times and that took a lot of pressure off of me. Mom and Dad, thanks for everything. I would not be here if you didn't push me to be my best when I was younger. The work ethic you instilled carried me throughout the most grueling bits of grad school.

Abstract

Acute Myeloid Leukemia (AML) is a genetically and phenotypically heterogeneous white blood cell cancer with a poor prognosis and limited therapeutic options. For many decades the current standard of care has been an intensive chemotherapy regimen, to which only a fraction of patients respond and are physically able to withstand. However, the advent of deep genetic sequencing has led to the discovery of a number of mutational lesions targetable by small-molecule inhibitors, which more patients can tolerate. Even so, the combination of extreme genetic variability and acquired/intrinsic drug resistance has caused many targeted therapies to fail clinically. It is therefore imperative that we more deeply characterize underlying molecular features of intrinsic drug resistance/refractoriness to targeted therapies as well as extrinsic factors which facilitate these responses, particularly the role of the tumor microenvironment. One class of inhibitors targeting bromodomain and extra-terminal (BET) family proteins (BETi) has become of interest in hematological settings due to their potent *in vitro* and *in vivo* activity, but it is still understudied. This dissertation has two main foci, 1.) Determination of tumor intrinsic mechanisms of resistance/sensitivity to inhibitors targeting BET family proteins (BETi) in AML and 2.) Extrinsic mechanisms of BETi activity on the tumor microenvironment of AML. Accordingly, this dissertation demonstrates that BETi response is tethered to leukemic differentiation state. We utilized patient RNA-seq, drug profiling, and differentiation state data from ~600 AML patient samples within the Beat AML biorepository, and multiple whole-genome CRISPR screens to identify regulators of monocytic differentiation as predictors of BETi response. Monocytic AML subtypes were intrinsically sensitive to BET inhibition, whereas undifferentiated AML subtypes were intrinsically resistant. This also revealed multiple targetable vulnerabilities to overcome BETi resistance via combinations with small-molecule inhibitors (SMIs), such as BCL2 inhibitors, which are more effective in undifferentiated AMLs as rational combination

treatment strategy to prevent drug resistance driven by tumor maturation state changes. Further, I identify a novel role for BET family proteins in regulating T cell differentiation in the AML microenvironment. This dissertation demonstrates that AML drives *in vivo* T cell exhaustion, which is coordinated by multiple T cell receptor (TCR) activated transcription factors and BET proteins. Additionally, I demonstrate that BET inhibition reinvigorates AML-induced exhausted T cells to a more functional subtype that expands with immune checkpoint therapy. Finally, I utilized cell type proportion data derived from deconvoluted bulk RNA-seq patient data to describe the functional immune landscape of AML -- immune cell type correlations with a number of clinical correlates (ELN2017, outcome, etc.), drug responses, immune exhaustion, and immune checkpoint blockade (ICB) responses. Taken together, this body of work identifies a novel mechanism of non-genetic drug resistance to BETi, extrinsic control of T cell differentiation regulated by BET proteins, the pre-clinical efficacy and mechanistic basis of combined BETi + anti-PD1, and globally characterizes the functional/genomic landscape of immune cells in AML.

Chapter 1

Introduction

The Hematopoietic System

The hematopoietic system is the combined processes in the body which generates all cells residing in the blood. The hematopoietic system is created early in developing embryos and begins as blood cells form in the yolk sac. Later in development, blood cells are formed in secondary lymphoid tissues such as lymph nodes, spleen, and liver. Lastly, the bone marrow niche develops and assumes the role of forming the majority of blood cells with the secondary lymphoid organs now primarily serving as a hub for maturation and proliferation for lymphoid cells(1,2). The process by which the blood cells of the hematopoietic system are generated is called hematopoiesis.

Hematopoiesis and Differentiation

Hematopoiesis is the highly coordinated process by which all blood cells are formed as a result of selective differentiation of self-renewing hematopoietic stem cells (HSCs), which starts during embryogenesis and continues throughout our lives(3-6). An average adult will produce approximately 10^{11} – 10^{12} new blood cells daily to maintain blood homeostasis. HSCs are driven by extrinsic cues, such as cytokines and chemokines, to differentiate along two main branches, myeloid and lymphoid, to generate over a dozen unique blood cells which constitute our innate and adaptive immune system (Figure 1(7))(8,9). These cues regulate expression of a multitude of hematopoietic transcription factors which determine the identity of the derivative blood cell into which the HSC differentiates. While there are numerous hematopoietic transcription factors that

contribute to HSC differentiation, the E twenty-six (ETS) family proteins play the most essential role. ETS transcription factors are a large evolutionarily conserved gene family which all share significant sequence homology in their DNA binding domain(10). These transcription factors are made up of 12 subfamilies(11) and, for myeloid cell differentiation, the most important transcription factor is SPI1 (encoding PU.1). PU.1 is considered the master regulator of myeloid differentiation and interacts with a number of epigenetic modifying machinery to promote cell fate-specifying gene programs(12-15). HSCs have a near unlimited self-renewal capacity, which wanes naturally with age(16), but self-renewing capacity and overall plasticity decrease as they differentiate into subsequent progenitor cells. Thus hematopoiesis, and the controlled differentiation of HSCs, must be tightly regulated to maintain homeostasis. This chapter will provide an introduction to acute myeloid leukemia, a cancer which is driven by the acquisition of mutations in a variety of early progenitor myeloid cells, leading to dysregulated differentiation and expansion of malignant myeloid cells.

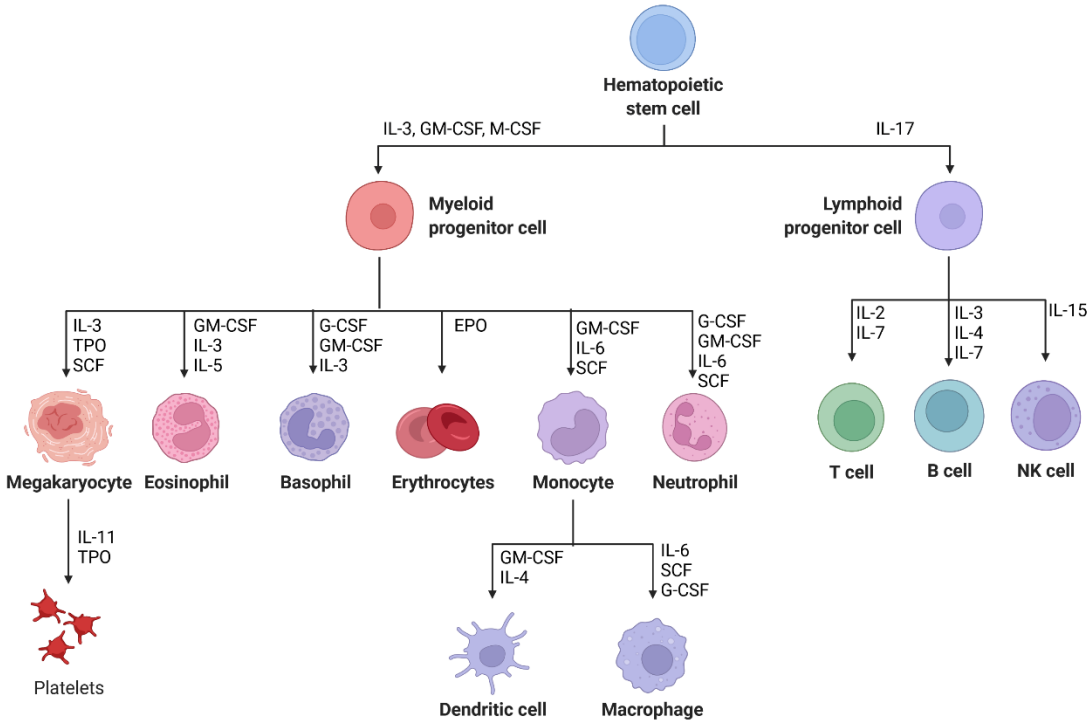

Figure 1 – Overview of the cytokines which promote differentiation of HSCs into all other blood cells. Adapted and created from Biorender hematopoiesis template. Cytokines derived from Metcalf et al. 2008.

Acute Myeloid Leukemia – Epidemiology, Treatments, and Subtypes

Epidemiology

Acute Myeloid Leukemia (AML) is a myeloid lineage white-blood cell cancer with a poor prognosis and limited therapeutic options(17,18). AML is characterized by an uncontrolled expansion of abnormal myeloid cells, commonly referred to as blasts, which ultimately causes global dysregulation of hematopoiesis and death as a result of the disease directly or from secondary issues such as infection and bleeding(17-21). AML has an exceptionally poor prognosis among the elderly, with an average 5 year survival of only ~25%(22) (Figure 2).

The only potential curative option is bone marrow transplantation post-chemotherapy – a procedure fraught with risks such as graft vs. host disease and bone marrow failure(17,18,23). In 2020 there were 60,530 new cases of leukemia and 23,100 leukemia deaths in the United States. AML accounted for only ~1/3 of new cases (19,940), but disproportionately made up approximately 50% of the new deaths (11,180). In total, AML encompasses approximately 1% of all new cancer diagnoses and 2% of cancer-related mortalities (SEER Cancer Stat Facts). AML is an extremely genetically heterogeneous cancer, with the most common mutations, *FLT3-ITD, NPM1,* and *DNMT3a*, only encompassing approximately ~30% of all AML patients(20). Broadly, AML can be characterized by acquisition of mutations targeting 4 main classes 1.) Proliferation Enhancers – *FLT3-ITD, N/*KRAS 2.) Differentiation Blocks – *RUNX1, CEBPA, GATA1* 3.) Epigenetic Dysregulation – *DNMT3A, TET2, ASXL1* and 4.) Splicing/DNA Repair mutations – *TP53, FANC, SF3B1(20)*.

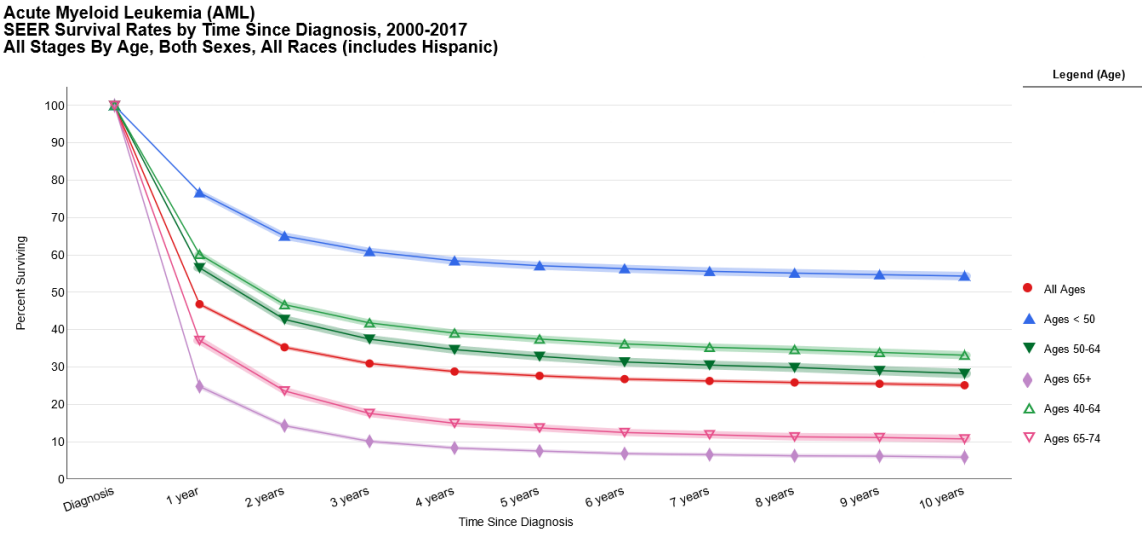

Figure 2 – SEER Cancer statistics describing the cumulative survival rates for AML patients stratified by age from 2000-2017

Treatment

The standard of care for *de novo* AML, chemotherapy, remains largely unchanged even after ~40 years since its introduction. Commonly referred to “induction chemotherapy” or “7 + 3,” this intensive chemotherapy regimen is composed of 7 days of continuous infusion of cytarabine (ara-c) followed by 3 days of short infusions of anthracyclines (e.g daunorubicin, idarubicin)(17,21,24). For patients with an adverse prognosis the goal of this treatment regimen is to get patients tumor burden low enough so that they can undergo a bone marrow transplantation from a suitable match, which essentially creates a graft vs. tumor response. Unfortunately, many patients cannot withstand such a difficult chemotherapy regimen and many will eventually relapse(25). Recent advancements in sequencing technologies have allowed for better characterization of genetic lesions which drive leukemogenesis as previously discussed. This has led to the development and FDA approval of a few therapies that specifically target these genetic lesions such as adaptation of combined BCL2 inhibitor + DNMT3a inhibitorsin chemotherapy ineligible or relapsed/refractory AML patients(26,27), as well as FLT3/FLT3-ITD inhibitors such as gilteritinib(28). However, drug resistance for targeted therapies is a recurring multi-faceted issue (Figure 3) and mechanistic understanding of these resistance drivers are needed to help discover more durable treatments. As it stands now, small-molecule inhibitors, either as monotherapies or combined with other targeted therapies, extend survival and are generally more tolerable than chemotherapy but they do not cure disease in patients.

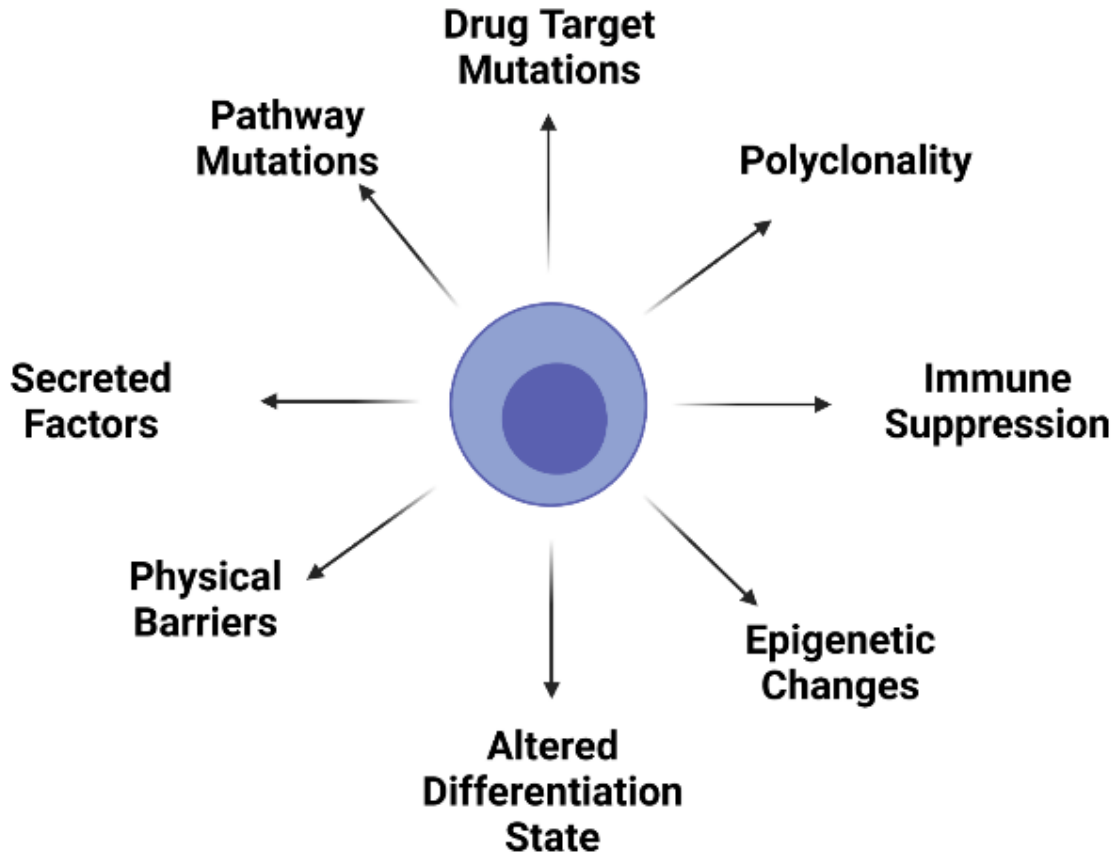

Figure 3- Cartoon schematic detailing the many described mechanisms of drug resistance that has been can occur in AML patients

Subtypes

Not only is AML genetically heterogeneous, it is also composed of multiple different subtypes based on differentiation state and/or cytogenetics. Several clinical classifications exist to subtype AML based on cytogenetic patterns, morphology, and genetics. One of the oldest designations systems is referred to as “French-American-British” (FAB) subtyping system, which was described in the 1970s and heavily relied on morphological features(29). While less popular now, the FAB classifications are still used clinically, usually in parallel with the newer WHO Classifications of AML(30). FAB subtypes range from M0 to M7 in order of least to most differentiated. M0-M2 resemble HSCs with increasing differentiation, M3 is a unique Promyelocytic leukemia discussed further in a later section, M4-M5 are monocytic, M6 are erythrocytic, and M7 are megakaryocytic. (Figure 4). WHO Classifications are much more specific and includes designations based on cytogenetic patterns, but includes designations based on morphology that are analogous to FAB subtyping supported by immunophenotyping (Figure 5). While these subtyping systems have been a standard diagnostic tool in characterizing AMLs, there are still very few targeted therapies which are designed around the patient’s leukemic differentiation stage. The only FDA therapy which is tailored to a leukemia subtype based on their differentiation state is arsenic trioxide (ATO)(31) and all-trans retinoic acid (ATRA)(32,33) in Acute Promyelocytic Leukemias (APLs), which is an M3 FAB. This leukemia is specifically characterized by the fusion protein PML-RARa which consists of the PML protein, a tumor suppressor that regulates TP53 and differentiation, and the retinoic acid receptor alpha (RARa) subunit. This fusion protein prevents normal PML signaling and leaves the cells in a trapped state of dedifferentiation where they are resistant to apoptosis but are rescuable via treatment with ATRA, the ligand of the RARa subunit. This derepresses proper PML signaling and leads to terminal granulocytic differentiation and death of the malignant cells. However,

as just described, there are many other mechanisms of leukemogenesis driven by underlying deficiencies in differentiation that may reveal novel synthetic vulnerabilities, like ATRA and ATO.

Classification	Cell Type	Description
M0	Myeloblasts	Undifferentiated AML
M1	Myeloblasts, minimal maturation	Myeloblastic AML with minimal maturation
M2	Myeloblast, with maturation	Myeloblastic AML with maturation, some cells developing
M3	Acute Promyelocytic Leukemia	Translocations between chromosome 15 and 17 (PML- RARa)
M4	Monoblasts	Myelomonocytic AML
M5	Monocytes	Monocytic AML
M6	Erythrocytes	Leukemia with features of erythrocytes
M7	Megakaryocytes	Leukemia have features of developing platelets

Figure 4 – Table describes the FAB subtyping system with the classification, cell type affected, and the clinical description

WHO myeloid neoplasm and acute leukemia classification	FAB Equivalent
Acute myeloid leukemia (AML) and related neoplasms	
AML with recurrent genetic abnormalities	
AML with t(8;21)(q22;q22.1);RUNX1-RUNX1T1	**M2**
AML with inv(16)(p13.1q22) or t(16;16)(p13.1;q22);CBFB-MYH11	**M4eo**
APL with PML-RARA	**M3**
AML with t(9;11)(p21.3;q23.3);MLLT3-KMT2A	
AML with t(6;9)(p23;q34.1);DEK-NUP214	
AML with inv(3)(q21.3q26.2) or t(3;3)(q21.3;q26.2); GATA2, MECOM	
AML (megakaryoblastic) with t(1;22)(p13.3;q13.3);RBM15-MKL1	
Provisional entity: AML with BCR-ABL1	
AML with mutated NPM1	
AML with biallelic mutations of CEBPA	
Provisional entity: AML with mutated RUNX1	
AML with myelodysplasia-related changes	
Therapy-related myeloid neoplasms	
AML, NOS	
AML with minimal differentiation	**M1**
AML without maturation	**M0**
AML with maturation	**M2**
Acute myelomonocytic leukemia	**M4**
Acute monoblastic/monocytic leukemia	**M5**
Pure erythroid leukemia	**M6**
Acute megakaryoblastic leukemia	**M7**
Acute basophilic leukemia	
Acute panmyelosis with myelofibrosis	
Myeloid sarcoma	
Myeloid proliferations related to Down syndrome	
Transient abnormal myelopoiesis (TAM)	
Myeloid leukemia associated with Down syndrome	
Acute leukemias of ambiguous lineage	
Acute undifferentiated leukemia	
Mixed phenotype acute leukemia (MPAL) with t(9;22)(q34.1;q11.2); BCR-ABL1	
MPAL with t(v;11q23.3); KMT2A rearranged	
MPAL, B/myeloid, NOS	
MPAL, T/myeloid, NOS	

Figure 5 – Describes the recently updated WHO 2016 Classifications of Acute leukemias (does not include MPN/MDS/related neoplasms) with the clinical annotations, incidence, and closest FAB equivalent where possible.

BET Family Proteins

Structures and Domains

BET proteins (Bromodomain and Extra Terminal domain), which include BRD2, BRD3, BRD4, and BRDT (testis specific), consist of a family of chromatin reading proteins which share similar binding domains. Each BRD protein has distinct expression patterns across different tissue types – BRD2 and BRD3 are expressed in the pancreas, testis, ovaries, brain, liver, spleen, lung, and kidney, whereas BRD4 is expressed ubiquitously (importantly, this includes the bone marrow and lymphoid cells)(34-36). The most well studied protein within the BET family is BRD4, due to its described role in regulating transcription and oncogenic potential. BRD4 is unique in that it contains an n- and c-terminal phosphorylation site (NPS/ CPS), a basic residue enriched interaction domain (BID), a pTEFb interaction domain (PID) and a c-terminal motif (CTM, unique to the BRD4L isoform). Like the other BET proteins, BRD4 consists of two bromodomains (BD1 and BD2), which serve to bind acetylated lysine residues, but is unique in that it recruits the transcription elongation factor pTEFb via its conserved PID and RNA polymerase II to promote gene transcription(37-39) (Figure 6). RNA Pol II remains transcriptionally paused until BRD4 proteins directly stimulates the pTEFb to phosphorylate the c-terminal domain (CTD) of RNA Pol II at its Serine 2, which further mediates the activation of Topoisomerase I and transcription(40). The NPS and CPS domains, which can be phosphorylated by casein kinase 2, regulate BRD4 activity during cell cycling. Additionally, all BRD proteins contain an extra terminal (ET) domain, which acts as recruiters for transcription regulator proteins(41).

BRD4 canonical and non-canonical functions

BRD4 was originally identified as a regulator of cell cycle control as it associates with chromosomes to promote transcription of genes critical in progressing from G1(42-44). In this context, BRD4 is critical during embryogenesis via the maintenance of embryonic

stem cells self-renewal and cooperation with cell state determining transcription factors such as Nanog(45) and OCT4(46). Thus BRD4-null embryos die shortly after implantation. As a chromatin regulator, it is perhaps not surprising that BRD4 has also been implicated in many other critical cellular processes such as osteoblast differentiation (47), adipogenesis, and myogenesis(48). BRD4 has a specific role in promoting recruitment of transcription machinery to super-enhancer regions, which are large clusters of enhancers that regulate expression of critical genes, such as those which determine cell fate(49), senescence(50), and many other critical biological processes(51). BRD4 has also been shown to directly bind and interact with a number of transcription factors as well, such as JMJD6(52), GATA1(53), and multiple replication factor proteins(54). BRD4 is thought to have increased affinity for super-enhancers via its increased binding affinity for multi-acetylated or acetylation-dense histones(55,56) but the exact mechanism is still relatively unclear. Most recent findings have pointed towards differences in acetylation affinity between BD1 and BD2 domains of BET proteins. Most notably, BD1 favors binding to acetylated residues on histone H4, whereas BD2 accommodates a wider range of acetylation markers(43,55,57). Further, it is established that BD1 is the primary domain required for binding to chromatin(58). Interestingly, BRD4 also has several non-canonical functions including interaction with splicing machinery(59), acting as a direct histone acetyltransferase(60), and acting as an atypical kinase that directly phosphorylates the CTD tail of RNA pol II, which is normally accomplished by the pTEFb complex(61). However, these mechanisms are still largely understudied and their impact or contributions to malignancies is unknown. The important point is that BRD4 is a chromatin reader and binds to acetylated histone residues to recruit the RNA transcribing machinery to super enhancer regions and promote their gene expression; however, it can also perform atypical functions.

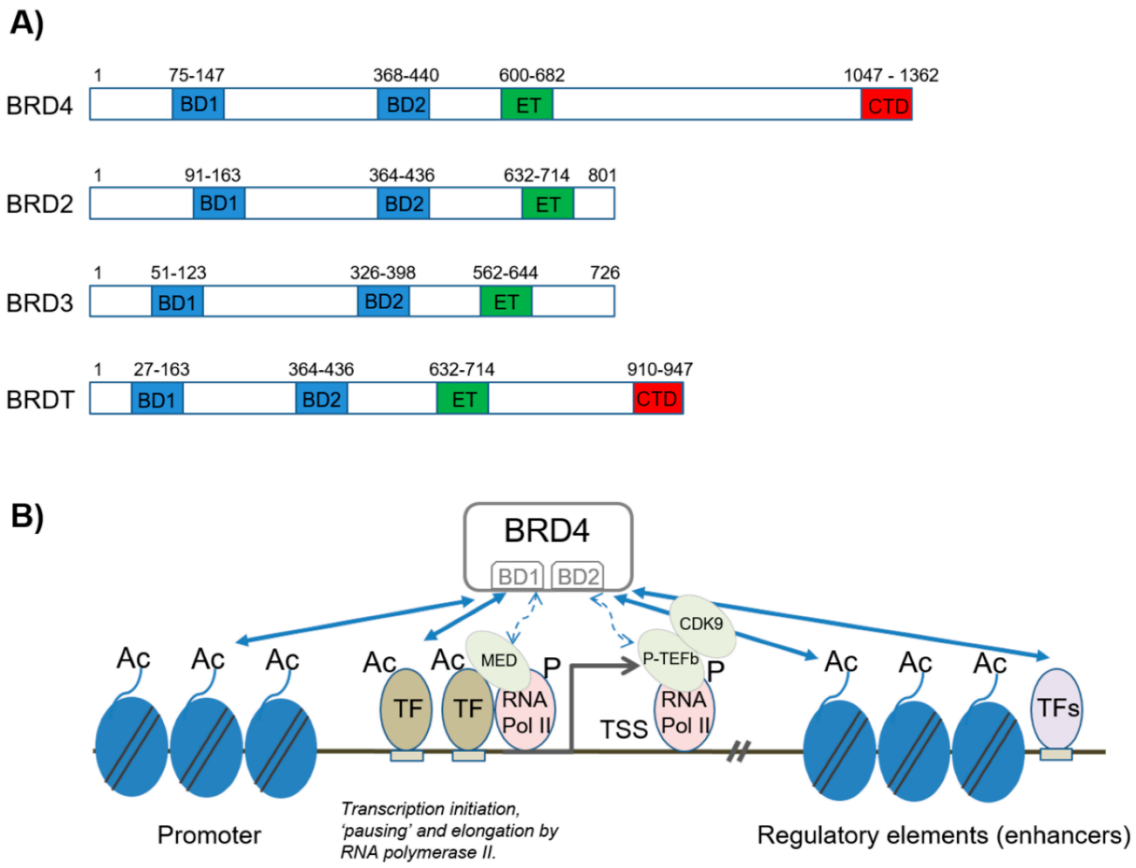

Figure 6 – A.) Details the location of the Bromodomain 1 (BD1), Bromodomain 2 (BD2), extra terminal (ET), and c-terminal domain (CTD) on BET family proteins. B.) Cartoon schematic details BRD4s interaction with acetylated histone residues and the RNA transcription machinery utilizing its different domains. Used with permission from Biomedicines.

Oncogenic Potential and Therapeutic Targeting

BRD4 itself is rarely mutated in cancer, with the exception of NUT midline carcinoma (NMC), which is driven by translocation of BRD4 with NUT genes(62,63). This translocation drives an incredibly aggressive cancer with a median survival of only 7 months. It is believed that the main mechanism of oncogenesis in NMC is via aberrant activation of MYC and SOX2, preventing differentiation and increasing proliferative capacity(64). Other fusions have been described, such as BRD4-NOTCH3(65) but are exceedingly rare and only described on a case-by-case basis. The role of BRD4 in promoting leukemia is more nuanced and is thought to be primarily due its regulation of *myc*, a well-described master-regulator of many oncogenes(66)(67). In addition, BRD4 has been shown to regulate the transcription of many hematopoietic transcription factors that determine cell differentiation state and are often dysregulated in AML, supporting previous data regarding BRD4 regulating super-enhancer regions(68) (Figure 7).

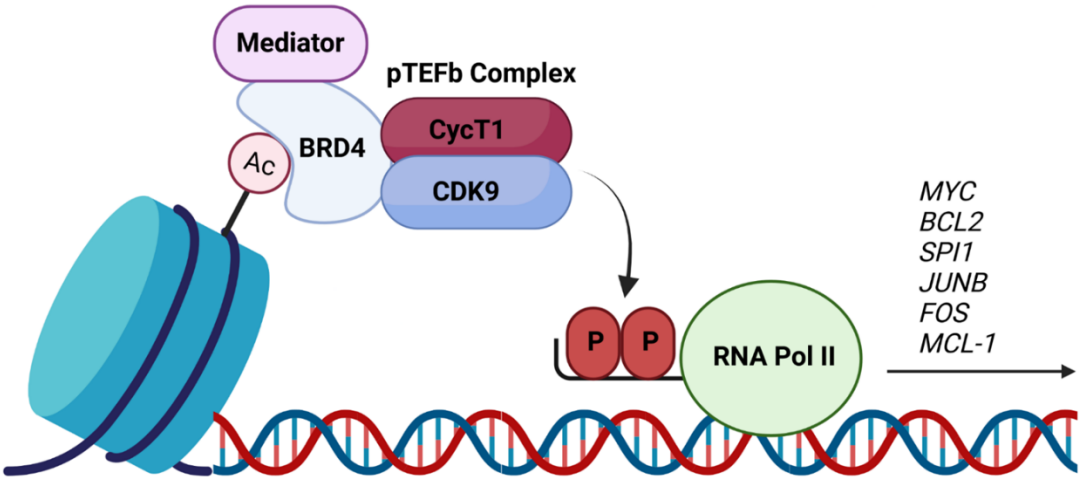

Figure 7 – Cartoon schematic detailing the mechanisms of action for BRD4. BRD4 binds to acetylated histone residues and recruits RNA transcribing machinery such as the mediator and pTEFb Complex to facilitate RNA pol II elongation. This is accomplished via phosphorylation of the RNA pol II tail by pTEFb Complex. BRD4 regulates many oncogenic genes in hematological malignancies. Created in biorender.

In summary, the exact role of BRD4 in promoting leukemia remains relatively unclear but is likely due to regulation of many pro-leukemia survival and differentiation programs. What is known, however, is that selective inhibition of BRD4 and other BET proteins is a potent inhibitor of leukemic growth *in vitro* and *in vivo*(69-73). Early RNAi dropout screens identified BRD4 loss as an inhibitor of leukemic growth(74). In addition, BETi treatment in leukemia cells has been shown to dramatically reduce transcription of the aforementioned oncogenes and induce cell death(70,75,76). Several BETi have been developed to date, the majority of which function by specifically blocking the acetyl-lysine binding pocket of BRD4 from interacting with acetylated histones. This dissertation will focus on three BETi -- JQ1, OTX-015, and CPI-0610, which all act mechanistically in this fashion(70,71,76,77). Newer generation of BETi exist which are composed of the recognition features of previously described BETi (e.g JQ1, etc.) conjugated to E3 Ubiquitin Ligase, which tags and ubiquitinates BRD4 for degradation. These inhibitors are commonly referred to as Proteolysis-Targeting Chimera (PROTACs). However, these inhibitors have had issues transitioning to the clinic due to their overt toxicity(78-80). Growing interest is garnering around selective inhibition of the BD1 and BD2 domains, rather than pan-BD targeting that is accomplished by older generation BETi, and have recently been described, but are too new to gauge their impact in hematological malignancies(81). As mentioned previously, the BD1 and BD2 domains have unique binding preferences and selective inhibition of one or the other may affect clinical activity. Clinically, BETi OTX-015 achieved complete remissions in a small subset of patients who failed alternative therapies, which is rarely achieved in monotherapy SMIs. However, many patients were unresponsive to OTX-015(82), prompting the investigation of potential intrinsic resistance mechanisms to BETi, which is the subject of the first body of work in this thesis.

T cell Exhaustion

Introduction

The second body of work in this thesis describes a role for BRD4 in regulating T cell exhaustion justifying synergistic combinations of BETi and anti-PD1 therapy in AML. This introductory section will describe the characteristics of immune exhaustion and the interplay with immune checkpoint blockade therapy.

Characteristics of T cell Exhaustion

T cells are lymphoid cells that develop in the thymus and differentiate into either $CD4^+$ T cells or $CD8^+$ T cells, which are the focus of this section(83). T cells protect the host in conjunction with antigen-presenting cells, which display antigens bound to major-histocompatibility complexes I (MHC) and are recognized by $CD8^+$ T cells, and on MHC II which are recognized by $CD4^+$ T cells. $CD8^+$ T cells engage with antigen-bound MHC I via their T Cell Receptors (TCRs) and undergo clonal expansion and differentiation into a wide variety of memory and effector subtypes(84). Effector $CD8^+$ T cells act primarily through generation of cytolytic molecules, such as granzyme B and perforin, and inflammatory cytokines. These short-lived T cells contract after approximately 10-14 days before undergoing programmed cell death, whereas memory T cells persist and provide immunological memory of the bacterial/viral/parasitic infections(85).

Broadly, T cell exhaustion is a phenomenon originally described during chronic viral infections in which T cells continuously exposed to antigens terminally differentiate into dysfunctional T cells. It was found that Armstrong LCMV infections, which generate acute infections that are quickly cleared by the animal, preferentially generate terminal effector T cells. Conversely, Clone 13 or Docile LCMV infections, which generate chronic infections, preferentially generate terminally exhausted T cells after an extended period of time(86,87). In this context “dysfunctional” refers to a multitude of changes, most notably decreases in effector molecule secretion (granzyme B, perforin, etc.), loss of

proliferative capacity, loss of transcriptional plasticity, and resistance to ICB therapy re-invigoration(88,89). Differentiation down a terminal exhaustion (TEx) lineage vs. terminal effector lineage is determined by antigen exposure type, acute vs chronic, and is regulated by large changes in the epigenetic landscape (Figure 8(88)). A set of TCR-activated transcription factors -- namely BATF, IRF4, NFATc1, and TOX, promote terminal exhaustion whereas transcription factors in the HMG-box family, such as TCF1 and SLAMF6, promote stemness and maintain what are referred to as progenitor exhausted T cells (TPEx)(86,87,90-95) (Figure 9(96)). These T cells are considered precursors to terminally exhausted T cells and retain many of their effector functions, described in detail in the following section. As described in Figure 9, TPEX are maintained and demarcated by the transcription factor TCF1. TCF1 is a key transcription factor in the canonical WNT signaling pathway and is considered a master regulator of T cell function and differentiation (reviewed(97)). In the context of TPEX cells, it is believed that TCF1 maintains the stemness of these cells via enhancing expression of *Eomes*, *Bcl6*, and *Bcl2* while inhibiting *Prmd1* (encodes BLIMP1). BLIMP1 has been well described as a negative regulator of a number of stemness programs in T cells, such as *Sell*, *Il7ra*, *Cxcr5*, and *Ccr7(98-100)*. Interestingly, TCF1 is also believed to be critical in the initiation of exhaustion differentiation and is considered a fate-decision transcription factor(91). Chen *et al*. demonstrate that TCF1, while maintaining memory programs, also promotes differentiation away from effector programs towards exhaustion via the TCF1-EOMES-BCL2 axis.

Epigenetic Regulation of T cell Exhaustion

The development of T cell exhaustion is driven by large epigenomic changes. Many studies have described the changes in chromatin architecture during $CD8^+$ T cell exhaustion differentiation(101-105). Additionally, several have demonstrated that PD1 blockade does not fully restore TCR signaling due to the altered epigenomes of $CD8^+$ T

cell (supporting my hypothesis of using epigenetic targeted inhibitors in parallel with aPD1 therapy)(101,106,107). It is believed that the primary players coordinating T cell exhaustion via epigenetic landscape alterations are NFAT, TOX, and NR4a which coordinate with DNA methylators like DNMT3a and histone acetylation machinery to alter chromatin accessibility at critical fate determining genes such as *Pdcd1, Ctla-4, Tcf7, Tbx21,* and Ifng(87,93,94,108). Deletion of any of these key players significantly disrupts Tex formation. In total, commitment away from effector programs towards exhaustion is driven by many coordinating TCR-activated transcription factors and is accompanied by large transcriptional and epigenetic changes.

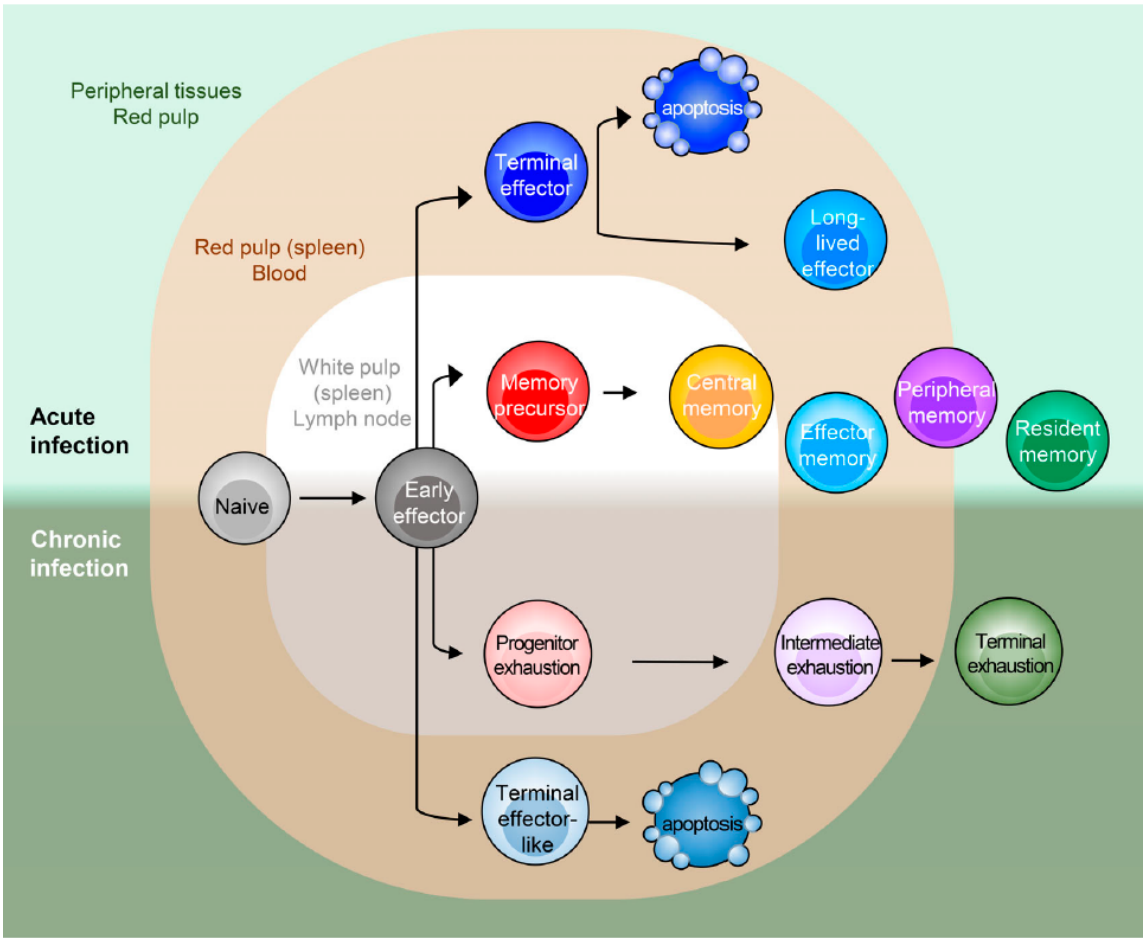

Figure 8 – Cartoon schematic (with permission from JEM.) detailing the opposing fates of $CD8^+$ T cells upon exposure to chronic or acute antigens. Acute infections generate short-lived effector T cells which undergo programmed cell death during contraction. Chronic antigen exposure instead drives generation of progenitor exhausted T cells which give rise to terminally exhausted T cells

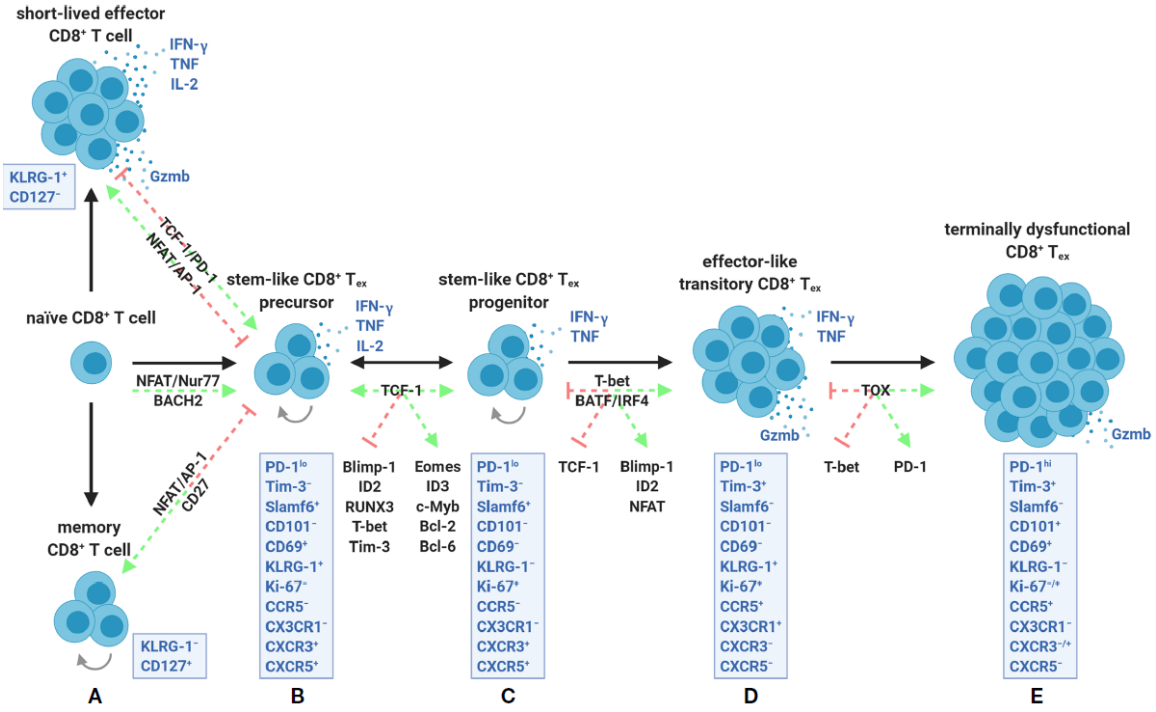

Figure 9 – Cartoon schematic (with permission from Frontiers in Immunology) detailing the transcription factors which regulate differentiation of naïve CD8+ T cells into progenitor exhausted and finally terminally exhausted T cells. In addition, the recently identified surface markers expressed on progenitor exhausted T cells (B/C) and terminally exhausted T cells (E) are shown.

T cell exhaustion and Immune Checkpoint Blockade Response

Not surprisingly, cancers of many types, which can be thought of as promoting a chronic antigenic environment, have been shown to preferentially generate terminally exhausted T cells in the same fashion as chronic LCMV infections (reviewed(89,96)). Immune checkpoint blockade has revolutionized how we think about cancer therapies and its discovery by James Allison and Tasuku Honjo awarded them the 2018 Novel Prize in Physiology and Medicine. Seminal work from both labs discovered that, upon activation, T cells rapidly upregulate several receptors, now referred to as "checkpoint" or "inhibitory" receptors, which engage with ligands to suppress T cell function (reviewed in(109-111)). It has been hypothesized that these receptors, which include PD1, TIM3, LAG3, TIGIT, VISTA, and others, are an evolutionary adaptation to chronic antigen exposures to prevent the development of auto-immunity after chronic infection. One of the most well studied checkpoint receptors is PD-1, which is engaged by its ligands PD-L1 and PD-L2(112). These ligands are highly expressed on antigen-presenting cells, as well as on several tumors, and are rapidly upregulated in response to IFNy produced by activated T cells(113,114). PD-1 is thought to suppress TCR signaling and thus, T cell activity, through several direct and indirect pathways upon engagement by its ligands PD-L1 and PD-L2(111): 1.) Dephosphorylation of ZAP70 and PI3K via recruitment of phosphatases SHP1 and SHP2 to PD-1s ITIM and ITSM domains(115) 2.) Regulation of CD28 co-stimulation via SHP1/SHP2 mediated dephosphorylation of CK2 which increases activity of PTEN and subsequently reduces PIP3 and PI3K activity(116) 3.) Cell cycle arrest at G0-G1 via accumulation of CDK inhibitor $p27^{Kip1\ (117\text{-}119)}$ 4.) CBL-b mediated internalization of the TCR complex, thus reducing TCR signaling(120-122) (Figure 10(111)).

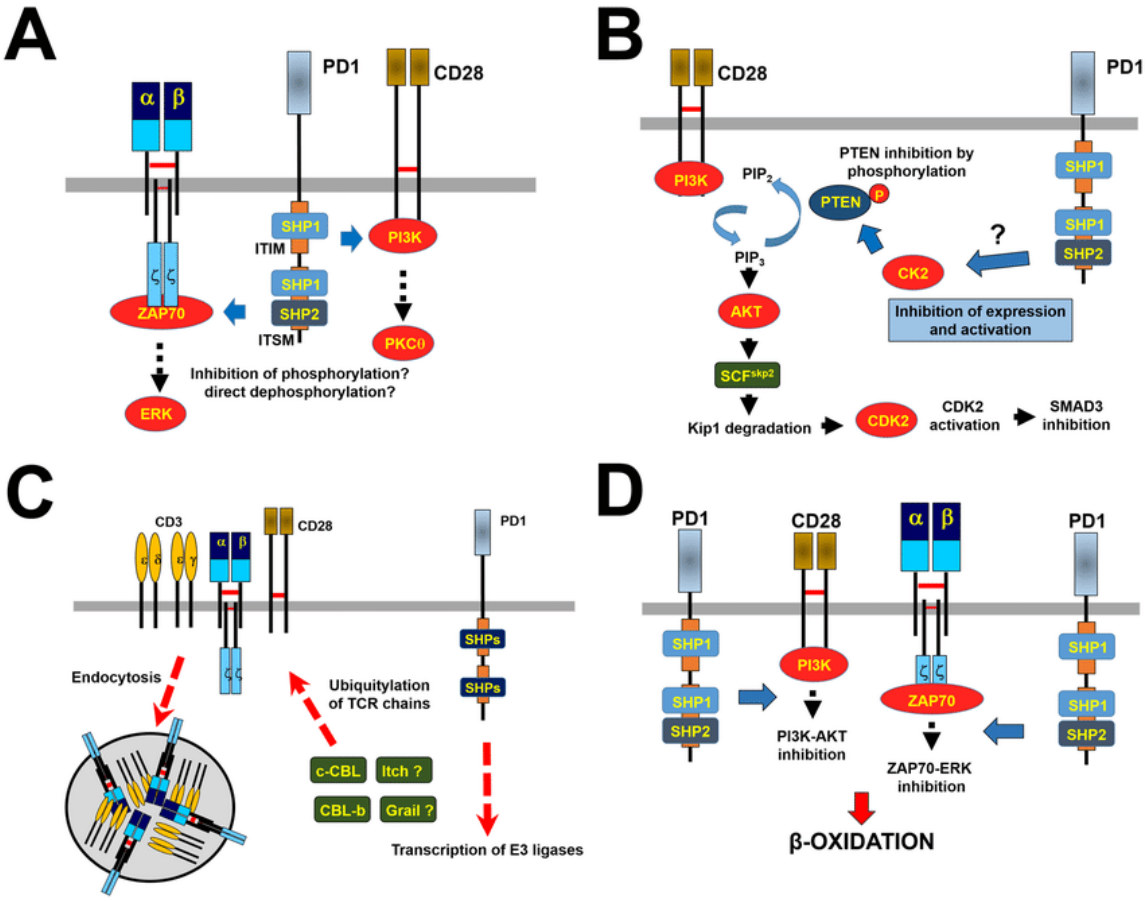

Figure 10 – Cartoon schematic detailing the 4 main mechanisms of PD-1 signaling regulation of T cell activation. Used with permission from Oncotarget.

Immune checkpoint blockade refers to the usage of blocking antibodies against the checkpoint receptor (e.g. PD-1), or the ligands (e.g. PD-L1/PD-L2 individually or combined). These therapies have increased survival across many tumor types, but of particular note is in the metastatic melanoma setting (reviewed (123,124)) where anti-PD1 therapy is now an FDA approved first-line therapy for this once considered "impossible to treat" cancer. Currently, there are over 100 clinical trials evaluating the efficacy of immune checkpoint blockade (ICB) therapy alone or in combination with targeted drugs/chemotherapies across dozens of different cancers.

The importance of understanding mechanisms of T cell exhaustion regulation in cancer has come to the forefront, particularly in areas studying mechanisms governing ICB responses as it has now been shown in several settings that the specific T cell subpopulations which are re-invigorated with ICB therapy and maintain the strongest anti-tumor responses are the $TCF1^+$ TPEx T cells discussed previously(100,106,125,126). Some of the earliest clinical trial data post-analyses by Sade-Feldman *et al.* in metastatic melanoma found that, while both TEX and TPEX could be identified in all patients, ICB responders had higher frequencies of intratumoral TCF1-expressing $CD8^+$ T cells(127). Higher proportions TEx is associated with worse clinical outcomes in multiple tumor types, including AML and other hematological malignancies(106,128-130). Thus, one potential approach to improving ICB therapies is to identify potential combinatorial or sequential treatment strategies that employ other small-molecule inhibitors which promote expansion of these TPEx cells and rescue ICB refractoriness, the topic of the second main body of work described in this thesis. Given the known epigenetic regulation of exhaustion differentiation, epigenetic targeting inhibitors are of particular interest.

Chapter 2

Monocytic Differentiation and AHR signaling as Primary Nodes of BET Inhibitor Response in Acute Myeloid Leukemia

Adapted from Romine *et al*. Blood Cancer Discovery. DOI: 10.1158/2643-3230.BCD-21-0012

Abstract

To understand mechanisms of response to BET inhibitors (BETi), we mined the Beat AML functional genomic dataset and performed genome-wide CRISPR screens on BETi- sensitive and BETi- resistant AML cells. Both strategies revealed regulators of monocytic differentiation, SPI1, JUNB, FOS, and aryl-hydrocarbon receptor signaling (AHR/ARNT), as determinants of BETi response. AHR activation synergized with BETi while inhibition antagonized BETi-mediated cytotoxicity. Consistent with BETi sensitivity dependence on monocytic differentiation, ex vivo sensitivity to BETi in primary AML patient samples correlated with higher expression of monocytic markers CSF1R, LILRs, and VCAN. In addition, HL-60 cell line differentiation enhanced its sensitivity to BETi. Further, screens to rescue BETi sensitivity identified BCL2 and CDK6 as druggable vulnerabilities. Finally, monocytic AML patient samples refractory to venetoclax ex vivo were significantly more sensitive to combined BETi + venetoclax. Together, our work highlights mechanisms that could predict BETi response and identifies combination strategies to overcome resistance.

Statement of Significance:

Drug resistance remains a challenge for AML and new therapies, such as BET inhibitors, will require combination approaches to boost single-agent responses. We conducted

genome-wide CRISPR screens and functional genomics on AML patient samples to identify leukemic differentiation state and AHR signaling as primary mediators of BETi response.

Introduction

Acute myeloid leukemia is an aggressive hematologic malignancy, diagnosed primarily in elderly patients. Many patients cannot tolerate the intensive 7 plus 3 chemotherapy regimen (cytarabine plus anthracycline), which has been a standard of care for >40 years(17). These patients rely on alternative treatment strategies, such as targeted small-molecule inhibitors. Recently, combinations of BCL2 inhibitor, venetoclax, with hypomethylating agents was approved for treatment of patients unfit for chemotherapy, but not all patients respond to this therapeutic regimen(27). Most patients, particularly those treated with monotherapy regimens, will develop resistance and relapse. Therefore, understanding molecular mechanisms driving drug resistance is critical for the development of drug combinations that yield durable remissions and extend survival.

AML is a heterogeneous cancer that is primarily driven by four classes of mutations: 1) activation of proliferative and anti-apoptotic genes, 2) block of differentiation, 3) epigenetic regulators, and 4) splicing machinery(19,20,131). As such, we have seen the implementation of many small-molecule inhibitors targeting these pathways(132).

The Bromodomain and Extra-Terminal domain (BET) protein family consists of bromodomain containing proteins BRD2, BRD3, BRD4, and BRDT, which interact with acetylated histone tails to facilitate many downstream functions such as chromatin remodeling and transcriptional regulation. Epigenetic inhibitors targeting BET family proteins, (BETi) have recently come to the forefront of development due to evident cytotoxicity in hematological settings(69-73). BRD4 binds acetylated histone tail and

recruits Positive Transcription Elongation Factor b (P-TEFb) to enhancer regions to mediate the phosphorylation of the c-terminal domain of RNA pol II, required for elongation of the nascent mRNA(133,134). BRD4 also acts as a histone acetyltransferase (HAT) (60), an atypical kinase(61), and interacts with splicing machinery(59). Previous RNAi studies identified BRD4 loss as a potent inhibitor of leukemic growth(74). BET proteins have also been linked to driving leukemia disease by recruiting transcription machinery to MYC and BCL2 promoters(68,75). BETi treatment in leukemia cells has been shown to dramatically reduce transcription of these oncogenes and induce cell death(70,75,76). Clinically, BETi OTX-015 achieved complete remissions in a small subset of patients who failed alternative therapies. However, many patients were unresponsive to OTX-015, prompting the investigation of potential intrinsic resistance mechanisms to BETi(82).

Several studies have reported on a wide scope of genetic resistance mechanisms to BETi involving autophagy(135), WNT signaling driven by leukemia stem cells and transcriptional plasticity(136,137), and PP2A(138). Further, Bell *et al.* have shown that non-genetic resistance can arise upon BETi exposure(139). These studies prompted us to mine the Beat AML functional genomic dataset and also utilize genome-wide CRISPR screens to further understand drivers of resistance to BETi in AML and identify therapeutically druggable dependencies.

Results

Monocytic markers correlate with BETi sensitivity in AML patient samples

To identify potential genetically driven BETi resistance mechanisms, we correlated *ex vivo* drug sensitivity data for three BETi (JQ1, OTX-015, and CPI-610) against recurrent genetic mutations using the Beat AML cohort, an integrative dataset containing ex vivo drug sensitivity, exome-, and RNA-sequencing for over 500 primary AML patient

specimens(20). Of the entire database, we were able to obtain BETi *ex vivo* data for 173 unique patient samples. Interestingly, we found no genetic mutations or cytogenetic patterns that significantly correlated with resistance or sensitivity to any of the three BETi (Figure 11a-f). In recent work by our lab and others, similar explorations of response to venetoclax identified leukemic differentiation state as a primary determinant of sensitivity and resistance(140-143). Accordingly, since no mutations correlated with BETi response, we next asked whether BETi sensitivity and resistance correlated with expression of cell surface markers that are known indicators of cell differentiation state. Indeed, within the Beat AML database, *ex vivo* responses to JQ1, OTX-015, and CPI-0610 in 173 primary human patient samples were significantly correlated with expression of monocytic markers such as CSF1R, VCAN, CD33, ITGAL, and LILRA1(Figure 12a,b). In addition, we found high congruence of drug sensitivity versus surface marker expression correlations across all three BETi (Figure 12c). Historically, AML cases have been classified based on the French-American-British (FAB) M0 to M7 classification system, where M0, M1, and M2 represent tumors comprised of minimally or undifferentiated cells, and

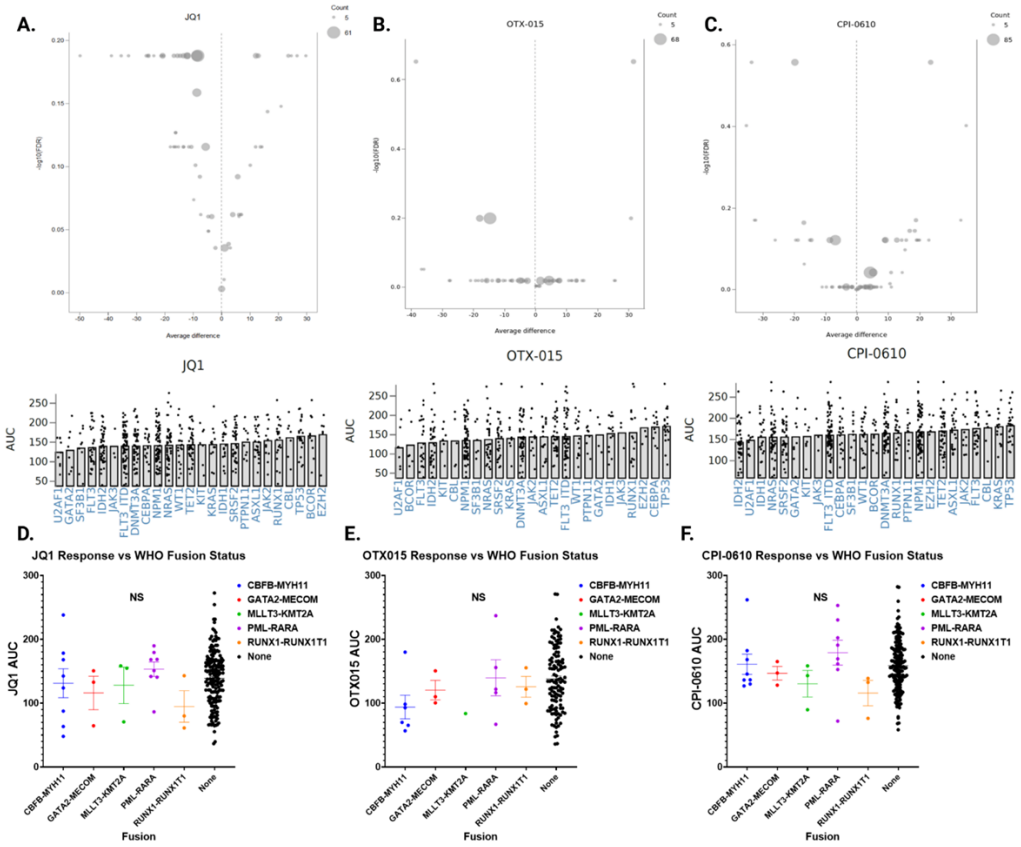

Figure 11 – **a-c.)** Volcano plots correlating BETi (JQ1 left, OTX-015 middle, and CPI-0610 right) ex vivo sensitivity of 173 AML patient samples, as determined by MTS viability assay, with genetic mutations in the Beat AML database, as previously described and publically available at http://www.vizome.org (no significance). Corresponding recurring genetic mutations vs individual AUCs are below the corresponding volcano plot (X-axis denotes a recurring genetic mutation, Y-axis the corresponding AUC, with each point representing a unique patient sample). In brief, recurring mutations (found in at least 5 patients) and inhibitor area-under-curves (AUC), as determined by MTS assay, were compared using a linear model and compared linear contrast (two-sided students T-test) of mutation/mutation sets to appropriate negatives (WT gene comparison). FDR was computed using the Benjamini-Hochberg method over all the drugs. **d-f.)** Ex vivo MTS assay sensitivities in AML patient samples to JQ1, OTX-015, and CPI-0610 were stratified by WHO-FUSION status (common fusion protein alterations known to occur in AML) within the beat AML biorepository. Significance was determined by one-way ANOVA. No WHO-FUSIONS correlated with any BETi sensitivity or resistance.

M4-M5 represent tumors of a myelomonocytic or monocytic cell state. As expected, we also found that CSF1R, VCAN, LILRA1, and LILRB1 were highly expressed in monocytic leukemia FAB subtypes (M4-M5) compared to undifferentiated cases (M0-M2) (Figure 12d-g). Together these findings indicate that BETi may be more efficacious in differentiated leukemias and highlights a novel vulnerability for these leukemias.

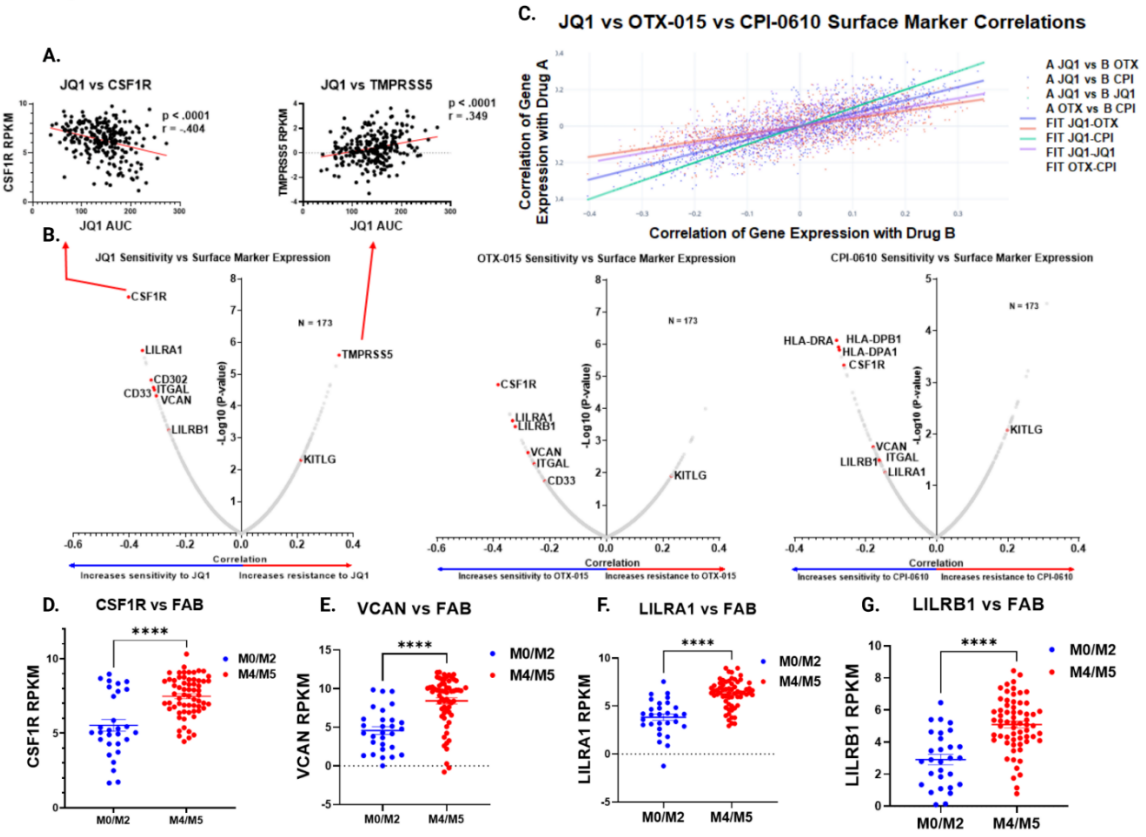

Figure 12 - **a.)** Correlations between ex vivo sensitivity to JQ1 in 173 patient samples and expression of monocytic differentiation markers with Beat AML dataset. Each dot represents a unique patient sample ex vivo response to a BETi (area under the curve, determined by MTS viability assay) plotted against mRNA level of the surface marker denoted (CSF1R, TMPRSS5, eg.). A simple linear regression model was fit separately for each inhibitor and gene with the inhibitor AUC values as the outcome. The T-statistic and P-value tests whether the slope is non-zero and corrected for multiple comparisons. Corresponding correlation coefficients were computed using the relationship to the linear model: slope*(sd(expr)/sd(auc)) where sd indicates standard deviation. **b)** Pearson correlation coefficients and significance, corrected for multiple comparisons, are calculated for each surface marker mRNA expression and ex vivo sensitivity to a BETi in 173 Beat AML patient sample dataset. Each dot represents a correlation coefficient and corresponding p-value for individual surface marker mRNA vs. BETi AUC (as shown in Fig a, extended to all known surface markers). Points of interest are highlighted in red. **c)** Pearson correlations for sensitivity to each individual BETi (JQ1, OTX015, CPI0610) vs surface marker expression calculated previously in 1b, plotted against each other with a line of best fit highlighting their congruence. Each point thus represents the XY coordinate location of correlations for a surface marker between two different BET inhibitors, for example a single point will be X =JQ1 vs CSF1R correlation, Y = OTX vs CSF1R correlation, or X = OTX vs ITGAL correlation vs Y = CPI ITGAL correlation, etc. Dark purple dots represent comparisons between JQ1 and OTX, orange represents comparisons between JQ1 and CPI, green represents comparisons between JQ1 against itself, and light purple represents comparisons between OTX and CPI. Corresponding lines of best fit match the above comparisons. **d-g.)** Comparison of RNA expression levels (RPKM) of **d.)** CSF1R, **e.)** **V**CAN, **f**.) LILRA1, and **g.)** across FAB groups (French-American-British subtyping; M0-M2 (29 samples), undifferentiated AML; M4-M5 (34 samples), myelomonocytic-monocytic AML (83)) within the Beat AML patient dataset (ref. 3.)). P-values determined by Mann-Whitney t-tests. X-axis denotes FAB subtype, Y-axis denotes RPKM expression of a given gene.

Genome-Wide CRISPR screen identifies monocytic differentiation regulators of BETi resistance

To further study mechanisms of resistance to BETi in AML, we performed a genome-wide CRISPR resistance screen in OCI-AML2 cells under selection of the BETi, CPI-0610. Distribution of sgRNAs in deep-sequenced libraries from drug-treated cells were compared to DMSO-treated controls using edgeR(144). To prioritize hits, we used a tiering structure that we previously developed for CRISPR screens(145). This scheme organizes top candidates into three tiers based on evidence (determined by the number of sgRNA guide hits per gene), concordance (indicated by the agreement across the set of guides for a given gene), and discovery (based on expanding effect size threshold). Using this prioritization scheme and focusing on tiered genes with a mid-log fold change of > 1.5, CPI-0610 (Figure 13a) selected cells showed enrichment for guides targeting hematopoietic transcription factors (e.g. *FOSL2*, *JUNB*) (Figure 13b) and aryl-hydrocarbon signaling (e.g. *AHR*, *ARNT*) (Figure 13c) compared with DMSO. We ran a parallel screen using overlay of a related BETi, JQ1, instead of CPI-0610. While the results of this screen did not yield hits that were as statistically significant as the CPI-0610 screen with no genes assigned to a Tier, we focused attention to genes with a mid-log fold change > 2. Using this threshold, we also identified resistance-enriched guides that targeted genes in the same category of transcription factors known to regulate myelopoiesis (*SPI1, FOS, CREB1;* Figure 14a, b). To prioritize hits for follow-up analysis, we assessed enrichment of hits from the two screens in a pathway context. We took the combined list of gene hits from both screens, and seeded a STRING(146) network to investigate associations between this union of candidate genes from both screens (Figure 13d, Figure 14c).

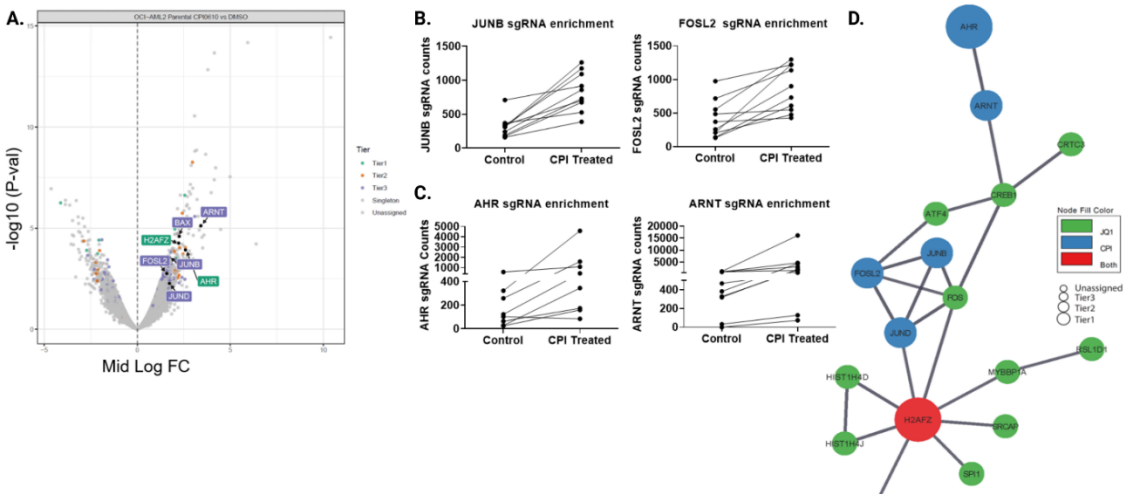

Figure 13 - Cas9 expressing OCI-AML2 were lentivirally transduced with a genome-wide CRISPR library containing an average of 5 guides per gene, collectively targeting 18,010 human genes (31) (32). Cells were treated with 500nM CPI-0610 or vehicle (DMSO) for 21 days followed by DNA harvest and PCR-amplification of sgRNA guide sequences. **(a.)** Volcano plot comparing enrichment of sgRNAs relative to DMSO control in CPI-0610 treated OCI-AML2 cells versus –log10 transformed median p-value after 21 days with corresponding significance tiers. Each dot represents a combined sgRNA KO enrichment score (combining ~5-6 unique sgRNAs targeting same gene) relative to control vs. corresponding p-value. Significance of each sgRNA was determined via edgeR (RRID: SCR_012802) after TMM(78) normalization. Briefly, considering only significant sgRNAs (FDR < .05), genes were classified into 5 ordered groups. Tier 1 genes had more than one significant sgRNA, a minimum log 2-fold change >= 2, 75% of sgRNAs per gene present and concordance among sgRNAs per gene >= 75%; Tier 2 hits had log 2-fold change >= 2 and 100 % concordance among sgRNAs per gene Tier 3 hits had log 2-fold change >= 1 and 100% concordance among sgRNAs per gene. Singleton hits represent significantly enriched genes with log 2 -fold change >= 2 but only a single significant sgRNA. Enriched hits not satisfying these criteria were classified into the Unassigned group. X – axis corresponds to median log fold change (CPI treated/Control treated) sgRNA counts. Y axis corresponds to –log10 median p-value. **b.)** Enrichment of cells containing the relative sgRNA KO relative to DMSO control (roughly ~5-6 unique sgRNAs per gene KO for Yusa library) targeting hematopoietic transcription factors JUNB (left) and FOSL2 (right) in CPI-0610 treated OCI-AML2. Each line represents the guide counts of the relevant unique sgRNA KOs in control or CPI0610 treated cells**. c.)** Enrichment of cells containing the relative sgRNA KO targeting aryl-hydrocarbon receptor signaling components AHR (left) and ARNT (right) in CPI-0610 treated OCI-AML2. Each line represents the guide counts of the relevant sgRNA KOs in control or CPI0610 treated cells. **d.)** A STRING(34) network, which is used to model known or predicted protein-protein interactions from custom gene lists, was seeded with significant hits from both the CPI0610 and JQ1 CRISPR screen, and identifies a concordant network of enriched hits of interest across both JQ1 and CPI-0610 CRISPR screens centered on hematopoietic transcription factors, AHR, and histone modifying machinery. Size of node denotes tier (largest = tier 1, smallest = unassigned), color denotes gene screen of origin.

In addition, we took these same hits and analyzed them via GO Cellular Components Ontology and found high concordance between genes from both screens under shared ontological components (Figure 14d). Using both methods, a core set of gene hits—SPI1, FOS, JUNB, AHR, and ARNT—were mapped in close proximity across multiple pathway annotations, and these genes were chosen for downstream validation.

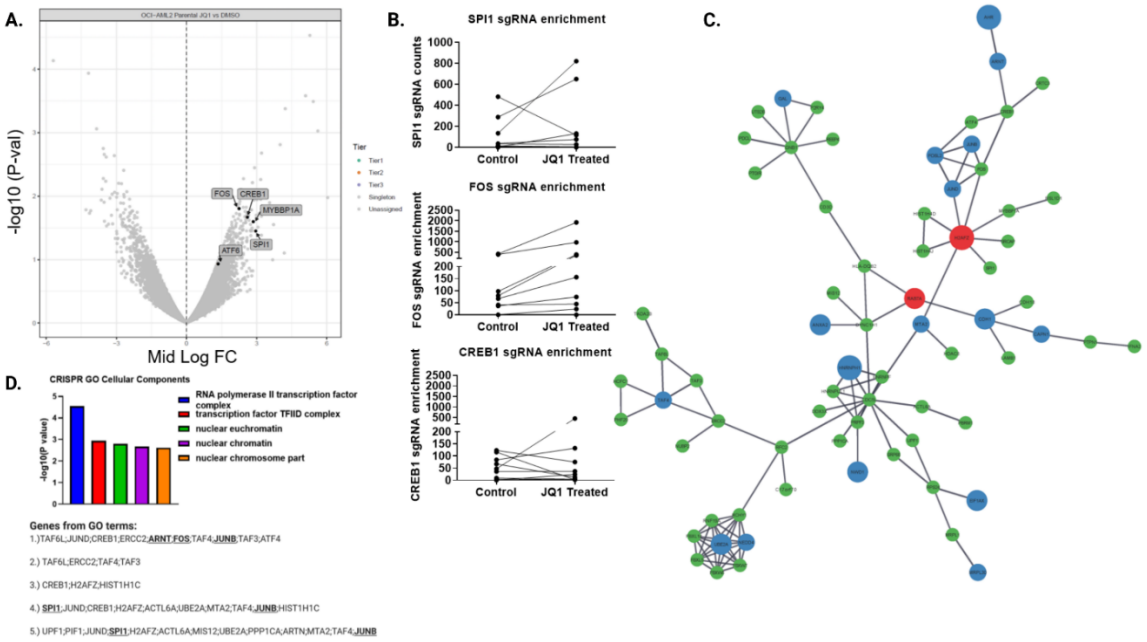

Figure 14 – **a.)** Volcano plot comparing enrichment of sgRNAs relative to DMSO control in JQ1 treated OCI-AML2 cells versus -log10 transformed median p-value after 14 days with corresponding significance tiers. Enrichment and associates p-values calculated as described in the methods and for the CPI-0610 screen. Y axis corresponds to –log10 median p-value, X – axis corresponds to median log fold change (JQ1 treated/Control treated) sgRNA counts. **b.)** Enrichment of cells containing the relative sgRNA KO targeting hematopoietic transcription factors SPI1 (Top), FOS (middle), and histone modifying machinery CREB1 (bottom) in JQ1 treated OCI-AML2. Each line represents the guide counts of the relevant unique sgRNA KOs in control or JQ1 treated cells. **c.)** Full string network plot incorporating hits from both JQ1 and CPI-0610 resistance screens. Size of node denotes tier (largest = tier 1, smallest = unassigned), color denotes gene screen of origin. **d.)** A GO Cellular Components Ontology, which identifies enriched ontological pathways from a gene list, was performed on the the combined JQ1 and CPI-0610 resistance screen hits and identifies RNA pol II transcription factor complex components as the most enriched ontological term.

Screen Validation

Since both the JQ1 and CPI screens pointed to the same pathways, but yielded less agreement at the level of individual genes, we wanted to determine whether these specific gene knockout events were truly causing differential resistance to the two drugs or whether targeting of these genes yields more of a pan-BETi resistance phenotype. Accordingly, we designed 2 sgRNAs per gene to target *SPI1*, *FOS*, *JUNB*, or non-targeting. Knockouts were validated by TIDE analysis or western blot (Table 1-3). Sensitivity to BETi (JQ1 and CPI-0610) was determined by MTS assay after selection of OCI-AML2 cells with control or gene-targeting sgRNAs. With this approach, we found that loss of SPI1, FOS, and JUNB resulted in pan-BETi resistance (Figure 15a-c). Small-molecule AHR inhibitors and activators are readily available and, thus, to investigate altered AHR signaling in mediating BETi resistance, we tested the combination of CPI-0610 with either AHR inhibitor (AHRi), CH-223191, or an AHR agonist, FICZ. As expected, the AHRi antagonized CPI-0610 cytotoxicity in OCI-AML2s (Figure 15d), with a ZIP synergy score of -3.493, while FICZ enhanced these affects, with a ZIP synergy score of 4.425 (Figure 15e). We validated these findings further by knocking out AHR and ARNT with single sgRNAs and observed multi-BETi resistance (Table 3). Convergent lines of evidence suggest that hematopoietic transcription factors (TFs)(147,148) and AHR(149,150) recruit histone modifying machinery to active transcription sites and interact with the P-TEFb complex(151,152). The subsequent hyperacetylation at these regions increases dependency on BRD4 and induces monocytic differentiation. Therefore, we hypothesized that monocytic leukemias, which characteristically have high expression of these genes, may exhibit greater sensitivity to BETi, and that undifferentiated blasts will be intrinsically resistant to BETi due to decreased expression of these genes.

Table S1

sgRNA Sequences and TIDE KO Efficiency		
Gene	**Sequence (5'-3')**	**Efficiency**
SPI1_1	GTCCCCCACAGACCATTACT	79%
SPI1_2	GGGGGTGGAAGTCCCAGTAA	85.80%
FOS_1	TTTGTTCTAGGACTTCTGCA	90.20%
FOS_2	CTAGGACTTCTGCACGGACC	63.70%
JUNB_1	TTCCATTTTAGTGCACATCC	Western
JUNB_2	TATGAGTCGTCGTGGTAGAA	Western
BCL2	TGGGAAGGATGGCGCACGCT	Western
AHR	AAGTCGGTCTCTATGCCGCT	Western
ARNT	GACATCAGATGTACCATCAC	Western

Table S2

CRISPR TIDE Primers	
Gene	Sequence (5'-3')
SPI1_1F	TCAACTGAGGTTAGAGAGGCCAC
SPI1_1R	GAGAGGCAGGGTCAGTAGAG
SPI1_2F	TGGTGAGGGTGCGAGAATTATC
SPI1_2R	TCAACTGAGGTTAGAGAGGCCAC
FOS_1F	GAGGCAGGTTCGTTCTGAGC
FOS_1R	TTGGGATGGAATGGGCTTGG
FOS_2F	GGAGGCAGGTTCGTTCTGAG
FOS_2R	GCTTCATCCTCTGTACTGGGCTC

Table S3

OCI-AML2 AHR/ARNT KO vs Fold Change Drug Sensitivity			
	OCI-AML2 Parental	**OCI-AML2 AHR KO**	**OCI-AML2 ARNT KO**
JQ1	1	2.574338	2.535132
OTX-015	1	1.82834	2.069636
CPI-0610	1	1.844004	1.586564
Venetoclax	1	0.094367	0.164157
Palbociclib	1	0.440321	0.371134

Table 1-3 - **Table 1:** sgRNA sequences used to generate single sgRNA mediated KOs for target genes and corresponding TIDE efficiencies. sgRNA sequences designed using synthego sgRNA design tool (https://design.synthego.com/#/) and corresponding TIDE KO Efficiency as determined by TIDE tool (https://tide.nki.nl/). **Table 2:** DNA primers used to amplify regions of DNA in OCI-AML2 cells to assess TIDE KO efficiency. **Table 3:** OCI-AML2 Parental cells, AHR KO, and ARNT KO cells were assessed for response to JQ1, OTX-015, CPI-0610, Venetoclax, and palbociclib by MTS assay. Here we represent the fold change in IC50 for corresponding inhibitor compared to parental cells.

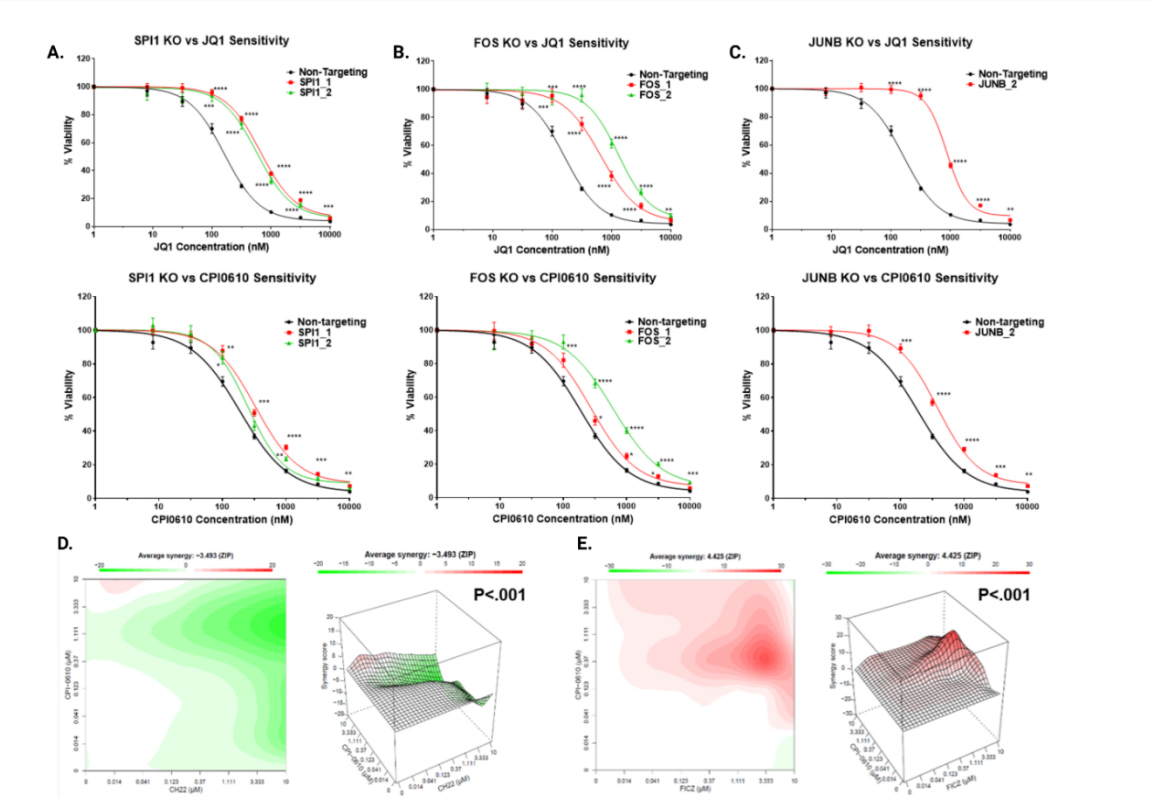

Figure 15 - **a-c.)** OCI-AML2 cells were transduced with lentiviruses carrying custom designed single sgRNA/Cas9 constructs (2 different sgRNAs/gene) targeting SPI1, FOS, JUNB, or non-targeting. After puromycin selection and 10 days of transduction, sensitivity to JQ1 (top row) and CPI-0610 (bottom row) was measured in replicates of 6 via colorimetric MTS-based viability assay. Plots represent sensitivity to BETi in a.) SPI1 KO (left), b.) FOS KO (middle), and c.) JUNB KO (right) in single sgRNA knockouts (colored) vs. non-targeting control (black) in OCI-AML2 cells. Error bars represent the standard error margin between the 6 replicates. Drug curve consists of 8 concentrations ranging from 0uM, and .0137uM-10 uM in log increments. P-values for individual sgRNAs vs non-targeting were calculated using a two-stage linear step-up procedure of Benjamini-Krieger-Yekutieli. X axis represents BETi-concentration, Y-axis represents OCI-AML2 viability. **d,e.)** OCI-AML2 cells were subjected to dilutions of CPI-0610 in combination with titrations of either d.) AHR inhibitor CH-232191 or e.) AHR ligand FICZ and evaluated for viability via colorimetric MTS-based assay. ZIP synergy score was calculated at each drug combination dose pair as previously described(81,82). The ZIP score average was computed across the dose matrix to provide an overall index of drug interaction. A positive average ZIP score indicates the combination was synergistic (red) whereas a negative average ZIP score indicates antagonism (green). ZIP Scores were -3.493 and 4.425 for CH-22191 and FICZ, respectively. Significance of synergy determined by One-Sample Wilcoxon signed rank test comparing individual dose-pair combinations across the entire 7x7 matrix. X axis represents increasing concentrations of AHRi CH22193 (left) or AHRa FICZ (right). Y axis represents increasing concentrations of CPI0610.

BETi-R cells exhibit decreased markers of leukemic differentiation and forced myeloid differentiation increases sensitivity to BETi

Given our proposed mechanism, which posited that BETi sensitivity is driven by monocytic differentiation, we asked whether acquired BETi-resistant (BETi-R) cells had reduced marks of myeloid differentiation. We generated JQ1 and CPI-0610 resistant OCI-AML2 cell models by serially passaging them under increasing selective pressure of BETi and reached IC50s five-fold higher than parental OCI-AML2 cells (JQ1 - 52nM parental, 1.8uM resistant, CPI0610 – 170nM parental, 1.1uM resistant) (Figure 16a). Immunophenotyping of OCI-AML2 parental and BETi-resistant cells revealed a significant reduction in myeloid differentiation marker CD33 expression in BETi-R cells at baseline (Figure 16b). To test whether BETi treatment selects for less differentiated clones, we treated both BETi-naïve and BETi-R OCI-AML2 and observed decreased CD33 expression in both BETi-naïve and BETi-R cells in a dose dependent manner, further suggesting that BETi may select for less differentiated clones (Figure 16c). HL-60s are an undifferentiated M2 FAB leukemia cell line which has been used as a model of myeloid differentiation due to their ability to differentiate in response to all-trans retinoic acid (ATRA), marked by a dramatic increase in expression of CD38. Upon exposure to ATRA HL-60s rapidly upregulate myeloid differentiation programs and dramatically increase expression of many genes such as SPI1, CDKN1A, AHR, FOS, JUN, CD38, and others(153). Given our previous findings which showed that BETi-R cells exhibit decreased marks of differentiation, and that loss of these differentiation regulators drive resistance, we directly asked whether inducing myeloid differentiation increases BETi sensitivity. Indeed, HL-60s, differentiated with 1uM ATRA for 72 hours prior to exposing to BETi, showed dramatically enhanced sensitivity to BETi as compared to undifferentiated HL-60s (Figure 16d, e). In addition, doxycycline inducible PU.1 overexpression in HL-60s sensitized to multiple BETi (Figure 16f). Lastly, to answer whether BETi directly target differentiation programs and, thus, support the

notion that BETi may modulate the process of differentiation, we added BETi concomitantly with ATRA in HL-60s and found that differentiation was significantly attenuated, as seen by a significant reduction in CD38 expression and morphological changes consistent with myeloid differentiation after 72 hours (Figure 16g). Taken together these findings validate that BETi treatment selects for less-differentiated clones and that forced differentiation can enhance sensitivity to BETi.

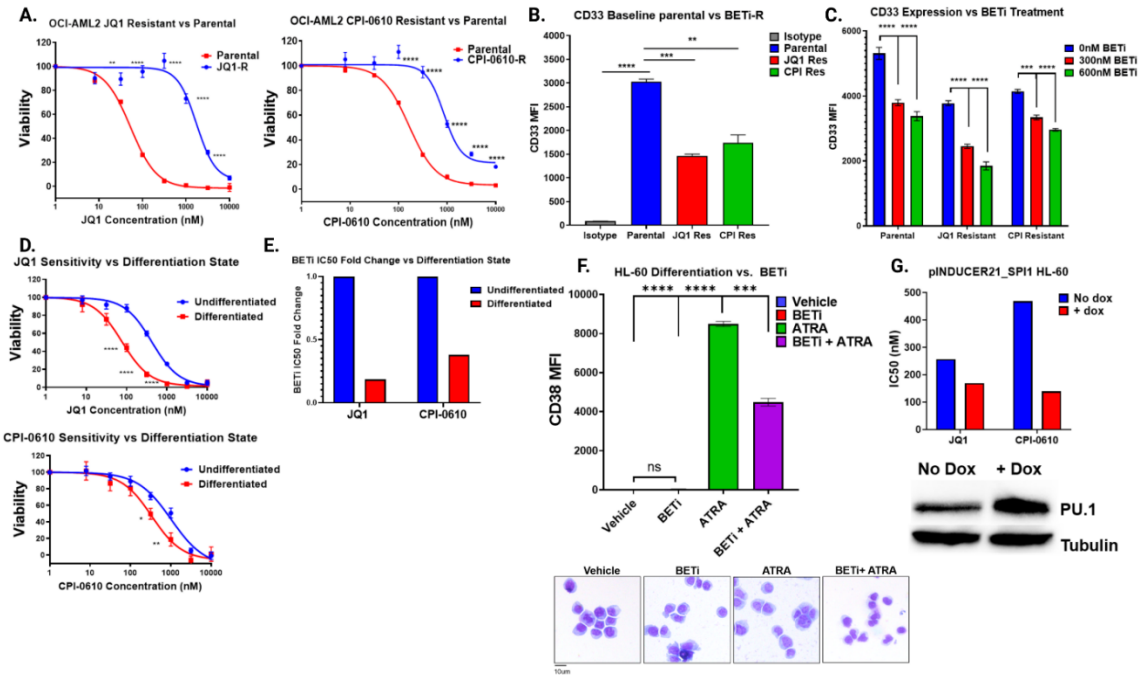

Figure 16 - **a-c.)** BETi resistant OCI-AML2 cells were generated via incubation with serially increasing concentration of JQ1 or CPI0610 over a several month period. **a.)** MTS viability assay after 72 hours was used to assay BETi dose response in the JQ1 resistant OCI-AML2 JQ1 (left) or CPI-0610 resistant OCI-AML2 (right) . Error bars represent the standard error margin between the 6 replicates. P-values were calculated using a two-stage linear step-up procedure of Benjamini-Krieger-Yekutieli comparing Parental to BETi-R OCI-AML2 cells. X axis represents BETi-concentration, Y-axis represents OCI-AML2 percent viability. **b.)** Median Fluorescence Intensity (MFI) of myeloid differentiation marker CD33, as determined by flow cytometry, on untreated BETi naïve OCI-AM2 cells and BETi-R OCI-AML2 cells withdrawn from drug for 1 week. Significance determined by ordinary one-way anova with multiple comparisons corrections from three replicates**. c.)** CD33 MFI, as determined by flow cytometry, of BETi naïve or BETi-R OCI-AML2 cells treated with vehicle, 300nM, or 600nM JQ1 for 72 hours**.** Significance determined by 2-way anova with multiple comparisons corrections from three replicates**. d.)** HL-60 cells were differentiated with 1uM ATRA for 72 hours or left undifferentiated in vehicle for 72 hours. The cells were then washed in PBS and viability assessed (>95%) by guava easycyte. Drug dose response curves, as determined by MTS viability assay, were then assessed for JQ1 (Top) and CPI-0610 (bottom) comparing undifferentiated (vehicle) and ATRA-differentiated HL-60 cells. Error bars represent the standard error margin between the 6 replicates. P-values were calculated using a two-stage linear step-up procedure of Benjamini-Krieger-Yekutieli comparing undifferentiated (vehicle treated cells) to differentiated (ATRA treated cells). X axis represents BETi-concentration, Y-axis represents HL-60 viability**. e.)** Fold change IC50 values for JQ1 and CPI-0610 in undifferentiated HL-60s vs ATRA-differentiated HL-60s from Fig d. **f.)** (Top) Flow cytometry measurement of CD38 MFI, which marks HL-60 differentiation state, in naïve HL-60s treated for 72 hours with vehicle (undifferentiated), BETi, ATRA (differentiated), or simultaneously added BETi and ATRA. Significance determined by One-way ANOVA from three replicates. (Bottom) Giemsa stain of HL-60 cells which were previously subjected to vehicle, BETi, ATRA, or BETi + ATRA for 72 hours**. g.)** HEK293T cells were used to generate inducible PU.1 virus (pINDUCER21-SPI1) with packaging vectors psPAX2 and VSVG . HL-60 cells were then lentivirally infected with the inducible virus or empty vector and GFP sorted. HL-60cells were then induced with doxycycline for 5 days and JQ1 and CPI-0610 IC50s determined by MTS assay. Corresponding western blot validating PU.1 overexpression in HL-60 cells at day 5 below. X axis denotes control vs pINDUCER21-SPI1 cells, Y-axis denotes IC50 to JQ1 or CPI-0610.

Genome-Wide CRISPR screening in BETi-R cells identifies BCL2 and CDK2/6 as re-sensitizing to BETi

To determine acquired vulnerabilities in BETi-R cells, we performed a genome-wide CRISPR dropout screen on JQ1-resistant OCI-AML2 cells, to generate knockout events that re-sensitize JQ1-R cells to BETi. Hits were identified by comparing depleted sgRNAs from JQ1-treated cells to DMSO. Using STRING analyses we identified a subnetwork consisting of cell cycle genes (CDK2 & CDK6) and anti-apoptotic genes (BCL2, ROCK1, & BIRC2) (Figure 17a, b). Independently derived sgRNA guides targeting BCL2 re-sensitized both JQ1-R and CPI-0610-R OCI-AML2 cells to BETi (Figure 17c). Data collected from the Beat AML biorepository, bloodspot.eu, and data deposited by Pei *et al(142)* show that SPI1, FOS, FOSL2, JUNB, and AHR are highly expressed in monocytic leukemias, whereas BCL2 and CDK2/4/6 are enriched in undifferentiated blasts (Figure 18a-f). Collectively these data further support our hypothesis that BETi sensitivity and resistance is tethered to differentiation state and identifies potentially targetable vulnerabilities BCL2 and CDK2/6.

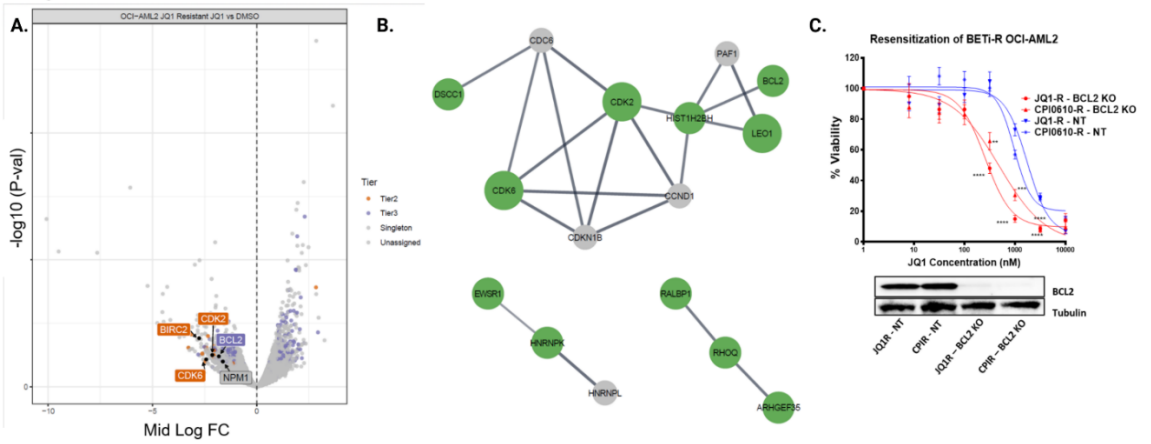

Figure 17 - Cas9-expressing BETI-R OCI-AML2 cells were generated using Cas9Blst. Loss-of-function screens were performed as described, using a human genome-wide sgRNA library. 100e6 cells were used for viral transduction at MOI 0.3, selected with puromycin and then subjected to DMSO or 200nM JQ1 for 14 days. **a.)** Volcano plot comparing enrichment of sgRNAs relative to DMSO control in JQ1 treated JQ1-resistant OCI-AML2 cells (generated in figure 14a) vs. –log10 transformed median p-value. Hits of interest are highlighted and identified. Significance and prioritization of hits performed as previously performed on JQ1 and CPI0610 screens (Fig 12 and Fig 14). X-axis denotes median log fold change of guides (Treated-control). Y-axis denotes –log10 p-val. **b.)** String analysis performed as previously in figure 12d from hits (defined as P<.05, median log fold change < -1.5x) identified in the JQ1 resistant OCI-AML2 CRISPR screen identifies a network of targetable genes BCL2, CDK2, and CDK6. **c.)** JQ1 resistant and CPI-0610 resistant OCI-AML2 cells were infected with either non-targeting or BCL2 targeting lentiviruses and selected for puromycin. **(Top)** MTS viability assay was then used to compare JQ1 sensitivity in single sgRNA KO of BCL2 or non-targeting in JQ1 resistant or CPI-0610 resistant OCI-AML2 cells**. (Bottom)** Whole cell extracts from JQ1-R, CPI-R, and non-targeting cells were evaluated by western blot showing BCL2 KO. Error bars represent the standard error margin between the 6 replicates. P-values were calculated using a two-stage linear step-up procedure of Benjamini-Krieger-Yekutieli comparing non-targeting BETi-R cells to BCL2 KO BETi-R OCI-AML2 cells. X axis represents BETi-concentration, Y-axis represents BETi-R OCI-AML2 viability.

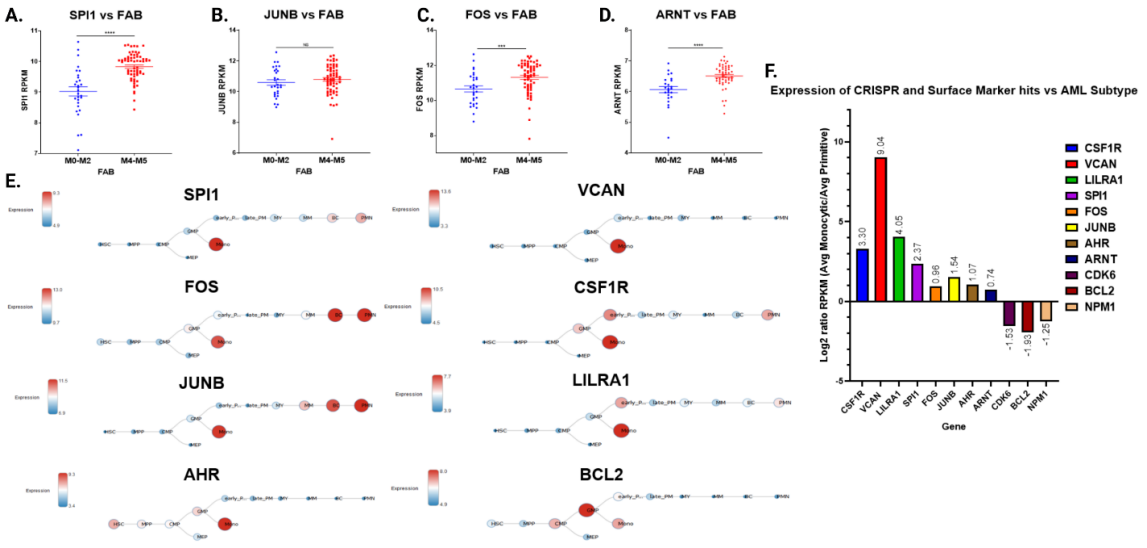

Figure 18 - **a-d.)** Beat AML RNA expression data (3) comparing RNA expression of identified CRISPR hits (SPI1, JUNB, FOS, ARNT) vs FAB subtype (M0-M2 undifferentiated – 29 AML patients, M4-M5 monocytic – 34 AML patients) e.) Bloodspot.eu data comparing RNA expression of CRISPR hits and surface markers against differentiation state. f.) RNA-seq data deposited by Pei et al. 2020 comparing expression of CRISPR hits and surface markers against primitive and monocytic leukemia patient samples.

BETi-R AML cells are sensitive to BCL-2i and the combination of BETi + BCL2i specifically rescues intrinsically BCL2i-resistant monocytic AMLs

We and others have shown that BCL2i are more effective in undifferentiated blasts and monocytic differentiation is a driver of BCL2i resistance in AML(140-143)—the inverse correlation that we have seen here where BETi are more effective on AML cells of monocytic differentiation state and an undifferentiated state promotes BETi resistance. Thus, we tested the efficacy of BCL2i venetoclax in BETi-naïve and BETi-R cells and found increased sensitivity in BETi-R cells (Figure 19a). This correlated with increased expression of BCL2, MCL1, and BCL2L1 (BCLXL) in the BETi-R cells (Figure 19b). In addition, the combination of venetoclax and BETi significantly increased cytotoxicity in undifferentiated c-kit+ cells in BETi-naïve and more so in BETi-R cells (Figure 19c). Finally, AML patient samples treated *ex vivo* with JQ1 showed enhanced sensitivity in M4/M5 FABs but were intrinsically resistant to venetoclax, as previously published(141-143). However, the combination of JQ1 + venetoclax showed significantly enhanced sensitivity compared to venetoclax alone, specifically in matched monocytic leukemias, rescuing intrinsic BCL2i resistance due to monocytic differentiation (Figure 19d, e).

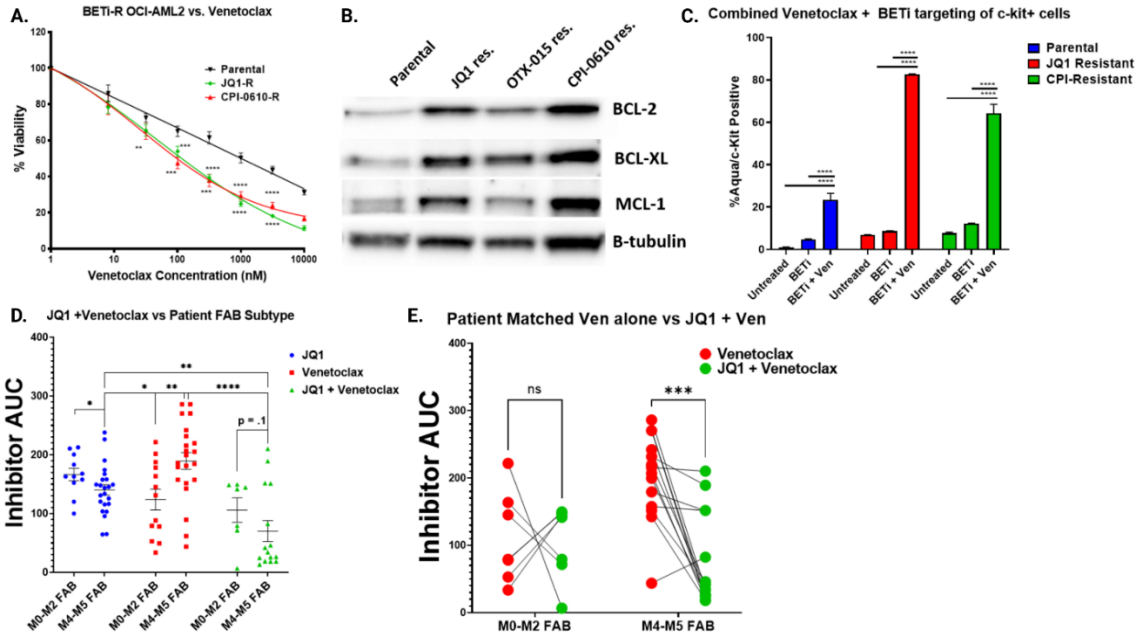

Figure 19 - **a.)** BETi-naïve and BETi-R OCI-AML2 cells were subjected to titrations of BCL2i Venetoclax for 72 hours and then assessed for viability by MTS assay. Error bars represent the standard error margin between the 6 replicates. P-values were calculated using a two-stage linear step-up procedure of Benjamini-Krieger-Yekutieli comparing Parental to BETi-R OCI-AML2 cells**. b.)** Whole cell extracts from naïve or BETi resistant OCI-AML2 cells were subjected to immunoblot analysis using antibodies specific for BCL2L1 (BCL-XL), MCL1, and BCL2. **c.)** Flow cytometric analysis of treatment of BETi naïve or BETi-R OCI-AML2 cells with vehicle, 600nM JQ1 48 hours, or 600nM JQ1 + 100nM Venetoclax 48hr vs viability by Zombie Aqua. Significance determined by 2-way anova with multiple comparisons corrections from three replicates**. d.)** ex vivo drug sensitivities, as determined by MTS assay, in Beat AML patient samples derived from the Beat AML biorepository(3), comparing responses to JQ1, Venetoclax, or JQ1 + Venetoclax combined and stratified by FAB subtype (M0-M2, undifferentiated AML; M4-M5, myelomonocytic-monocytic AML). Significance determined by two-way ANOVA. N= 11 JQ1 M0-M2, 23 M4-M5 ; N = 13 Venetoclax M0-M2, 22 M4-M5 ; N= 7 JQ1 + Venetoclax M0-M2, 15 M4-M5. **e.)** Sensitivity to venetoclax alone and, separately, JQ1 in combination with venetoclax, as determined by MTS assay in matched Beat AML patient samples stratified by FAB subtype. Lines connect individual patient samples response to single agent venetoclax (red) compared to their response to JQ1 + venetoclax (green). N= 7 M0-M2, 14 M4-M5. Significance determined by 2 way ANOVA.

As discussed previously, our data indicates that BETi selects for less differentiated clones, which correlates with increased CDK2/6 expression and was resensitized by sgRNAs targeted these genes. Thus, we tested the combination of CDK4/6i, palbociclib or abemaciclib, with JQ1, OTX-015, or CPI-203 in BETi-naïve OCI-AML2 and OCI-AML3 cells and observed strong synergy (Figure 20a). In concordance with our proposed mechanism, we found that palbociclib resistance correlates with increased monocytic markers, inverse of BETi (Figure 20b), and that forced myeloid differentiation of HL-60s drove strong resistance to palbociclib (59.45nM IC50 undifferentiated, 3766nM IC50 differentiated) (Figure 20c). In addition, AML patient samples treated with palbociclib or JQ1 + palbociclib recapitulated our findings with venetoclax, with M4/M5 FAB patient samples exhibiting resistance to single agent palbociclib treatment but enhanced sensitivity with BETi combination treatment (Figure 20d, e). Collectively, these data suggest that the synergy shown here and by others previously between BCL2i or CDK4/6i with BETi is driven by differentiation state, and that myeloid differentiation can drive resistance to CDK4/6i and BCL2i.

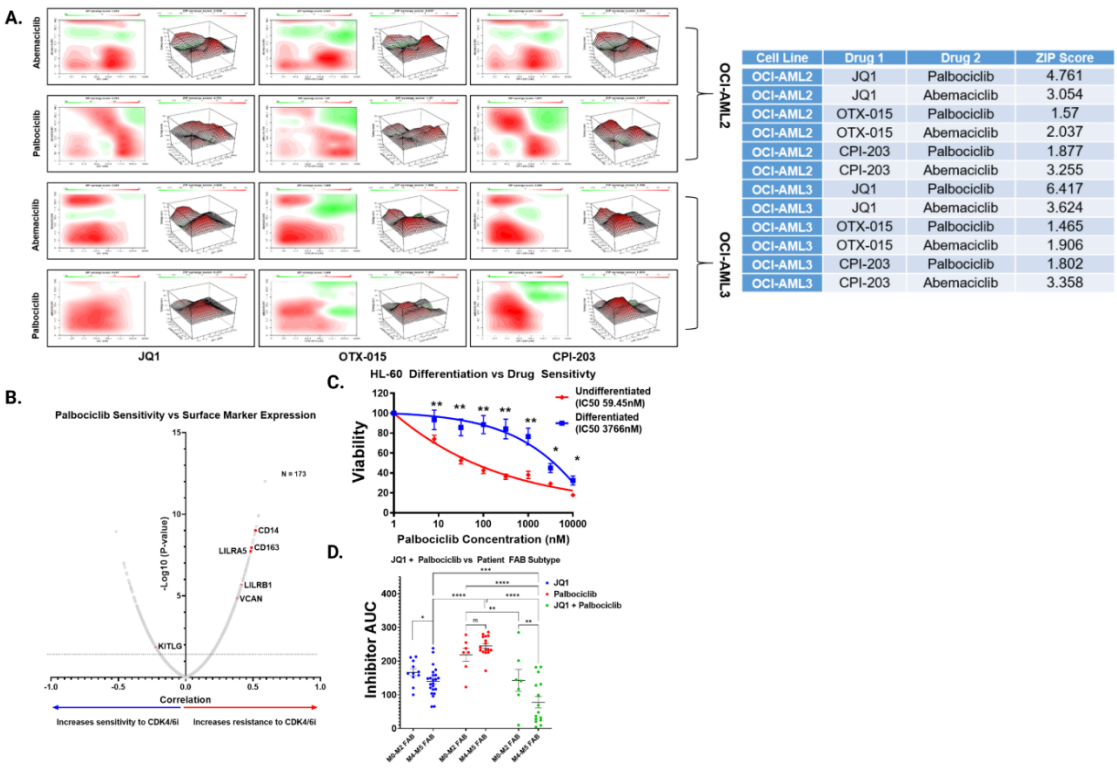

Cell Line	Drug 1	Drug 2	ZIP Score
OCI-AML2	JQ1	Palbociclib	4.761
OCI-AML2	JQ1	Abemaciclib	3.054
OCI-AML2	OTX-015	Palbociclib	1.57
OCI-AML2	OTX-015	Abemaciclib	2.037
OCI-AML2	CPI-203	Palbociclib	1.877
OCI-AML2	CPI-203	Abemaciclib	3.255
OCI-AML3	JQ1	Palbociclib	6.417
OCI-AML3	JQ1	Abemaciclib	3.624
OCI-AML3	OTX-015	Palbociclib	1.465
OCI-AML3	OTX-015	Abemaciclib	1.906
OCI-AML3	CPI-203	Palbociclib	1.802
OCI-AML3	CPI-203	Abemaciclib	3.358

Figure 20 - **a.)** ZIP Synergy plots for drug combinations, tested over a 72 hour incubation, involving a BETi (JQ1, OTX-015, or CPI-203) and a CDK4/6i (palbociclib or abemaciclib) in OCI-AML2 and OCI-AML3 cells. Summary tables of all ZIP scores given to the right. The ZIP score average was computed across the dose matrix to provide an overall index of drug interaction. A positive average ZIP score indicates the combination was synergistic (red) whereas a negative average ZIP score indicates antagonism (green). **b.)** Correlations derived from RNA expression of surface markers vs. ex vivo sensitivity to palbociclib collected in the Beat AML dataset as performed previously with BETi, figure 10a-b. Pearson correlation coefficients and associated p-values were derived from comparisons of inhibitor AUC to gene expression and corrected for multiple comparisons. Y-axis plots –log10 p-val vs X-axis Pearson correlation between palbociclib and a given surface marker's RNA expression. **c.)** Drug dose response curve, as determined by MTS-assay, for CDK4/6i palbociclib in HL-60 cells with vehicle or differentiated with ATRA for 72 hours prior to dosing with palbociclib. X-axis plots Palbociclib concentration (nM) vs Y-axis MTS-percent viability of HL-60 cells. **d.)** ex vivo drug sensitivities in Beat AML patient samples, as determined by MTS assay, comparing responses to JQ1, Palbociclib, or JQ1 + Palbociclib combined and stratified by FAB subtype. Significance determined by two-way ANOVA as performed previously with venetoclax, figure 17d.

H3K27Ac ChIP-seq stratified by FAB subtype reveal enrichment of AHR signaling and HTFs in monocytic leukemias

Finally, to determine whether undifferentiated blasts (FAB subtype: M0-M2) have differentially acetylated histone residue profiles in comparison to monocytic leukemias (FAB subtype: M4-M5), as a consequence of differential expression of the monocytic differentiation regulators (SPI1, FOS, AHR, eg.) which recruit histone modifying machinery, we analyzed H3K27Ac ChIP-seq data deposited by McKeown and Corces *et al.(154)* and called differentially acetylated regions by FAB subtype. The undifferentiated M0-M2 FAB subtype samples separated distinctly by PCA from the differentiated M4-M5 subtypes (Figure 21a). 6,076 differential affinity peaks were identified between M0-M2 and M4-M5 samples. As expected, we observed increased acetylation at monocytic surface markers such as VCAN/LILRs and most significantly increased acetylation at the canonical AHR transcriptional target CYP1B1(155,156) and its repressor AHRR, which is induced during constitutive AHR signaling(157,158) (Figure 21b). This suggests increased AHR signaling in monocytic AMLs. To further validate that enhanced AHR signaling is found in monocytic leukemias, we asked whether M4-M5 patient samples had increased expression of canonical AHR regulated genes, CYP1B1 and CDKN1A. Indeed, both were found to be significantly increased in M4-M5 AML (Figure 21c). In addition, we evaluated genes co-expressed with CYP1B1 and AHR within AML patient samples in the Beat AML database and found significant positive correlations with monocytic surface markers, hematopoietic transcription factors previously identified within the Beat AML database, and BETi-naïve whole-genome CRISPR screens as well as negative correlations with CDKs and BCL2 (Figure 22a, b). In conclusion, these data show that monocytic AML patient samples have increased binding at BRD4 targets as well as AHR. Further, we show that AHR signaling is enhanced in monocytic leukemias,

validating our findings in the initial whole-genome CRISPR screens and subsequent validation with AHR agonists and antagonists.

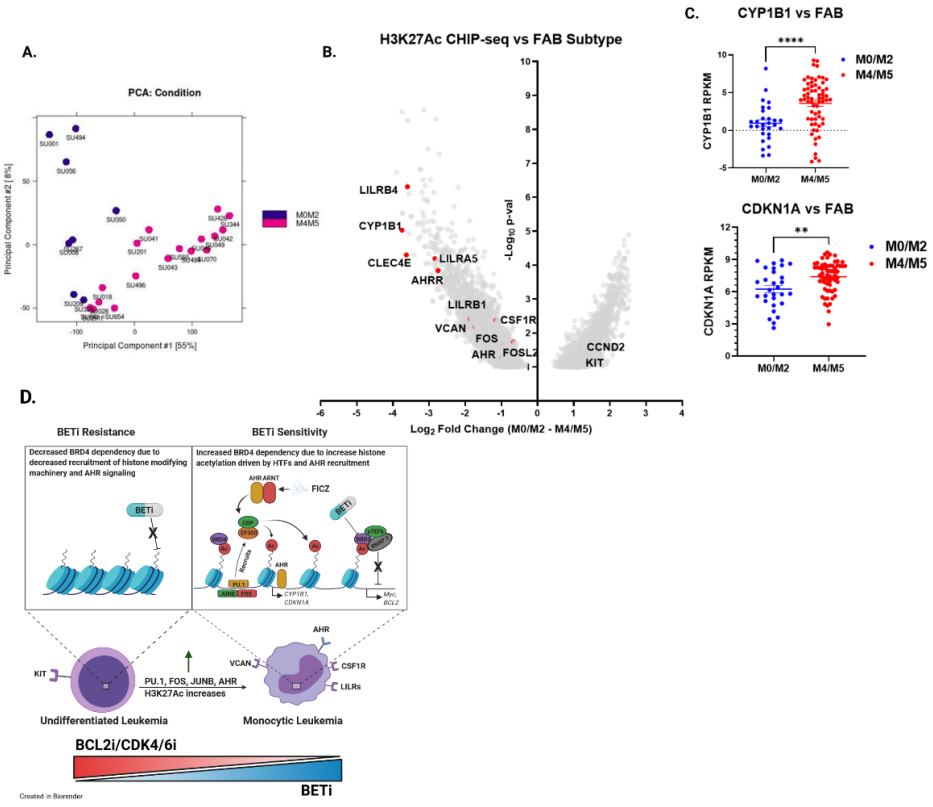

Figure 21 - **a, b.)** Analysis of H3K27Ac ChIP-Seq AML samples with known FAB designations (n=8 M0-M2 FAB, 17 M4-M5). **a.)** Principal component analysis (PCA). **b.)** Volcano plots representing the 6,076 differentially H3K27-acetylated genes between the undifferentiated M0-M2 FAB subtype and M4-M5 FAB monocytic subtype. Each point represents a single gene enrichment vs –log10 p-val. **c.)** Relative expression levels (RPKM) of canonical AHR genes across FAB groups within Beat AML patient RNA-seq dataset (all samples with both RNA-seq data and FAB subtype data, 29 M0-M2 samples and 34 M4-M5 samples) **d.)** Cartoon schematic detailing findings and hypothesis. In brief, we hypothesize that BETi sensitivity and resistance is governed by leukemic differentiation state. Monocytic AMLs have higher expression of transcription factors (SPI1, FOS, JUNB, etc.) and increased AHR signaling which recruit histone acetylation machinery to acetylate histone residues which BRD4 binds to mediate downstream affects. Thus monocytic AMLs have more targetable sites for BETi, and increased sensitivity. Conversely, BCL2i/CDK4/6i are more efficacious in undifferentiated leukemias, which characteristically have higher expression of these genes, and the combination with BETi may help overcome drug resistance development as a consequence of altered maturation state.

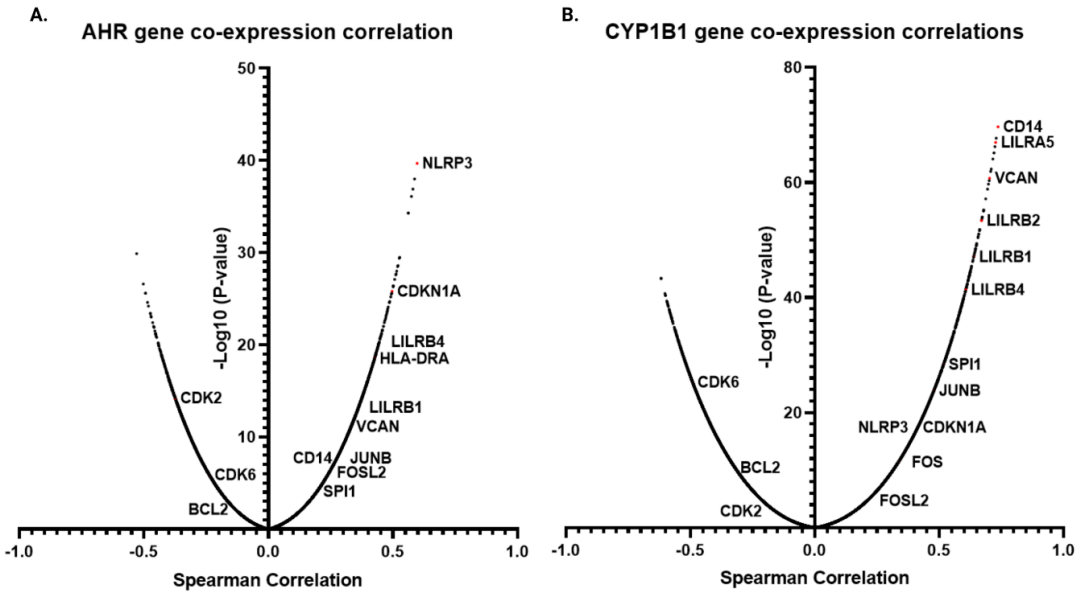

Figure 22 - a,b.) Volcano plot showing spearman correlations of genes co-expressed with AHR (left) and CYP1B1 (right) in AML patient samples within the Beat AML biorepository. Spearman correlations and corresponding p-values derived from cBioPortal analyses of the Beat AML biorepository (https://www.cbioportal.org/).

Discussion

BETi have shown clinical promise in a small subset of patients but most are intrinsically resistant to BET inhibition as a monotherapy(77), which is consistent with Beat AML biorepository data, with 48 of 287 (17%) patients exhibiting *ex vivo* sensitivity (<100 nM IC50, average 886nM) to BETi JQ1(20). While we found no association of BETi sensitivity with known mutations, our data correlates dependency of intrinsic resistance to BETi on leukemic differentiation state. Our study indicates that primary patient samples with higher expression of genes associated with a more differentiated, monocytic phenotype exhibit enhanced sensitivity to BETi, and reveals a potential therapeutic strategy for monocytic leukemias.

Consistent with primary patient sample BETi sensitivities, our CRISPR BETi resistance screen for identified SPI1, FOS, JUNB, and AHR – genes with high expression in monocytic leukemias and play a critical role in transcribing monocyte/macrophage-differentiation genes(159-162). Our CRISPR resensitization screen of BETi-R cells revealed CDK4/6, BCL2 and NPM1, as top hits in re-sensitizing to BETi. Thus, our study identified both resistance and re-sensitization components of BETi sensitivities, tethered to blast differentiation state. Loss of function of genes, expression-enriched in monocytic AML, such as hematopoietic TFs SPI1, FOS, and JUNB, as well AHR signaling is revealed as a primary driver of resistance to BET inhibition, while inactivation of genes that are expression-enriched in primitive AML, such as CDK6, NPM1, and BCL2 re-sensitizes resistant cells to BETi inhibitors.

Dysregulation of Hematopoietic Transcription Factors in AML

Hematopoietic TFs such as SPI1 and JUNB suppress myeloid leukemias by enabling proper differentiation(163-165). Not surprisingly, mutations that cause reduced function in these TFs are frequently found in AML and generally associate with a poor

prognosis(20,166-168). Despite the large body of evidence surrounding the biology of TFs in hematological malignancies, the manner by which they can impact drug sensitivity is largely unknown.

In normal hematopoiesis, SPI1 drives monocytic differentiation by positively regulating the AP-1 TFs, JUN/FOS, and, as such, their expression highly correlates with AML-M4 and M5 subtypes(163). Interestingly, SPI1 expression in AML has demonstrated the ability to bi-directionally transition between differentiated and undifferentiated states(169), which supports the notion that leukemia cells could acquire BETi resistance by selecting for cells in a repressed SPI1 state without acquiring *de novo* mutations. Both the AP-1 complex, and AHR signaling regulates cellular proliferation by directly (indirectly for AHR, via upregulation of CDKN1A/p21) repressing Cyclin D1 and regulating expression of CDK2 and CDK4(164,170). Together these data may explain our findings that CDK4/6i and BETi synergize. We also noted increased sensitivity to BCL2i and re-sensitization to genetic knockdown in acquired BETi-resistant cells that overexpressed BCL family member proteins. Previous work has shown that sustained expression of NFkB-regulated anti-apoptotic genes occurs in SPI1 depleted AML cells (171).

Monocytic surface markers as correlates of BETi efficacy

We identified monocytic markers CSF1R, VCAN, LILRA1, as strongly correlating with BETi sensitivity in AML patient samples. Of particular interest is CSF1R, as there are highly-specific flow cytometry antibodies, which could be integrated into clinical immunophenotyping panels. CSF1R is a surface receptor that binds CSF1 or IL34 to promote proliferation, survival, and differentiation of monocytes and macrophages. Upon activation, CSF1R activates proliferation and survival pathways which upregulates the SPI1(172). VCAN is an extracellular matrix proteoglycan expressed across many human

tissues. It increases activation and adhesion of monocytes through interactions with CD44. Interestingly, monocytes highly upregulate VCAN, allowing a stronger self-promoting response to inflammation(173-175). LILRs are highly expressed in monocytes/macrophages, neutrophils, and B-cells and interact with HLA class I molecules with have both activating or inhibitory functions(176). Together, our findings suggest a possibility of predicting BETi sensitivity based on CSF1R/VCAN/LILR expression and further suggest the impetus for investigating efficacy of combining CSF1R and BET inhibitors in monocytic leukemias.

Combined BETi resistant and BETi naïve genome-wide screening to identify novel combinatorial treatment strategies to overcome BETi resistance

Our study highlights the power of performing genome-wide CRISPR drug screens on both treatment naïve and treatment resistant AML cells to identify rational combinatorial treatment strategies to overcome resistance. We identified in both settings that targeting BCL2 or CDK4/6 may sensitize BETi-resistant AML cells. Several groups have published *in vitro* and *in vivo* efficacy of targeting BCL2 in combination with BETi, lending credence to these approaches(148,177-180). However, we believe we are first to rationally describe this phenomenon in the context of differentiation state and highlight a novel therapeutic vulnerability in differentiated AMLs. In addition, we describe a novel role for AHR signaling in mediating BETi response in AML and as a measure of leukemic differentiation state, a topic of which we will be exploring further. Further, *in silico* predictions based on the Beat AML dataset identified BETi and CDK4/6i as a synergistic combination strategy, indicating a potentially viable combination strategy for both treatment-naïve and BETi resistant settings(181,182). Future studies will investigate unreported combination strategies identified in the screens, such as AHR agonists with BETi.

BETi vulnerability as a consequence of leukemic differentiation state

Hematopoietic differentiation is accompanied by large changes to the chromatin landscape and requires histone acetyltransferases (HATs), methyltransferases, and others(4,183). Monocytic differentiation in particular is associated with stark increases in histone acetylation and chromatin accessibility at hematopoietic TF binding sites(184). Hematopoietic TFs recruit BRD4 by directly stimulating activity of HATs, such as EP300, which is corroborated by studies demonstrating that EP300 inhibition phenocopies BRD4 inhibition(51,69,134,147). In this context BRD4 acts as a cofactor for hematopoietic TFs, offering a likely explanation of increased sensitivity to BETi in hematological malignancies.

Our findings suggest that BETi resistance is driven by differentiation state as a consequence of evolving histone acetylation status. This is consistent with studies demonstrating WNT-driven transcriptional plasticity as a driver for BETi resistance in AML(136,139). Further, Sheng *et al.* have recently described a mechanism for WNT signaling blocking monocytic differentiation through inhibition of SPI1(185). Intriguingly, studies also have shown that AHR activation induces SPI1 production and monocytic markers in human AML(153,186). Thus, we propose a unified mechanism of resistance involving decreased expression of hematopoietic TFs as a consequence of differentiation state, which can be driven by loss of WNT signaling, that consequently decreases BRD4 dependence and BETi sensitivity. Differentiated leukemia cells upregulate hematopoietic TFs, which recruit histone modifying machinery and serve to attract BRD4 to target sites, resulting in increased BETi sensitivity (Figure 19d). Conversely, less differentiated cells have lower expression of these TFs, thus, having reduced BRD4 recruitment and, subsequently, reduced sensitivity to a BETi. Further complexity to the proposed mechanisms could result from transient and often unpredictable nature of differentiation/epigenetic dysregulation in leukemia, driven by

differences in patient specific mutations. These are important topics for investigation moving forward. However, we believe these data support more targeted clinical exploration of BETi in AML, such as an emphasis on recruiting M4-M5 FAB subtypes or patients with high expression of CSF1R. In addition, our findings provide further mechanistic rationale to a potentially effective drug combination strategies bridging compounds targeting more undifferentiated AML cells (e.g. BCL2i or CDK4/6i) with therapies that are more effective against AML cells further differentiated along the monocytic lineage (e.g. BETi). This strategy may mitigate relapse due to changed maturation state of the tumor.

Methods

Cell Lines

OCI-AML2 (DSMZ Cat# AC-99, RRID: CVCL_1619), OCI-AML3 (DSMZ Cat# AC-582, RRID: CVCL_1844), and HL-60 (CLS Cat# 300209/p671_HL-60, RRID: CVCL_0002) were obtained from ATCC. Cell lines were authenticated using the Oregon Health & Science DNA Serviced Core Facility and tested bi-weekly for *Mycoplasma*. All cell lines were maintained in RPMI, 20% FBS, L-Glutamine, penicillin/streptomycin, amphotericin-B, and normocin. BETi-R cells were generated by incubating OCI-AML2s at respective JQ1 IC90 or CPI-0610 IC90 concentration twice weekly and viability monitored 3 times per week by guava easyCyte. Once viability returned to ~80% their sensitivity was re-measured and incubated at their increased IC90 concentration. This was repeated until a 5x IC50 increase was achieved. Cells were maintained resistant by treating with 800nM JQ1 or 800nM CPI-0610 weekly.

CRISPR/Cas9 library screen and CRISPR/Cas9 gene inactivation by individual sgRNA

Cas9-expressing cells were generated using Cas9Blst (Addgene, #52962). Loss-of-function screens were performed as described[9], using a human genome-wide sgRNA

library(187), purchased form Addgene (#67989). High titer lentivirus was generated using calcium phosphate precipitation procedures in HEK293T cells (NCBI Cat# C498, RRID: CVCL_0063). Viral supernatant was concentrated and tittered using viral titration kit (ABMgood, Canada). $100e^6$ cells were used for viral transduction at MOI 0.3, selected with puromycin for 5-7 days. Cells were screened with 200nM JQ1, or 500nM CPI-0610, or DMSO. DNA was harvested after puromycin selection day 14 (JQ1) and day 21(CPI-0610). PCR-amplified barcode libraries were generated as previously described(187), and deep sequenced using Illumina platform.

Single sgRNA knockouts

Single sgRNA sequences were designed using Synthego design tool (https://design.synthego.com/#/) and converted into DNA sequences (Supplementary Table 2). Individual sgRNAs were cloned into plentiCRISPRV2 (Addgene, #52961, RRID: Addgene_127644). Phosphorylated complementary oligonucleotides were annealed and ligated into *BsmbI*-digested pLentiCRISPRV2 backbone which contains sequences for Cas9 and puromycin resistance, then validated by Sanger sequencing. Lipofectamine-2000 (Invitrogen, #11668019) was used to transfect HEK 293T cells with single transfer vectors with packaging plasmids, psPax2 (Addgene, #12260, RRID: Addgene_12260) and VSVG (Invitrogen) to generate virus. Viral supernatants were collected, filtered through 0.45 uM filters and used for transduction of AML cells using spinoculation method as described(187). Cells were selected with 2 ug/mL of puromycin for 5-7 days and outgrown for 14 days in culture before testing for BETi resistance.

Biostatistical Analysis of CRISPR Screens

Pipeline for executing analyses of CRISPR libraries sequences were performed using modified Mageck analyses. Adaptor sequences were removed using cutadapt and reads were aligned to the K.Yusa library using bowtie2 (RRID: SCR_016368). Sequences that aligned to more than 1 region were discarded. An overall alignment rate of 92% was

achieved. The overall set of sgRNAs were first filtered to remove any that had zero reads in all samples or in the plasmid. For each contrast, sgRNAs that did not achieve 100 reads (adjusting for library size) in at least half the samples were also removed. Significance of each sgRNA was determined via edgeR (RRID: SCR_012802) after TMM(188) normalization for the following contrasts: JQ1 screen at day 14 to DMSO screen at day 14, and CPI-0610 screen at day 21 to DMSO screen day 21. Sequencing data is deposited at GEO (GSE159689). Hits were prioritized according to previously described tiering structure(145). Briefly, considering only significant sgRNAs (FDR < .05), genes were classified into 5 ordered groups. Tier 1 genes had more than one significant sgRNA, a minimum log 2-fold change >= 2, 75% of sgRNAs per gene present and concordance among sgRNAs per gene >= 75%; Tier 2 hits had log 2-fold change >= 2 and 100 % concordance among sgRNAs per gene Tier 3 hits had log 2-fold change >= 1 and 100% concordance among sgRNAs per gene. Singleton hits represent significantly enriched genes with log 2 -fold change >= 2 but only a single significant sgRNA. Enriched hits not satisfying these criteria were classified into the Unassigned group.

Biostatistical Analysis of H3K27Ac ChIP-seq dataset

Processing was performed using ENCODE's protocol for unreplicated H3K27Ac ChIP-seq experiments. Differential binding was determined using DIffBind (RRID: SCR_012918) from Bioconductor (RRID: SCR_006442)(189). The Annotatr Package from Bioconductor (RRID: SCR_006442) was then used to annotate regions 1-5kb from gene(190). Volcano plots were generated by plotting $-\log_{10}$ transformed p-val and $\log_2$ transformed fold changes (M0-M2 – M4-M5).

Drug Viability Testing and ZIP Synergy Scores

Drug viability testing was performed as previously described(20,181) using MTS based assays. Absorbance values were normalized to a kill control (10uM FSV) and

media/cells only. AML cells were plated for 72hr in replicates of 6 at 1250 cells/well in R20 and titrated using a log scale (0 – 10uM) against JQ1 and CPI-0610. Viability of the cells was measured using a Guava easyCyte prior to plating to ensure >90% viability. P-values for individual sgRNAs vs non-targeting were calculated using a two-stage linear step-up procedure of Benjamini-Krieger-Yekutieli. Combinations of CPI-0610 with CH-223191 or FICZ were tested for efficacy using the MTS assay and a matrix dose layout wherein each drug/ligand in the combination was titrated over 8 concentrations. Dose-specific normalized cell viability percentages were averaged across replicates and ZIP (Zero Interaction Potency) synergy scores were calculated as previously described(191,192) using the 'synergyfinder' R package.

Beat AML Patient Sample Surface Marker Analyses

A simple linear regression model was fit separately for each inhibitor and gene with the inhibitor AUC values as the outcome. The T-statistic and P-value tests whether the slope is non-zero and corrected for multiple comparisons. Corresponding correlation coefficients were computed using the relationship to the linear model: slope*(sd(expr)/sd(auc)) where sd indicates standard deviation. Log_2 RPKM values are available in Tyner *et al.* 2018(20).

HL-60 Differentiation Assays and Drug Sensitivity

In triplicate, 250,000 HL-60 cells (>95% Viability) were plated in a 6 well dish in 3 mL R20 and treated with either vehicle (100% EtOH) 300nM JQ1, 1 uM ATRA (Sigma, #R2625) suspended in 100% EtOH, or 1uM ATRA and 300nM BETi. After 72 hours cells were resuspended in fresh R20.A portion of the vehicle and and ATRA alone treated cells were taken and assessed for BETi sensitivity by MTS as previously described. The rest of the vehicle, BETi alone, ATRA alone, or BETi + ATRA cells were stained for viability and differentiation marker CD38 as described below.

HL-60 Morphological Assessment

HL-60 cells were subjected to vehicle, 300nM JQ1, 1uM ATRA, or 300nM JQ1 + 1uM ATRA for 72 hours as described previously for flow cytometric assessment. Cells were then spun onto glass slides via Cytospin (800rpm/3min), fixed in methanol, and stained with 1:20 Giemsa (Sigma-Aldrich) for 20 minutes prior to brightfield imaging (Leica).

Doxycycline-inducible SPI1 expressing HL-60s

Lipofectamine 2000 was used to transfect HEK 293T cells with pINDUCER21-SPI1 (Addgene #97039), packaging plasmids, psPax2 (Addgene, #12260, RRID: Addgene_12260) and VSVG (Invitrogen) to generate virus. Viral supernatants were collected, filtered through 0.45 uM filters and used for transduction of AML cells using spinoculation method as described(187). GFP+ HL-60 cells were then sorted via FACSARIAIII.

HL-60s were then induced with vehicle control or 1ug/mL doxycycline for 5 days, washed with media, and then tested for BETi sensitivity using MTS assay as previously described. A portion of cells were taken for western blotting prior to plating for MTS.

Flow Cytometry Staining

500K OCI-AML2 parental, JQ1-R, or CPI-R cells were treated with BETi, BETi combined with Venetoclax, or left untreated and washed in PBS and resuspended in 100 uL PBS. 1 uL ZombieAqua (Biolegend, #423101) was added to the cells and incubated for 15 minutes at room temperature, in the dark. Cells were then washed with FACS buffer (PBS, 2% bovine calf serum 0.005% sodium azide) and resuspended in 20uL/sample 1:50 Human Fc block (Biolegend, #422302) in FACS buffer and incubated for 5 minutes on ice. Without washing, a 20 uL/ sample cocktail in FACS buffer of 1:20 human antibodies, which include anti-CD33 BV711 (Biolegend, #303424, RRID: AB_2565775), 1:20 human anti-c-kit (Biolegend, #313228, RRID: AB_2566215), and 1:20 anti-CD38 A647 (Biolegend, #303514, RRID: AB_493090) for a final staining concentration of 1:100

Fc block and 1:40 antibodies, was added. The cells were then incubated in the dark, on ice, for 30 minutes, at which point they were washed, fixed for 20 minutes in PFA, and resuspended in FACS buffer prior to running on a BD Fortessa. Data were analyzed using FloJo Software.

Western Blotting

Briefly, lysates were generated using Cell Lysis Buffer (CST #9803S), 1mM complete mini protease inhibitor (Roche), 1mM Phosphatase Inhibitor (Sigma) and 1mM PMSF. Protein concentration was quantified and normalized via BCA. Lysates were given a solution of 6% SDS, 150mM Tris (pH 6.8), 30% Glycerol, .1% bromophenol Blue, and BME were added to the samples and boiled at 95^0 C for 5 minutes before gel separation. Proteins were transferred to a PVDF membrane using an iblot2 dry transfer system, blocked with BSA, and incubated with 1:1000 in TBST primary antibody overnight at 4C. The membrane was then washed with TBST before incubation in appropriate HRP-conjugated secondary for 3 hours and activated for imaging. Antibodies used: BCL2 (CST #4223S), JUNB(CST #3746S), Tubulin(CST #2146S), PU.1(CST #2258S), MCL-1 (CST# 94269S), BCL-XL (CST# 2764S).

Statistical Analyses

Specific statistical analyses described in figure legends. In all figures, “ns” denotes not significant (P>.05), and *, **, ***, **** correspond to P<.05, P<.01, P<.001, P<.0001, respectively.

Chapter 3

BET inhibitors synergize with anti-PD1 by rescuing TCF1$^+$ progenitor exhausted CD8$^+$ T cells in Acute Myeloid Leukemia

Adapted from Romine *et al.* 2021. bioRxiv. DOI: 10.1101/2021.08.04.455147

Abstract

Many acute myeloid leukemia (AML) patients exhibit hallmarks of immune exhaustion, such as increased myeloid derived suppressor cells (MDSCs), suppressive regulatory T cells (Tregs) and dysfunctional T cells. Similarly, our mouse model of AML driven by *Flt3-ITD and Tet2* deficiency displays these immune-related features, including CD8$^+$ T cells exhibiting a terminally exhausted phenotype (TEx). This T cell subset has been shown to be refractory to immune checkpoint blockade (ICB) monotherapy. Here we show that small molecule inhibitors which target bromodomain and extra-terminal domain (BET) proteins affect both tumor-intrinsic factors but also rescue T cell exhaustion and ICB resistance. *Ex vivo* treatment of cells from AML mice and AML patients with BET inhibitors (BETi) reversed CD8$^+$ T cell exhaustion by restoring proliferative capacity and expansion of the more functional precursor exhausted T cells (TPEx). This reversal is enhanced by combined BETi and anti-PD1 treatment. We show that BETi synergizes with anti-PD1 *in vivo*, resulting in the reduction of circulating leukemia cells, enrichment of CD8$^+$ T cells in the bone marrow, and increased expression of *Tcf7*, *Slamf6,* and *Cxcr5* in CD8$^+$ T cells. Finally, we profiled the epigenomes of *in vivo* JQ1 treated AML-derived CD8$^+$ T cells by single-cell ATAC seq and find that JQ1 increases *Tcf7* accessibility specifically in Tex cells, suggesting that

BETi likely mechanistically acts by reprogramming Tex cells to a more functional TCF1 expressing subtype.

Introduction

Acute myeloid leukemia (AML) is a genetically heterogeneous myeloid lineage cancer with a 5-year survival of 29% and with limited therapeutic options for those who cannot withstand current frontline therapies(17,19,131). The most common mutation, which encompasses 30% of AML patients and is associated with an exceptionally poor prognosis, is an internal tandem duplication in the FLT3 receptor (FLT3-ITD), which leads to ligand-independent signaling to many proliferation pathways. FLT3-ITD is commonly mutated with epigenetic regulators such as those involved in DNA methylation like DNMT3a and TET2(20). For other difficult-to-treat cancers, such as metastatic melanoma, therapy with immune checkpoint blockade (ICB) has made meaningful increases in life expectancy(123,124). ICB functions to reinvigorate cancer-specific T cells via blockade of inhibitory immune checkpoint (IC) receptors which suppress T cell activity and function. Expression of IC receptors, which include CTLA-4, PD1, TIM3, LAG3, TIGIT, VISTA and others, increases after initial antigen exposure and regulates T cell function through various signaling pathways. It has been hypothesized that these receptors are an evolutionary adaptation to chronic antigen exposure to prevent the development of autoimmunity after infection. Recent work has identified unique subsets of $CD8^+$ T cells that are generated specifically during chronic antigen exposure. Terminally exhausted T cells (TEx) have been shown to express high levels of IC receptors such as PD1 and TIM3 and low TCF1, while progenitor exhausted T cells (TPEx) are $PD1^+$, $TIM3^-$ and display high expression of TCF1 and SLAMF6. Importantly, the TPEx population has specifically been shown to expand in response to anti-PD1 therapy and retain anti-tumor capacity(86,87,90,125,126). In contrast, TEx are

significantly more dysfunctional with a lack of proliferative capacity and dramatically reduced secretion of effector molecules, such as granzyme B and perforin(87,89-92,95,125). Our lab and others have recently shown that a proportion of blood and bone marrow specimens from AML patients have an immunosuppressive microenvironment and have hallmarks of immune exhaustion: increased frequencies of regulatory T cells (Tregs)(193) and myeloid-derived suppressor cells (MDSCs)(194), decreased T-cell proliferation(195), elevated expression of immune checkpoint molecules(196-198) and increased TEx vs. TPEx(128,198) populations. Importantly, a subset of these patient samples containing dysfunctional T cells can be rescued by ICB(195). This prompted us to further investigate potential combination treatment regimens by which immune exhaustion could be reduced in AML.

The Bromodomain and Extra-Terminal domain (BET) protein family is made up of bromodomain-containing proteins BRD2, BRD3, BRD4, and BRDT(69,74,133,134,199). BET proteins are epigenetic readers which bind acetylated histone residues via conserved BD1 and BD2 domains and mediate downstream functions, such as histone acetylation recognition, chromatin remodeling, and transcription regulation. BRD4 binds acetylated histone tails and recruits Positive Transcription Elongation Factor b (P-TEFb) to enhancer regions to mediate the phosphorylation of the c-terminal domain of RNA polymerase II, required for elongation of the mRNA strand(133,200). Loss of function RNAi screening studies identified BRD4 loss as a potent and selective inhibitor of leukemic growth, and treatment with BET inhibitor (BETi) induced leukemia cell death *in vitro* and *in vivo*(69,71,74,76,134,201,202). Clinically, however, BETi therapy was able to elicit some complete remissions but only in a small subset of patients(82). Interestingly, BETi have also been shown to positively affect $CD8^+$ T cells, directly or indirectly, via reduction of PD-L1 expression on myeloid cells(203,204) and inhibition of chronic TCR activation genes, such as basic leucine zipper transcription factor, ATF-like (*Batf*), which

increased the persistence of stem-cell like memory $CD8^+$ T cells(205). Therefore, we hypothesized that BETi may synergize with anti-PD1 therapy in AML through targeting of tumor-intrinsic factors, such as *myc*, and tumor-extrinsic factors, such as promoting T cell stemness. Accordingly, we showed that a *Flt3-ITD/Tet2* AML mouse model, similar to the previously described *Vav-Cre Flt3-ITD/Tet2* model(206), phenocopies the immune exhaustion and PD-1 refractoriness found in many patients with AML. We found that these mice have a dramatically increased ratio of TEx:TPEx compared to wild-type (WT) mice and that BETi can rescue immune exhaustion by promoting proliferation of TPEx $CD8^+$ T cells and reprogramming Tex cells. BETi treatment was found to have a synergistic effect with anti-PD1 *in vivo* and *ex vivo* by reducing leukemic tumor burden and increased RNA expression of TPEx gene programs while decreasing that of TEx. In addition to the mouse model, we observed that BETi rescued T cell exhaustion in a subset of primary AML patient samples. Finally, we characterized the chromatin landscape of T cells treated *in vivo* with BETi by S3-ATAC-seq and found that BETi-treated Tex had greater *Tcf7* accessibility compared to vehicle treated throughout TPEx to TEx differentiation.

Results

Flt3-ITD/Tet2 *Mice Exhibit hallmarks of immune exhaustion.*

We previously showed that a genetically-engineered mouse model, *Flt3-ITD*$^{+/-}$ *Tet2*$^{flox/+}$ *LysM-Cre*$^{+/-}$ displays a profound defect in T cell proliferative capacity(207). To further characterize the tumor microenvironment and functional capacity of T cells in these mice, we assessed changes in myeloid and lymphoid populations at multiple organ sites. We found dramatically increased levels of $CD11b^+$ myeloid cells in the spleens and blood of AML mice compared to WT mice (Figure 23a, b). In addition, we observed significant evidence of myeloid infiltration in the spleen causing splenic follicle disruption,

and infiltration in liver portal veins and bone marrow (Figure 23c). Furthermore, we found increased levels of GR1$^+$ MDSCs and CD4$^+$FOXP3$^+$ Tregs, a frequent occurrence in AML patients(193-195,197,208)(Figure 24a, b), but no difference in T cell frequency (Figure 24c). We also identified significant increases in multiple exhaustion markers in both the CD4$^+$ and CD8$^+$ T cell populations but most notably a significant decrease in T cell stem-like maintenance transcription factor TCF1 (Figure 23d,e). Taken together, we concluded that these AML mice exhibited a tumor microenvironment characterized by severe immune exhaustion.

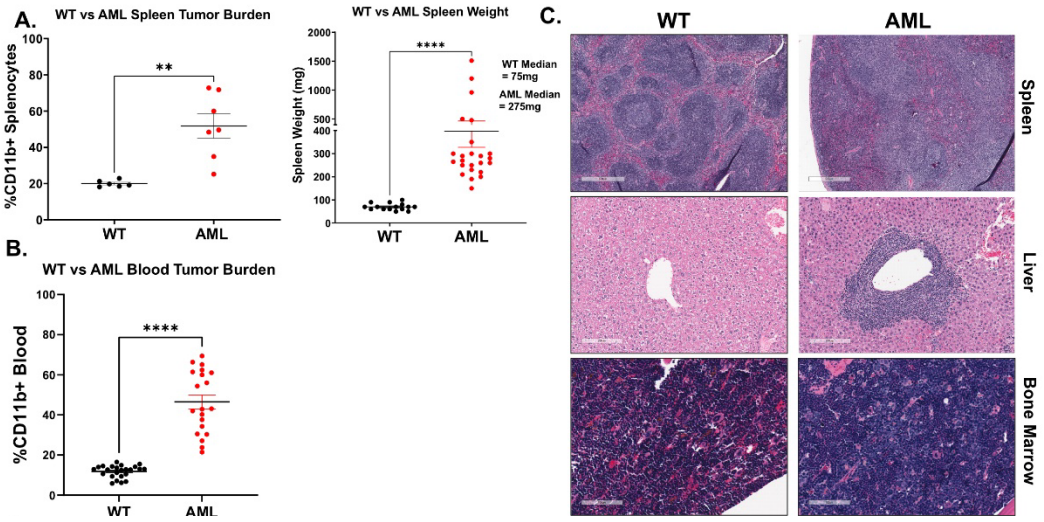

Figure 23- **a.)** Left: Splenocytes isolated from C57BL/6 (WT, black) or Flt3-ITD +/-, Tet2 +/-, Lys-Cre +/- (AML, red) mice were stained for live CD11b+ cells and evaluated by flow cytometry. Significance determined by Mann-Whitney T-test. Right: Whole spleens isolated from 15 WT (black) and 24 AML (red) mice were weighed. Median weights for each group are displayed on the right side of plot. Significance determined by Mann-Whitney T-test. **b.)** Blood isolated from 24 WT (black) and 20 AML (red) mice were stained for live CD11b+ cells and evaluated by flow cytometry. Significance determined by Mann-Whitney T-test. **c.)** Representative H&E staining of WT and AML mice-derived spleen (Top row, 500 μm scale), liver (middle row, 200 μm scale), and bone marrow (bottom row, 100 μm scale).

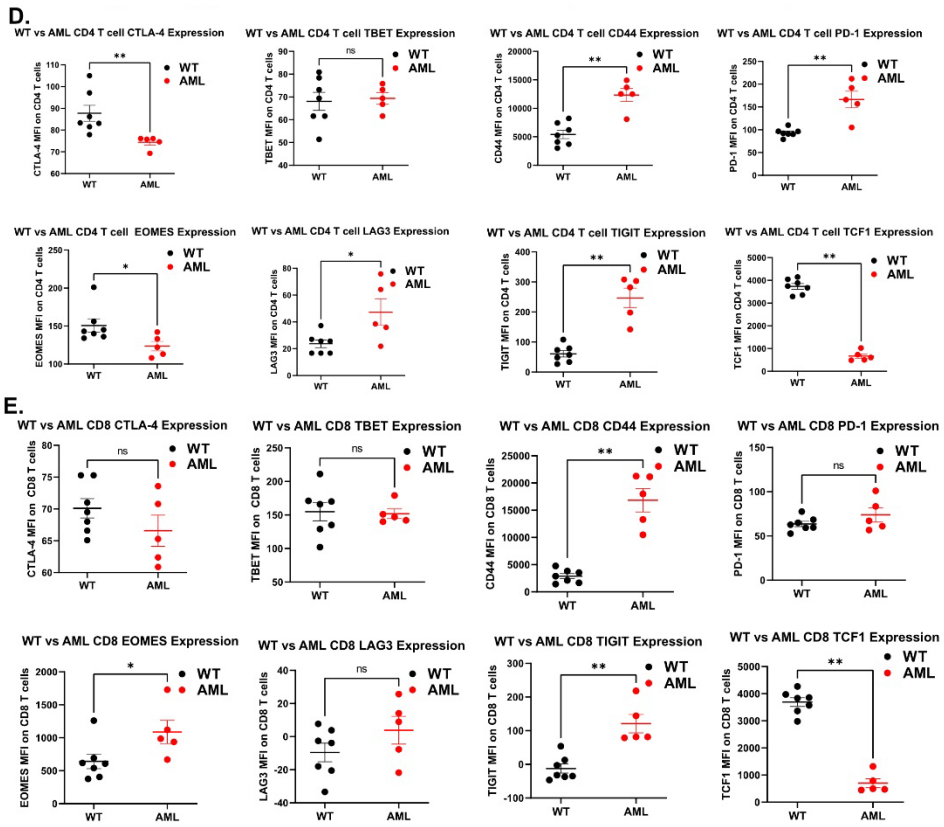

Figure 23 – **d.)** Splenocytes from untreated WT (black) and AML (red) mice were assessed for expression (median fluorescence intensity) of markers of immune exhaustion on CD4$^+$ T cells (Live, CD11b-, CD3$^+$, CD4$^+$). Top row, left to right: CTLA-4, TBET, CD44, PD-1). Bottom Row, left to right: EOMES, LAG3, TIGIT, TCF1). Significance determined by multiple Mann-Whitney T-tests. CD44, PD-1, LAG3 are significantly increased in AML mice. CTLA-4, EOMES, and TCF1 are significantly decreased in AML mice. **e.)** Splenocytes from untreated WT (black) and AML (red) mice were assessed for expression (median fluorescence intensity) of markers of immune exhaustion on CD8$^+$ T cells, as in (d). Significance determined by multiple Mann-Whitney T-tests. CD44, EOMES, and TIGIT are significantly increased in AML mice. TCF1 is significantly decreased in AML mice.

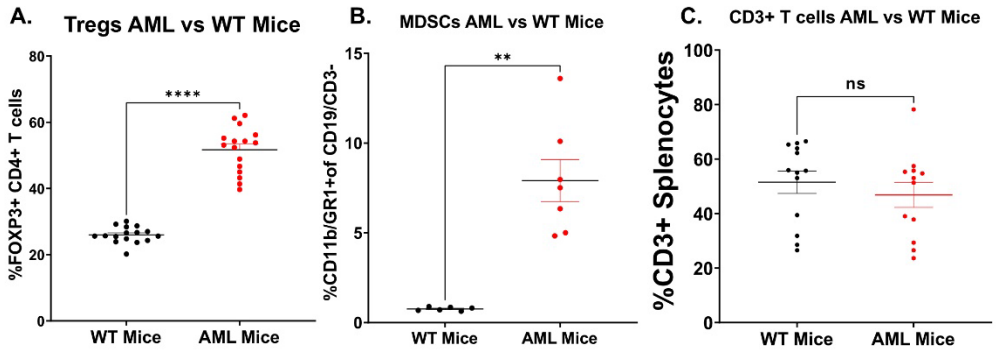

Figure 24 - Splenocytes isolated from Flt3-ITD +/-, Tet2 +/-, LysCre +/- (AML, red) or C57BL/6 (WT, black) mice were isolated and stained for 22a.) Treg cells ($CD4^+$, $FOXP3^+$), 22b.) MDSCs ($CD11b^+$, $GR1^+$) and 22c.) all T cells ($CD3^+$) and evaluated by flow cytometry. Significances determined by Mann-Whitney t-tests.

T cells derived from AML mice are phenotypically and functionally exhausted.
We previously showed that T cells from the AML mice are dysfunctional and unresponsive to TCR stimulation (207). We assessed the proliferative potential of $CD4^+$ and $CD8^+$ T cells derived from AML or WT mice by culturing whole splenocytes on anti-CD3 coated plates for 3 days, thus relying on naturally occurring antigen-presenting cells for co-stimulation. As shown previously, both $CD4^+$ and $CD8^+$ T cells derived from AML mice exhibited significantly reduced proliferation compared to WT mice in response to TCR stimulation (Figure 25a, b). We next asked whether the T cells were intrinsically dysfunctional or if the effect on proliferation occurred only when the T cells were in proximity to tumor cells. We isolated $CD3^+$ T cells by negative selection magnetic bead sorting and assessed proliferation with both anti-CD3 and anti-CD28 co-stimulation. The purified T cells from AML mice still lacked proliferative capacity compared to WT, indicating that the T cells are intrinsically dysfunctional (Figure 25c). Finally, we asked whether the AML-derived $CD8^+$ T cells were phenotypically terminally exhausted (TEx; $PD1^+$, $TIM3^+$, $TCF1^-$) or TPEx ($PD1^+$, $TCF1^+$, $TIM3^-$), the latter having been shown to retain anti-tumor activity, predict clinical outcome, and expand with ICB(106,125-127,129,209). Flow cytometric analysis of $PD1^+$ $CD8^+$ T cells derived from AML mice were primarily consistent with a TEx phenotype, in contrast to WT mice, which were primarily TPEx (Figure 25d, 25e, 26a). Thus, the AML mice generate an immunosuppressive microenvironment which supports $CD8^+$ and $CD4^+$ T cell exhaustion.

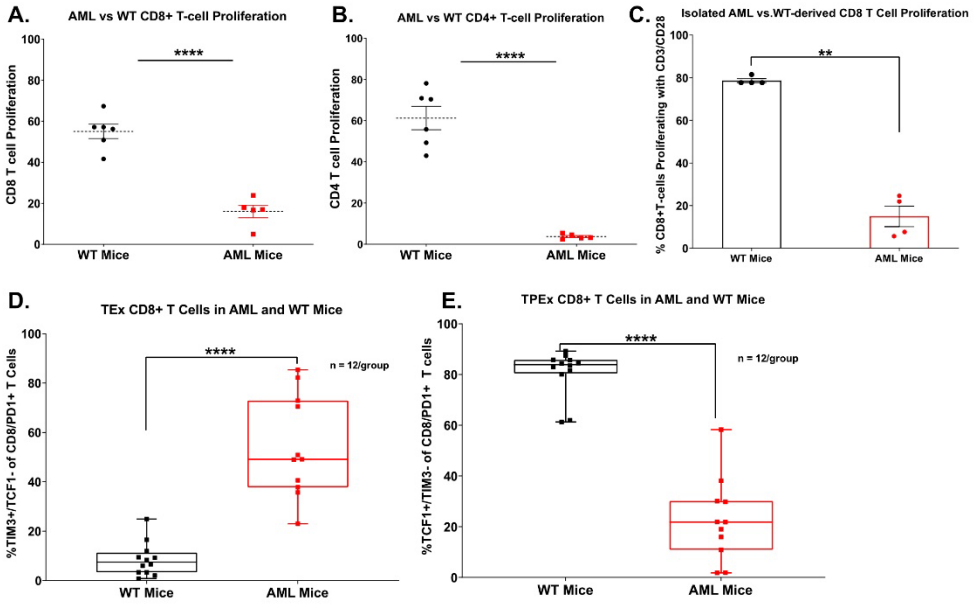

Figure 25 – **a,b.)** WT (black) and AML (red) splenocytes were isolated, stained with proliferation dye (CFSE), and cultured for 72 hours with anti-CD3. Proliferation of a.) $CD8^+$ T cells and b.) $CD4^+$ T cells was then assessed by flow cytometry, staining with viability and markers to identify T cells. Proliferation displayed is percent CFSE diluted relative to unstimulated (HIgG) control for each cell type. Significance determined by Mann-Whitney T-tests. **c.)** WT (black) and AML (red) T cells were isolated from splenocytes via CD3 negative isolation magnetic beads. The T cells were then stained with CFSE and plated for 72 hours with anti-CD3 and anti-CD28 stimulation. The cells were then harvested and assessed by flow cytometry. Significance determined by Mann-Whitney T-test. Splenocytes derived from WT (black) and AML (red) mice were stained for surface and intracellular markers of T cells exhaustion and evaluated by flow cytometry. **d.)** Terminally Exhausted CD8 T cells (TEx) are represented as $\%TIM3^+/TCF1^-$ of the $CD8^+/PD1^+$ T cells. **e.)** Progenitor Exhausted CD8 T cells (TPEx) are represented as $\%TCF1^+/TIM3^-$ of the $CD8^+/PD1^+$ T cells. Significance determined by Mann-Whitney T-tests.

Ex vivo *treatment of splenocytes from AML mice with BETi rescues T cell dysfunction*

To identify rationally-derived combination treatment strategies which target tumor-intrinsic and extrinsic factors, we performed high-capacity drug screening as previously described(20) on tumor cells cultured from the AML mice. Interestingly, we found that three of the top six most efficacious small molecule inhibitors (SMIs) targeted BET proteins (JQ1, OTX-015, CPI-0610) (Figure 27a). Given previous works by Kagoya *et al.*, Zhu *et al.*, and Hogg *et al*. which established the role for BETi in maintaining stemness of $CD8^+$ T cells via inhibition of TCR-activated transcription factor BATF(205) and that BETi reduce immunosuppressive ligand PD-L1(203,204) expression, we asked whether BETi + anti-PD1 could impact the exhausted phenotype found in T cells from our AML mice. To test whether BETi could rescue T cell dysfunction and rescue ICB therapy resistance, we performed proliferation assays as previously described with whole splenocytes and anti-CD3 stimulation but also in the presence of 60nM BETi JQ1, 120nM JQ1, 60nM JQ1 + 10ug/mL anti-PD1, 120nM JQ1 + anti-PD1, or anti-PD1 alone. As expected, treatment with anti-PD1 alone had no effect on proliferation, as the T cells were shown to be primarily terminally exhausted (Figure 25d-g). However, treatment with JQ1 at 60nM, and more so with 120nM, significantly increased proliferation of AML-derived $CD8^+$ T cells, whereas WT T cells were unaffected. Moreover, the combination of 120nM JQ1 and anti-PD1 had the largest effect, with a median three-fold increase in $CD8^+$ T cell proliferation compared to anti-CD3 stimulation alone (Figure 27b, c). The benefit of adding BETi with anti-PD1 was also observed in $CD4^+$ T cells, but was more variable between individual mice, with some mice only marginally benefitting from combined treatment while others were dramatically enhanced (Figure 26b). We next asked what phenotype characterized these newly proliferating $CD8^+$ T cells from the AML mice and found that they expressed high levels of TCF1 and low levels of TIM3, indicating that BETi mechanistically act by increasing TPEx:TEx ratios (Figure 27d-g).

Moreover, we tested the efficacy of combining BETi + anti-PD1 in five primary AML patient samples with an array of mutational backgrounds. All patient samples were displayed T cell dysfunction. Interestingly, 3/5 samples were at least partially responsive, with one sample dramatically so, to treatment with BETi or BETi + anti-PD1 in both the $CD8^+$ and $CD4^+$ T cell subsets (Figure 27h, 26c).

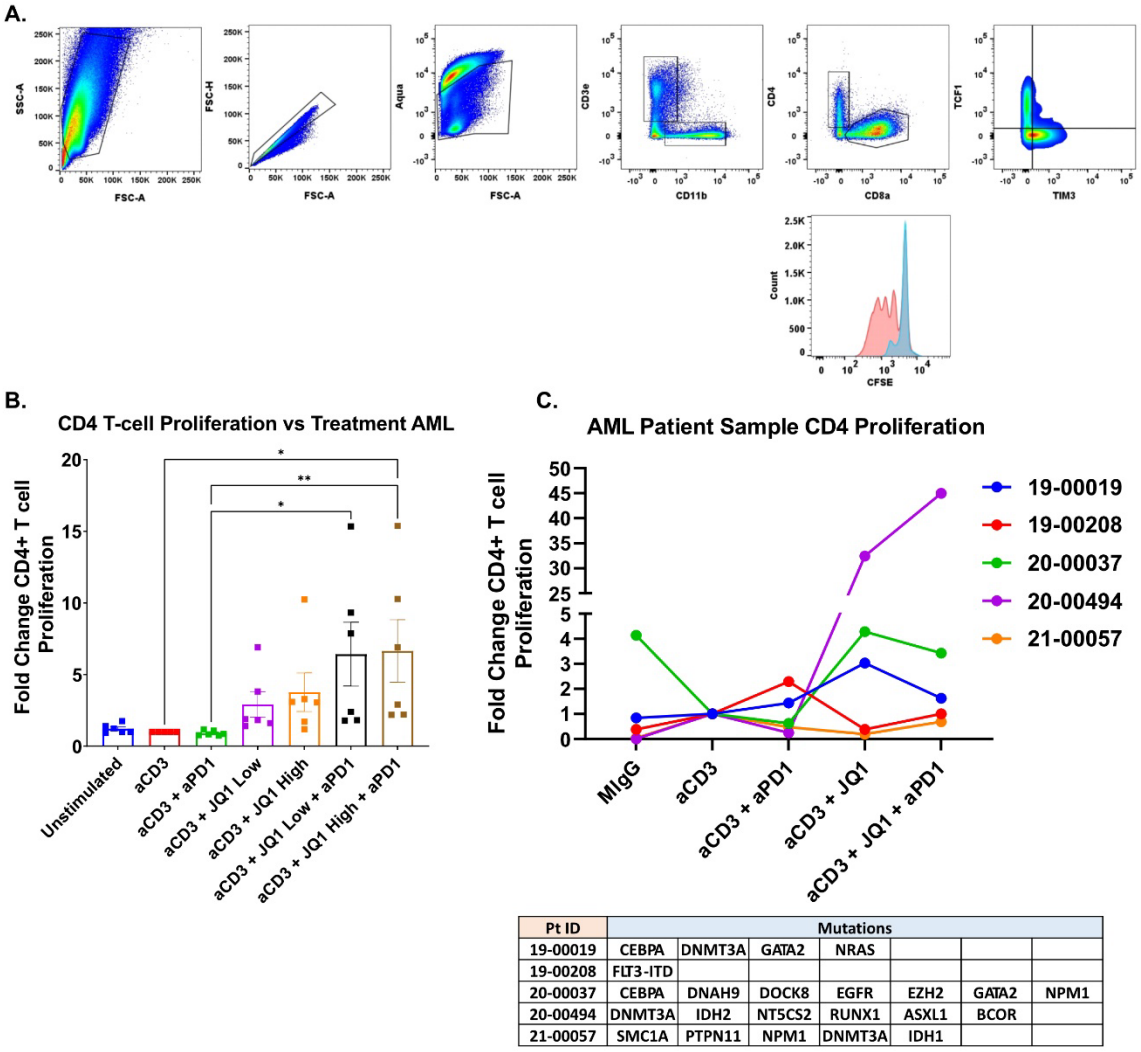

Pt ID	Mutations						
19-00019	CEBPA	DNMT3A	GATA2	NRAS			
19-00208	FLT3-ITD						
20-00037	CEBPA	DNAH9	DOCK8	EGFR	EZH2	GATA2	NPM1
20-00494	DNMT3A	IDH2	NT5CS2	RUNX1	ASXL1	BCOR	
21-00057	SMC1A	PTPN11	NPM1	DNMT3A	IDH1		

Figure 26 – **a.)** Plots below are a representative example from an AML mouse demonstrating the gating scheme used to assess T cell phenotype and proliferation. **b.)** Splenocytes were isolated from 6 AML mice were cultured for 72 hours without TCR stimulation (HIgG), anti-CD3 alone, anti-CD3 with anti-PD1 and titrations of anti-CD3 with JQ1 or anti-CD3 with both JQ1 and anti-PD1. Cells were stained for assessment by flow cytometry. Plots represent the fold-change in proliferation in CD4+ T cells, as measured by percent CFSE diluted relative to anti-CD3 stimulated alone. Significance determined by Kruskal-Wallis multiple comparisons t-tests. **c.)** Fresh mononuclear cells from bone marrow aspirates or peripheral blood obtained from 5 AML patients were stained with CTV and cultured for 5 days without TCR stimulation (mIgG), anti-CD3, anti-CD3 with anti-PD1, anti-CD3 with 120 nM JQ1, or anti-CD3 with 120 nM JQ1 plus anti-PD1. Cells were then stained for assessment by flow cytometry. Plots represent CD4+ T cell proliferation for each patient sample. Corresponding patient sample mutations listed in table below.

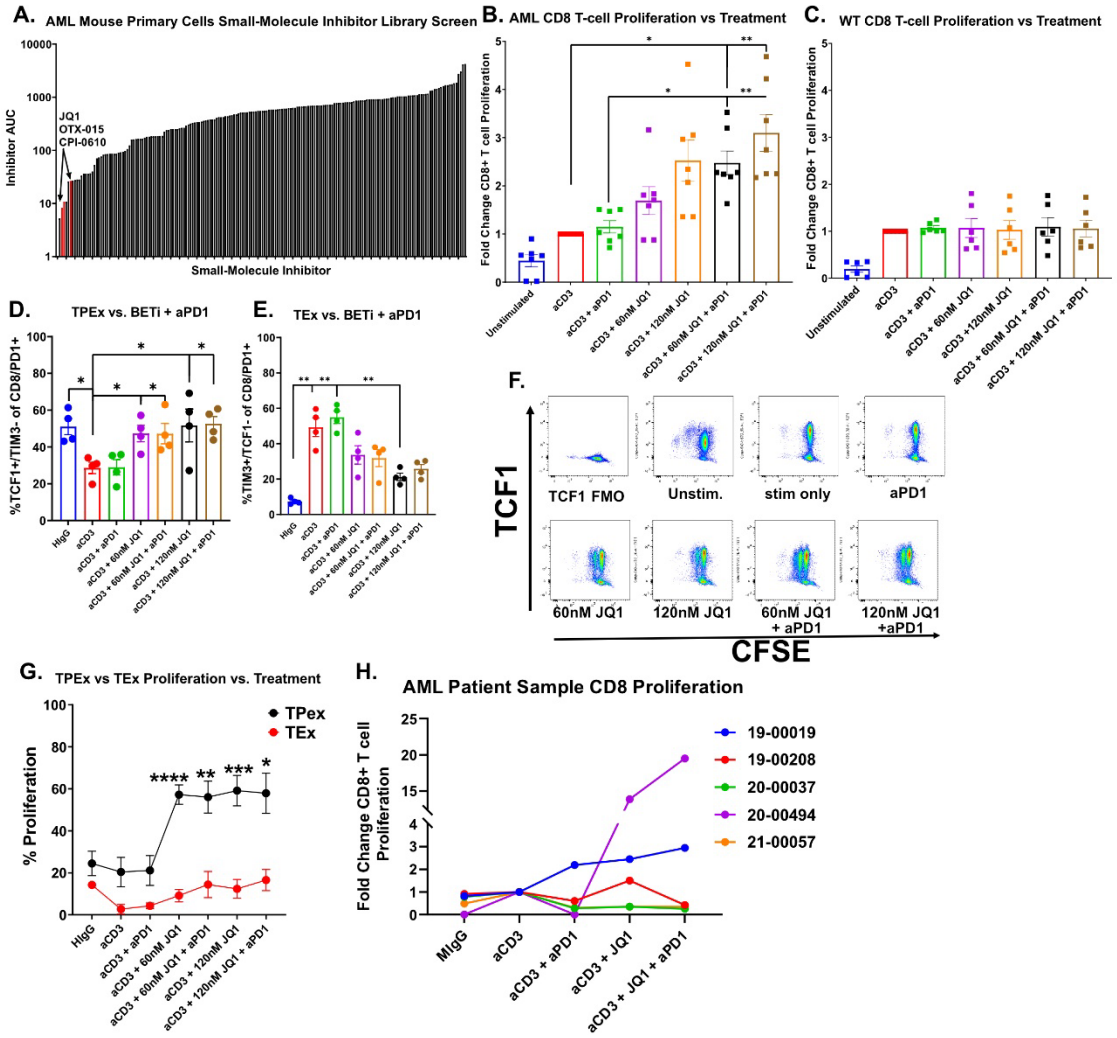

Figure 27 – **a.)** Cells from AML mice passaged for ~ 1 month were subjected to an inhibitor library panel, as previously described. Cells were seeded into multiple 384 well plates containing titrations of 188 inhibitors, incubated for 72 hours, and viability assessed by MTS assay. Plot represents each Areas Under the Curve (AUC) for every inhibitor on the panel. BET inhibitors JQ1, OTX-015, and CPI-0610 are highlighted in red. **b,c.)** Splenocytes were isolated from 7 AML (b) or 6 WT mice (c), stained with CFSE, and cultured for 72 hours without TCR stimulation (HIgG), anti-CD3 alone, anti-CD3 with anti-PD1 or titrations of anti-CD3 with JQ1 or anti-CD3 with both JQ1 and anti-PD1. Cells were stained and analyzed by flow cytometry. Plots represent the fold-change in proliferation in CD8+ T cells, as measured by percent CFSE diluted relative to anti-CD3 stimulated alone. Significance determined by Kruskal-Wallis multiple comparisons T-tests**. d,e.)** Effect of BETi, anti-PD1, or BETi + anti-PD1 treatment on the percent of TPEx CD8+ T cells (d) and TEx CD8+ T cells (e) after culturing for 72 hours as previously in b-c. Significance determined by Kruskal-Wallis multiple comparisons T-tests. **f.)** Representative dot plots of CD8+ T cells from an AML mouse treated as described in 3b,c comparing TCF1 expression vs. CFSE. **g.)** Splenocytes from 4 AML mice were stained with CFSE and plated for 72 hours without TCR stimulation (HIgG), anti-CD3 alone, anti-CD3 with anti-PD1 and titrations of anti-CD3 with JQ1 or anti-CD3 with both JQ1 and anti-PD1. Proliferation of TPEx (black) and TEx (red) CD8+ T cells from AML mice was assessed by flow cytometry. Significance determined by Kruskal-Wallis multiple comparisons t-tests. **h.)** Fresh mononuclear cells from bone marrow aspirates or peripheral blood obtained from 5 patients with AML were stained with CTV and cultured for 5 days without TCR stimulation (mIgG), anti-CD3, anti-CD3 with anti-PD1, anti-CD3 with 120 nM JQ1 or anti-CD3 with 120 nM JQ1 and anti-PD1. Cells were stained and analyzed by flow cytometry. Plots represent CD8+ T cell proliferation for each patient sample.

In vivo-*treated AML mice have reduced tumor burden and increased T cell TPEx gene program expression*

Given the results showing the effect of BETi on T cells from the AML mice *in vitro*, we sought to determine the *in vivo* therapeutic efficacy of BETi in combination with anti-PD1 and whether they also modulate the tumor immune microenvironment. AML or WT mice were treated with RIgG (8mg/kg), JQ1 (50mg/kg), anti-PD1 (8mg/kg), or combined JQ1 and anti-PD1 (50mg/kg and 8mg/kg, respectively) for 14 days. We monitored white blood cell (WBC) count in blood pre-treatment, mid-treatment, and at endpoint and characterized the tumor microenvironment (Figure 28a). Measurement of WBC counts over time by hematology analyzer found that only the combination of JQ1 + anti-PD1 significantly reduced tumor burden and, as expected from the *ex vivo* proliferation assays, anti-PD1 alone had no effect (Figure 28b). Characterization of the tumor microenvironment by flow cytometry showed no significant changes to the frequency of Treg cells, MDSCs, or splenic $CD3^+$ T cells (Figure 29a,b, 28c). However, we observed a significant increase in $CD8^+$ T cells in the bone marrow of mice in the JQ1 + anti-PD1 treatment group, suggesting that the combination has a greater impact on $CD8^+$ T cells specifically and not on other immunosuppressive cell types (Figure 28d). Finally, evaluation of RNA-transcripts in isolated $CD8^+$ T cells derived from JQ1-treated AML mice identified significantly increased expression of TPEx genes such as *Tcf7*, *Slamf6*, and *Cxcr5* (Figure 28e). Together, these results highlight the potential of combining BETi and anti-PD1 to treat immunosuppressed T cells in AML, particularly in ICB-refractory cases.

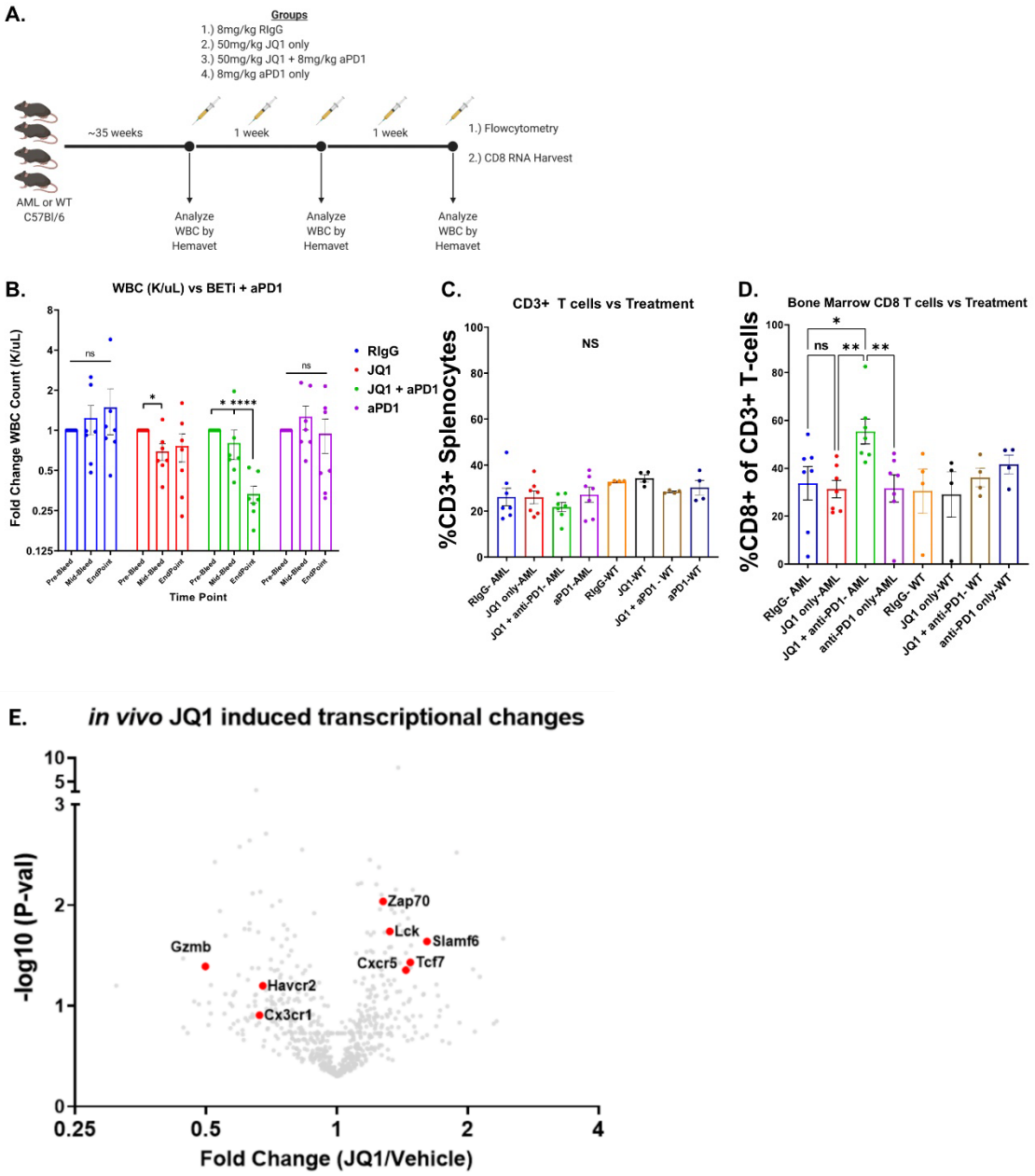

Figure 28 - **a.)** Schematic detailing in vivo BETi + anti-PD1 treatment strategy and functional readouts of efficacy. **b.)** Mice treated with RIgG, JQ1, JQ1 with anti-PD1, or anti-PD1 alone were bled periodically over a two-week period and assessed for WBC. Data displays fold-change WBC (k/μL) normalized per mouse in comparison to pre-treatment bleed WBC. Significance determined by one-way ANOVA. Timepoints are Pre-Bleed, Mid-bleed (day 7), Endpoint (day 14). **c,d.)** Bone marrow cells were isolated from treated AML and WT mice and assessed by flow cytometry. Graph denotes %CD3+ T cells in the bone marrow (c) and %CD8+ T cells in the bone marrow as a percent of all T cells (d). Significance derived from combining two experimental replicates and determined by one-way ANOVA. **e.)** CD8+ T cells were isolated from JQ1-treated and RIgG-treated AML mice and RNA harvested and analyzed by Nanostring. Volcano plot shows the fold-change in normalized transcript levels of JQ1-treated mice vs RIgG treated AML mice vs. –log10 P-value as determined by multiple t-tests. Hits of interest are highlighted in red. Dashed red line denotes significance threshold (0.05).

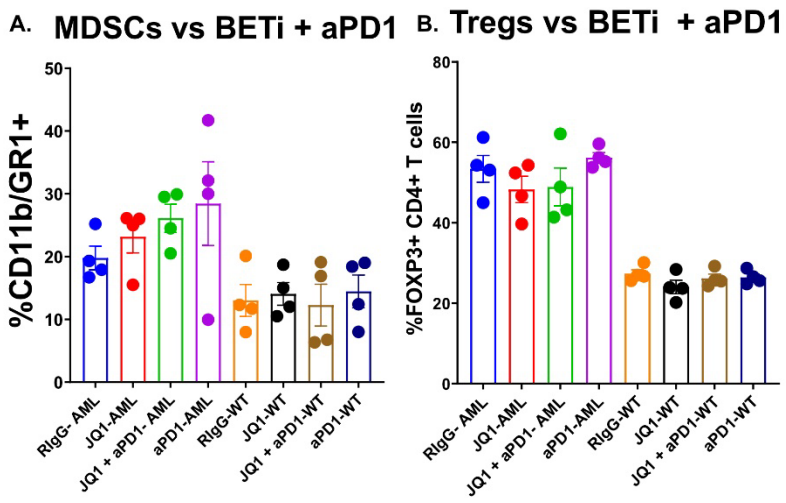

Figure 29 – **a,b.)** Splenocytes derived from AML mice treated with RIgG, JQ1, JQ1 + aPD1, or anti-PD1 were assessed by flow cytometry to determine a.) %MDSCs (CD11b+GR1+) and b.) %Tregs (CD4+FOXP3+). No significance was observed between treatments in AML or WT mice independently.

S3-ATAC-seq identifies in vivo JQ1 treated T cells have increased chromatin accessibility at the TCF7 promoter specifically in Tex cells

To ask whether BETi reprogram Tex directly or block TPex differentiation we evaluated the chromatin landscape of 5 *in vivo* JQ1 and 5 vehicle treated AML mouse T cells at a single-cell level by S3-ATAC-seq. S3-ATAC-seq is an optimized single-cell ATAC platform which provides vastly increased numbers of viable fragments via utilization of a uracil-intolerant polymerase and template oligos containing blocking uracil residues(210). We treated AML mice with vehicle or 50mg/kg JQ1 daily for 5 days before enriching spleen-derived $CD8^+$ T cells by magnetic bead sorting and sequencing via S3-ATAC. This resulted in exceptional TSS enrichment with an average TSS of 39.31 and ~4000 cells passing QC (Figure 30a-c). Using the R package ArchR we performed iterative clustering and identified 14 unique clusters of cells distributed between JQ1 and Vehicle treated splenocytes (Figure 31a-d). We next called ATAC-peaks using MACS2 and calculated gene scores for all cells and were able to easily distinguish between our cell types of interest. Cluster 4 identified Tregs as denoted by high CD4, FOXP3, and IL2RA gene scores. Clusters 5-8 were $CD8^+$ T cells with Cluster 5 making up Tex with high *Pdcd1, Tox, Lag3,* and *Havcr2* accessibility. Cluster 6 we denoted as naïve or related $CD8^+$ T cells due to their high accessibility at *Sell* and *Tcf7* with low expression of any canonical exhaustion or activation markers. Clusters 7 and 8 were assigned as TPex due to their high accessibility at *Cxcr3, Tcf7*, and intermediate accessibility at *Pdcd1* and *Sell* (Figure 32). Given our *in vivo* and *ex vivo* data demonstrating that JQ1 induces TCF1 expression in $CD8^+$ T cells, we investigated *Tcf7* accessibility through pseudotime trajectory as Naïve/Stem (C6) differentiate into TPEx (C7/C8) and finally Tex (C5). Here, we found that JQ1 treated T cells specifically enhances *Tcf7* chromatin accessibility in Tex, suggesting that BETi mechanistically act by reprogramming Tex cells (Figure 33a-e).

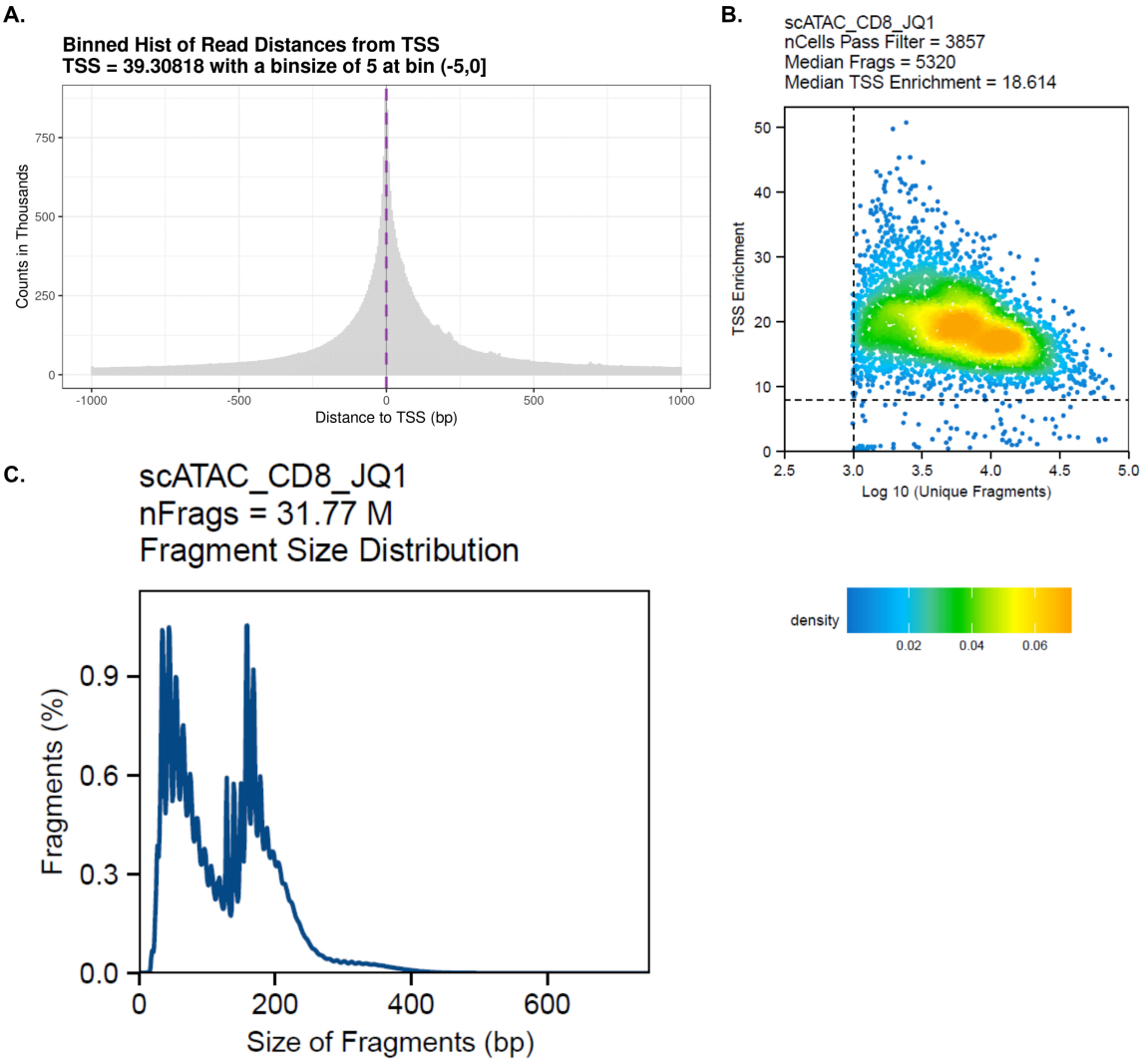

Figure 30 **– a.)** Represents the batched TSS enrichment score which was calculated using the ENCODE method. **b.)** TSS enrichment scores vs. Unique fragments for the batched dataset. A minimum threshold of 8 median TSS was used for downstream analysis. **c.)** Fragment size vs percent fragments for the batched dataset. Plots were generated with the ArchR package.

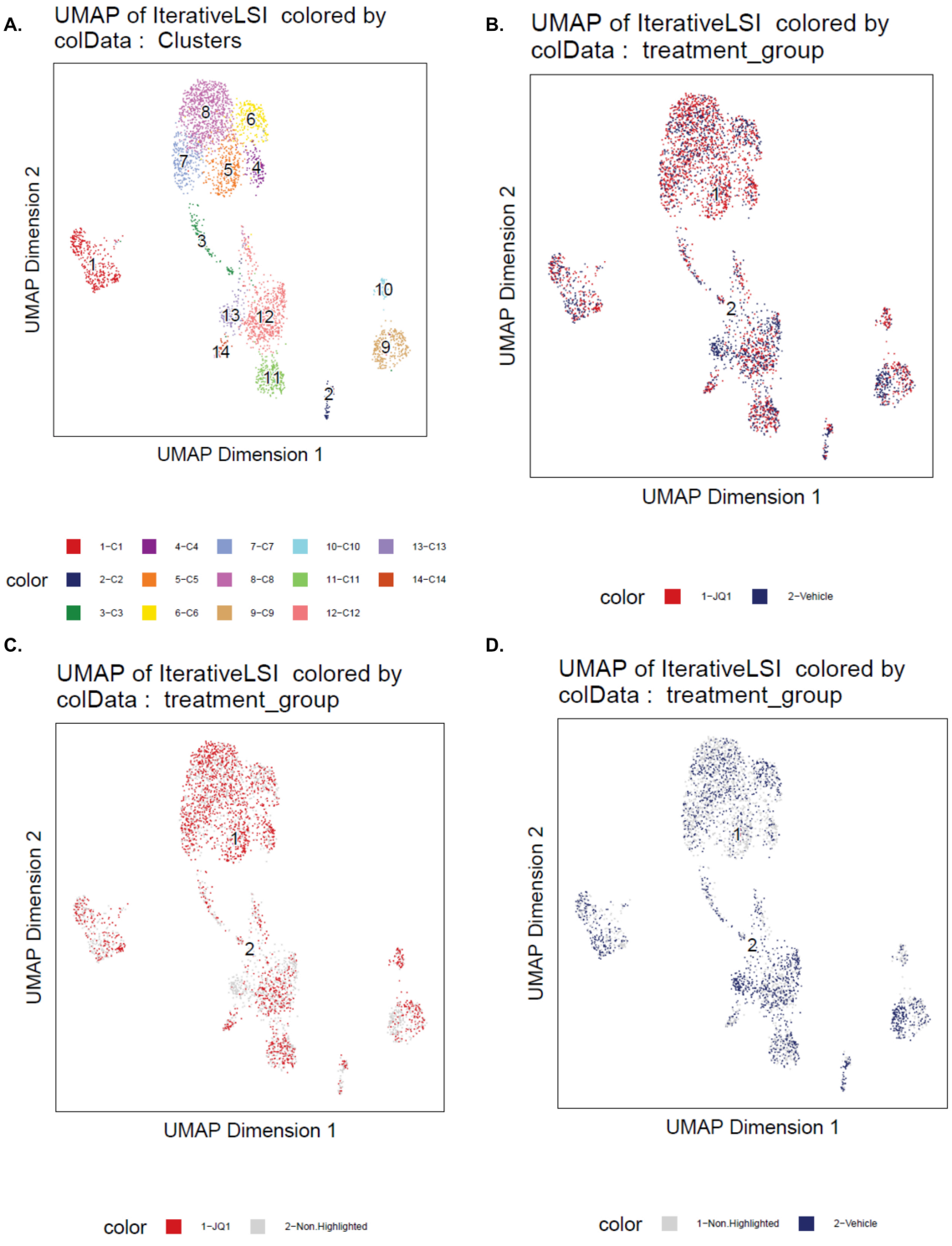

***Figure 31* – a.)** UMAP clustering using the iterative LSI dimensionality reduction method to predict cell type identities in the batched S3-ATAC data set. The legend below denotes the cluster identity. **b-d.)** UMAP plots with overlaid **b**.) JQ1 and vehicle treated cells **c**.) JQ1 only cells and **d**.) Vehicle cells only. All plots created using the ArchR package.

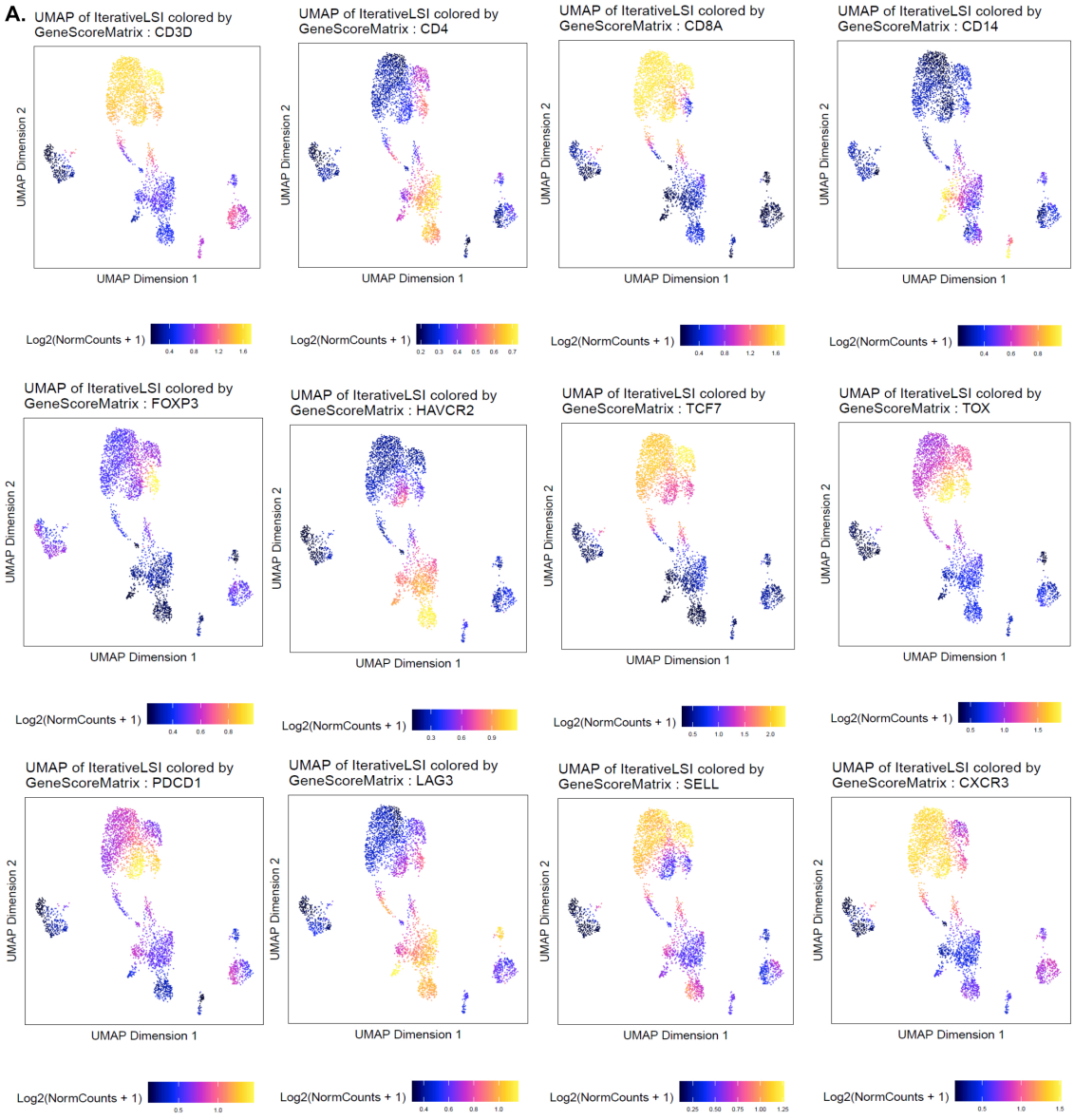

***Figure 32* – a.)** A Gene Score Matrix was calculated using the ArchR package. UMAP plots were then generated with the respective normalized gene score counts for the following genes (beginning at the top left corner): (row 1) *Cd3d, Cd4, Cd8a, CD14,* (row 2) *Foxp3, Havcr2, Tcf7, Tox,* (row 3) *Pdcd1, Lag3, Sell,* and *Cxcr3*.

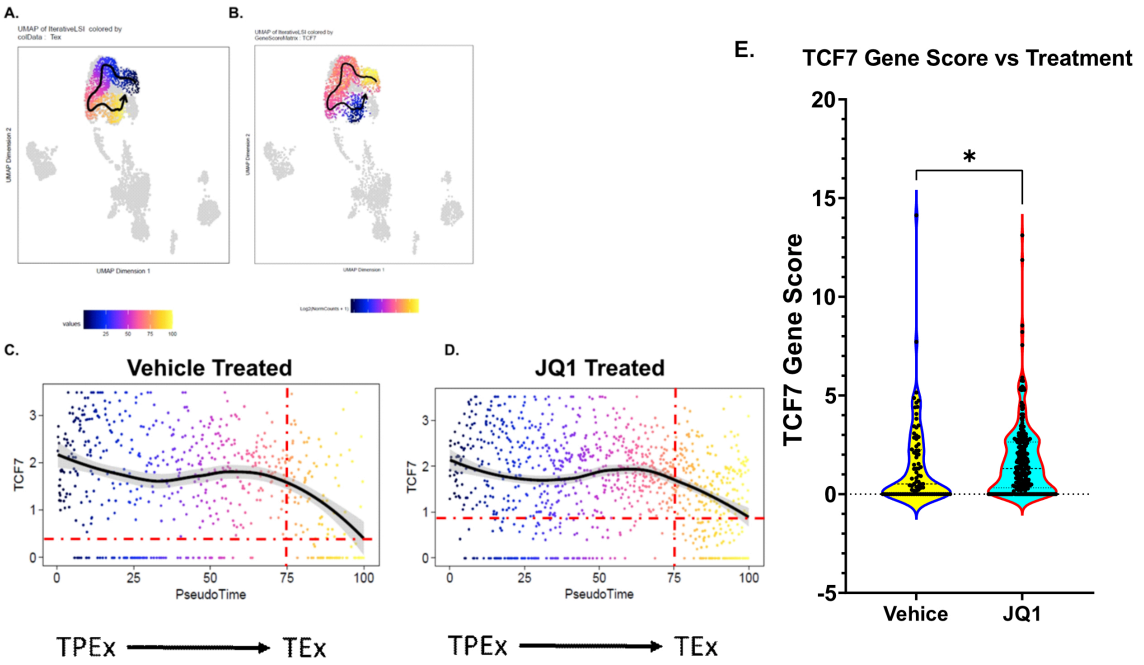

***Figure 33* – a.)** Tex differentiation trajectory plotted as pseudotime. Trajectory is fit to traverse from previously described Cluster 6→ Cluster 8 → Cluster 7 → Cluster 5. Plot represents both vehicle and JQ1 treated CD8 T cells. **b.)** *Tcf7* gene score throughout Tex differentiation trajectory. **c,d.)** Linearized pseudotime trajectory representing *Tcf7* gene scores throughout Tex differentiation separated by treatment with **c.)** Vehicle or **d.)** JQ1 treated. Red vertical line denotes the start of the third quartile where the most exhausted T cells reside and the horizontal dashed line marks the lowest TCF7 point. **e.)** Quantification of TCF7 gene scores from cells derived from the T cell exhaustion pseudotime trajectory. Significance calculated by mann-whitney.

Discussion

Immune checkpoint blockade in hematological malignancies

ICB therapy in the blood cancer setting is relatively new and although dozens of clinical trials are ongoing and actively recruiting (211), no large-scale study has been completed evaluating the efficacy of anti-PD1 therapies in AML. Our lab previously described the functional immune microenvironment of 50 newly-diagnosed AML patient bone marrow samples(211) and found that only 41% showed $CD8^+$ T cell proliferative capacity that was comparable to healthy donor. Further, we found that the AML patient samples with the most profound proliferative defect (37% of those tested) had severely dysfunctional T cells with significantly decreased production of effector cytokines such as IFN-γ, IL-2, and TNF-α, and increased expression of inhibitory checkpoint markers such as CTLA-4. Of these non-proliferating AML samples, 6 of 18 samples were not rescued with ICB treatment *in vitro*, maintaining the defects in proliferation and effector molecules upregulation seen without ICB. However, 12 of 18 samples did respond, at least partially, to ICB indicating that suppressive mechanisms may be overcome by altering the capacity of T cells to receive inhibitory signals through IC in the tumor environment. Combination treatment regimens that target both the tumor and immune environment to rescue terminally exhausted T cells may be the key to greater success with ICB therapy clinically. Smaller clinical trials have evaluated the efficacy of anti-PD1 + hypomethylating agents (HMA) but only a small subset, approximately 33%, responded to therapy(212), which is consistent with our *ex vivo* findings(211). Phenotypic profiling of these responsive patients before and after anti-PD1 +/- HMA identified pre-therapy bone marrow and peripheral blood $CD3^+$ and $CD8^+$ levels as predictive of response. In addition, we previously described the synergistic effects of combining MEKi and anti-PD1(207). We found that MEKi acted directly on both tumor cells and immune cells globally by reducing PD-L1 expression on patient samples and, at low doses, restored

some proliferative function of AML-derived T cells. These data provide evidence that treatment strategies that target both tumor-intrinsic factors as well as T cell suppression will be more effective.

Epigenetic regulation of T cell exhaustion

T cell exhaustion is driven by chronic antigen exposure and is accompanied by vast changes in the epigenetic landscape(91-94,104). This T cell state is identifiable by three main traits: 1) increased expression of inhibitory receptors such as PD1, LAG3, TIGIT, and CTLA-4, 2) decreased secretion of effector cytokines such as IL-2, IFN-γ, TNF-α and 3) loss of proliferative capacity(92,102,213-215). Epigenetic changes are largely driven by a pool of coordinating T cell receptor (TCR)-responsive transcription factors, such as BATF, IRF4, TOX, and NFAT(87,102,214,215), chromatin remodeling complexes such as EZH2, and other polycomb repressive complex 2 proteins(216-219). Generation of TPEx cells relies on the de-repression of many critical pro-memory transcription factors such as TCF1, FOX01, and others as a consequence of targeted DNA methylation deposition acquired during early effector differentiation. Interestingly, the pro-exhaustion transcription factor TOX was found to also directly modulate histone acetylation via direct binding to histone acetyltransferase KAT7(92,104,220). This critical role for epigenetic regulation of T cell exhaustion has garnered much interest in investigating the potential of several epigenetic targeting SMI, whose original design was directed towards targeting tumor-intrinsic epigenetic dysregulation(89). Very recently, Milner *et al.* showed that BRD4 regulates T cell differentiation by promoting super-enhancer activity at regions regulating key pro-exhaustion/differentiation genes such as *Id2*, *Cx3cr1*, and *Runx1(221)*. Using our unique mouse model of AML, we find that BET inhibition in combination with ICB therapy can lead to a shift from predominantly non-responsive T cells with a TEx phenotype to TPEx and the production of functional $CD8^+$ T cells. These results form the basis for further study of such combination therapies in

AML. Additionally, our s3-ATAC-seq data suggests that BETi act directly on Tex cells and enhance their functionality by affecting *Tcf7* accessibility. Further studies will focus on understanding the heterogeneity in AML patient responses to BETi + anti-PD1 and deeper characterization of the cell specificity of BETi.

Methods

AML murine model

Mice expressing FLT3-ITD under the endogenous *Flt3* promotor (strain B6.129-Flt3tm1Dgg/J, The Jackson Laboratory, stock no. 011112) were crossed to mice with the *Tet2* gene flanked by LoxP sites (strain B6;129S-Tet2tm1.1Iaai/J, The Jackson Laboratory, stock no. 017573). The *Flt3-ITD/Tet2*^{flox} mice were then crossed to mice expressing Cre recombinase under the *Lys*m promotor (strain B6.129P2-Lyz2tm1(cre)Ifo/J, The Jackson Laboratory, stock no. 004781). All breeding animals were purchased from The Jackson Laboratory. All mice used in these experiments were bred as heterozygous for FLT3-ITD, TET2, and LysCre. All mouse experiments were performed in accordance with the OHSU Institutional Animal Care and Use Committee protocol IP00000907.

Flow Cytometry Staining

Bone marrow, blood, or splenocytes were processed and subjected to red blood cell (RBC) lysis by ACK before counting via hemacytometer. Five million cells were resuspended in PBS and stained with Zombie Aqua viability dye (BioLegend, Cat# 423102) for 15 minutes at room temperature, covered from light. The cells were then washed with FACS buffer (PBS, 2% calf serum, 0.02% sodium azide) and resuspended in 25 µL 1:50 mouse FC block (TruStain FcX, BioLegend Cat# 101320), and left on ice for 5 minutes. 25 µL of a 2x cell surface staining antibody cocktail was added directly on top of the cells (final FC block 1:100, 1x Ab concentration) and stained on ice for 30 minutes. For intracellular staining, the cells were then washed with FACS buffer,

permeabilized and stained for intracellular targets according to manufacturer's protocol (eBioscience FOXP3 Transcription Factor Staining Buffer Set, Cat# 00-5523-00), then resuspended in FACS buffer before analyzing on either a BD Fortessa or Cytek Aurora flow cytometer. Data was analyzed using FlowJo software.

H&E Histology

Liver, spleen, and bone marrow snips were fixed and cut into paraffin blocks for H&E staining. The slides were then scanned using an Aperio AT2 scanner and analyzed with ImageScope.

Long-term culture of AML mouse-derived bone marrow cells and Inhibitor Library Screen

Bone marrow aspirates from three AML mice were combined, isolated, and cultured in RPMI containing 20% fetal bovine serum (FBS), streptomycin/penicillin, 50 μM 2-mercaptoethanol (RPMI-20), and supplemented with murine SCF (10 ng/ml) and IL-3 (10 ng/ml) (Peprotech or BioLegend). The cells were serially passaged for ~1 month. Inhibitor library screening to evaluate drug sensitivity was performed as previously described(20). Briefly, cultured AML mouse-derived cells were counted and seeded into four 384-well plates at a concentration of 2000 cells/well. The cells were then subjected to titrations of 188 unique small-molecule inhibitors in culture for 72 hours. MTS reagent (CellTiter96 AQueous One; Promega) was added and the optical density was read at 490 nm to assess viability.

Mouse* ex vivo *proliferation assays

96-well round-bottom plates were coated with either 2.5 μg/mL anti-CD3 (Biolegend, clone 145-2C11,Cat# 100359) or HIgG (Biolegend, clone HTK888, Cat#400959), at 4° C overnight, then washed with PBS. Splenocytes were harvested from AML or WT mice and stained with 2 μM CFSE (Life Technologies, Thermo Fisher) at $5x10^6$/mL at 37° C in the dark. After 15 minutes, the CFSE was quenched with 10 mL calf serum and washed with PBS. Cells were then plated at $5x10^5$/well in RPMI with 10% FBS with BME

supplementation and penicillin/streptomycin (RPMI-10). After a 72-hour incubation at 37° C the cells were stained for flow cytometric analysis with antibodies listed below and analyzed as previously described. Anti-PD1 (Clone RMP1-14) and RIgG (2A3) were purchased from BioXCell. JQ1 was purchased from Cayman Chemical (#11187).

Marker	Clone	Vendor
Tbet	4B10	BioLegend
LAG-3	C9B7W	BioLegend
TIM3	RMT3-23	BioLegend
CD44	IM7	BioLegend
CD62L	MEL-14	BioLegend
PD-L1	10F.9G2	BioLegend
CD11b	M1/70	BioLegend
CD8a	53-6.7	BioLegend
GR1	RB6-8C5	BioLegend
PD-1	29F.1A12	BioLegend
BATF	S39-1060	BioLegend
CD34	HM34	BioLegend
CD3e	400A2	BioLegend
TCF1	C63D9	Cell Signaling Technologies
CD4	GK1.5	BioLegend
FOXP3	FJK-16S	BioLegend

Human* ex vivo *proliferation assays

Bone marrow aspirates and peripheral blood samples were separated by Ficoll density gradient centrifugation. All experiments were performed using freshly isolated cells. Cells were labeled with CellTrace Violet (CTV, ThermoFisher) and cultured in 96-well plates coated with 1µg/ml anti-CD3 (BioLegend, Clone UCHT1) or control mIgG (BioLegend, Clone MOPC-21). Groups of wells were then treated with either 10µg/ml control mIgG, 10µg/ml anti-PD-1 (EH12.2H7), 60nM JQ1, or 60nM JQ1 + 10µg/ml anti-PD-1. After 5 days, cells were stained for flow cytometry. Viability was determined by Zombie Aqua staining and doublets were gated out of analysis by FSC-A vs FSC-H. Flow cytometry data was acquired on a BD LSRFortessa or Cytek Aurora and analyzed using FlowJo v10 software.

Marker	Clone	Vendor

CD19	HIB19	BioLegend
CD45	HI30	BioLegend
CD8	RPA-T8	BioLegend
CTLA4	BNI3	BioLegend
PDL1	29E.2A3	BioLegend
CD33	WM53	BioLegend
CD4	RPA-T4	BioLegend
PDL2	24F.10C12	BioLegend
CD56	HCD56	BioLegend
TIGIT	MBSA43	ThermoFisher
TIM3	7D3	BD
PD1	EH12.2H7	BioLegend
CD3	HIT3a	BioLegend

***BETi + anti-PD1 treatment* in vivo**

Age range of AML mice used in *in vivo* experiments was 25 to 54 weeks. WT and AML mice were given seven doses of 8 mg/kg RIgG, 50 mg/kg JQ1, 200 8 mg/kg anti-PD1 or 50 mg/kg JQ1 + 8 mg/kg anti-PD1 via i.p injection over two weeks (3 times per week, harvesting 1 day after 7th/final injection). For S3-ATAC daily 50mg/kg JQ1 or 10% cyclodextrin for 5 days was given. Drug solutions were prepared in a solvent of 10% cyclodextrin in PBS from a stock solution of JQ1 (50 mg/mL) in DMSO, followed by sonication/heat bath to dissolve the JQ1. Assessment of tumor burden in the blood, as determined by WBC measurements from Hemavet (950FS, Drew Scientific), was monitored weekly pre-, mid-, and post-treatment. At endpoint, single cell suspensions of bone marrow, blood, and spleen tissues were stained for flow staining as previously described.

Evaluation of CD8$^+$ T cell transcripts via Nanostring

AML mice were given 7 doses of vehicle (10% cyclodextrin) n = 5 or 50 mg/kg JQ1, n = 5, via i.p injection over two weeks (3 times per week, harvesting 1 day after 7th/final injection) as previously. CD8$^+$ T cells were isolated by magnetic bead isolation (Biolegend #480136) and RNA extracted according to manufacturer's protocol (PureLink

RNA kit, ThermoFisher). Samples were hybridized and loaded onto the Nanostring Chipset according to manufacturer's instructions (Nanostring Panel NS_MM_CANCERIMM_C3400) and analyzed using the nSOLVER4.0 tool.

S3-ATAC-seq

AML mouse $CD8^+$ T cells were enriched with one round of mojosort magnetic bead sort as described previously. Cells were then prepared as described in Mulqueen *et al*. 2021(210) before sequencing. Data was analyzed using the ArchR package (https://www.archrproject.com/index.html)

Chapter 4

Functional Immune Landscape of AML

Abstract

The implementation of small-molecule and immunotherapies in Acute Myeloid Leukemia (AML) has been met with many challenges due to widespread genetic and epigenetic variability amongst patients. Many mechanisms of response to therapies have been reported which are driven by underlying genetic and non-genetic mechanisms. There are many potential mechanisms by which immune cells can influence small-molecule or immunotherapy responses but is an area still largely understudied. Here we utilized the xCell webtool to perform cell type enrichment analysis from over 600 AML patient bone marrow and peripheral blood samples deposited in the Beat AML biorepository to describe the functional immune landscape. We identify multiple cell types which significantly correlate with mutational statuses, drug responses, differentiation state, clinical correlates, and *ex vivo* immunotherapy responses. Additionally, we generated a signature of terminally exhausted T cells (T_{ex}) and identified monocytes/monocytic AMLs as strongly correlating with increased proportions of these immunosuppressive T cells.

Our work, which is accessible through the Beat AML data viewer (Vizome), can be leveraged to investigate potential contributions of different immune cells on many facets of the biology of AML.

Introduction

AML is a devastating blood cancer with an average 5 year survival of approximately 29%(22) and is characterized by an uncontrolled expansion of abnormal myeloid-lineage cells commonly referred to as “blasts”. In the United States for the year 2020 there were 60,530 new cases of leukemia of which AML encompassed roughly 1/3 (19,940), but disproportionately accounted for nearly half of the deaths (11,180 of 23,100 all leukemia) (SEER). AML is an extremely genetically heterogeneous cancer, with the most common mutations, *FLT3-ITD, NPM1,* and *DNMT3a*, only encompassing approximately ~30% of all AML patients(20). While targeted therapy discoveries have expanded greatly in the past decade, there are still many confounding variables which dampen responses in patients. Understanding these underlying variables affecting drug responses are critical to achieving durable remissions by treating patients with tailor-made regimens.

As a blood cancer, AML cells are uniquely situated to interact with a plethora of immune cells either in the bone marrow or in the periphery. Many have reported on a number of different mechanisms by which AML cells interact with immune cells to disrupt homeostasis via secretion of and/or increased responsiveness to pro-inflammatory cytokines(222-224), promotion of T cell exhaustion(195,208,225), and more. Further, groups have begun investigating the connection between certain somatic mutations and expansion of immunosuppressive cell types, such as TP53 mutations increasing Tregs(226) and DNMT3a mutations attenuating T_H1 macrophage polarization(227). However, these studies are limited by small patient cohorts or restricted to murine models. This prompted us to describe the functional immune landscape of AML via

deconvolution of bulk RNA-seq from ~600 AML patient samples and mapping to a myriad of clinical annotations and drug responses.

Results

Immune landscape of AML

To assess the immune landscape of AML we deconvoluted bulk RNA-seq data using the xCell webtool(228) in 600 AML patients within the Beat AML registry and annotated multiple clinical correlates (Figure 34a, 35a). We found significant differences in immune cell repertoire based on specimen type -- bone marrow aspirates or peripheral blood. As expected, we found bone marrow aspirate samples had significantly decreased proportions of lymphoid populations as compared to the peripheral blood samples (Figure 35b-e). We validated the accuracy of the xCell proportion estimates by leveraging available clinical flow data, and found accurate predictions for all cell types with corresponding clinical flow annotations (Figure 34b-e).

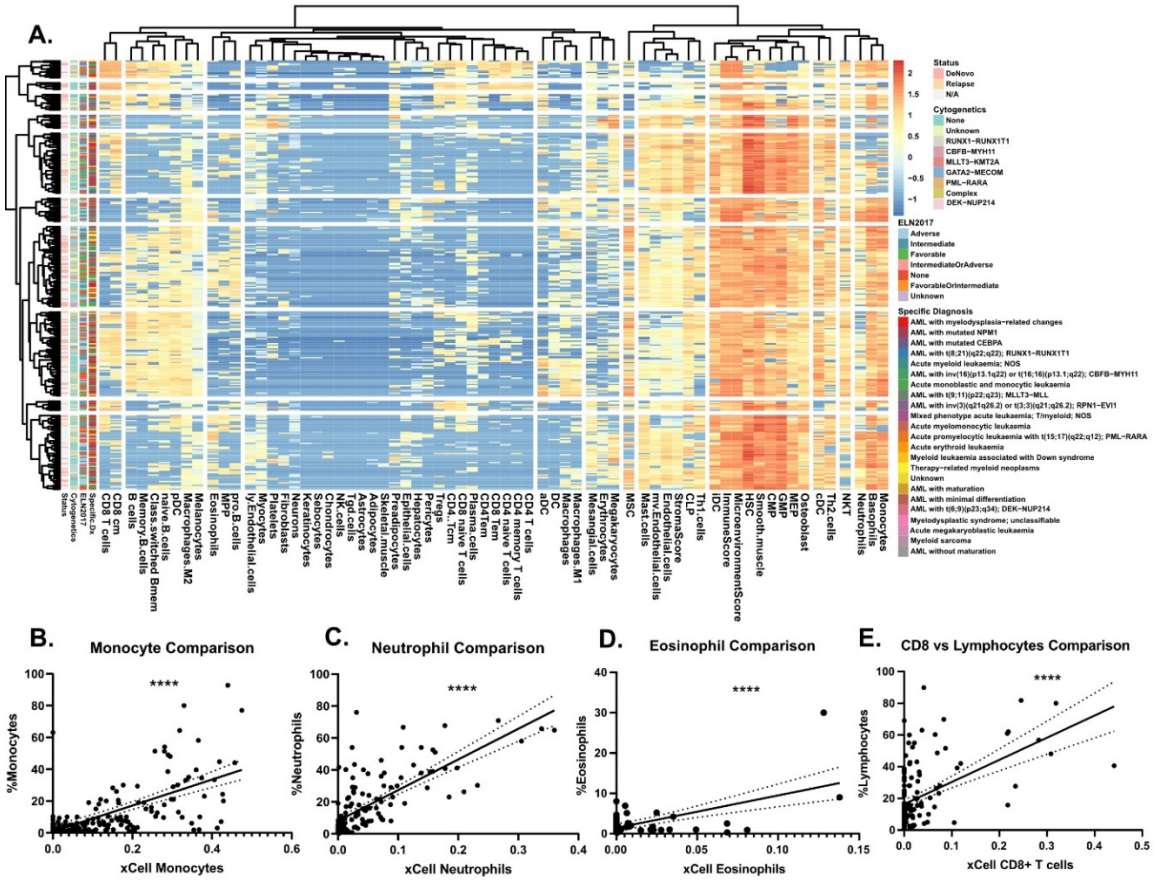

Figure 34 – a.) Heatmap representing log2 normalized immune cell proportion estimations calculated by xCell for 309 AML patient sample peripheral blood aspirates. Cell types are grouped by Euclidean distance and patient samples by correlation. Where possible, Relapse vs De novo status, ELN2017, and Specific Diagnosis denoted on left axis. b-e.) Comparison of real cell type proportions as determined by clinical flow cytometry at specimen acquisition vs xCell estimations for b.) monocytes, c.) neutrophils, d.) eosinophils, and e.) CD8+ T cells vs lymphocytes. Significance determined by spearman correlation. Solid black line represents the linear line of best fit and the dotted lines on either side represent the 95% clearance.

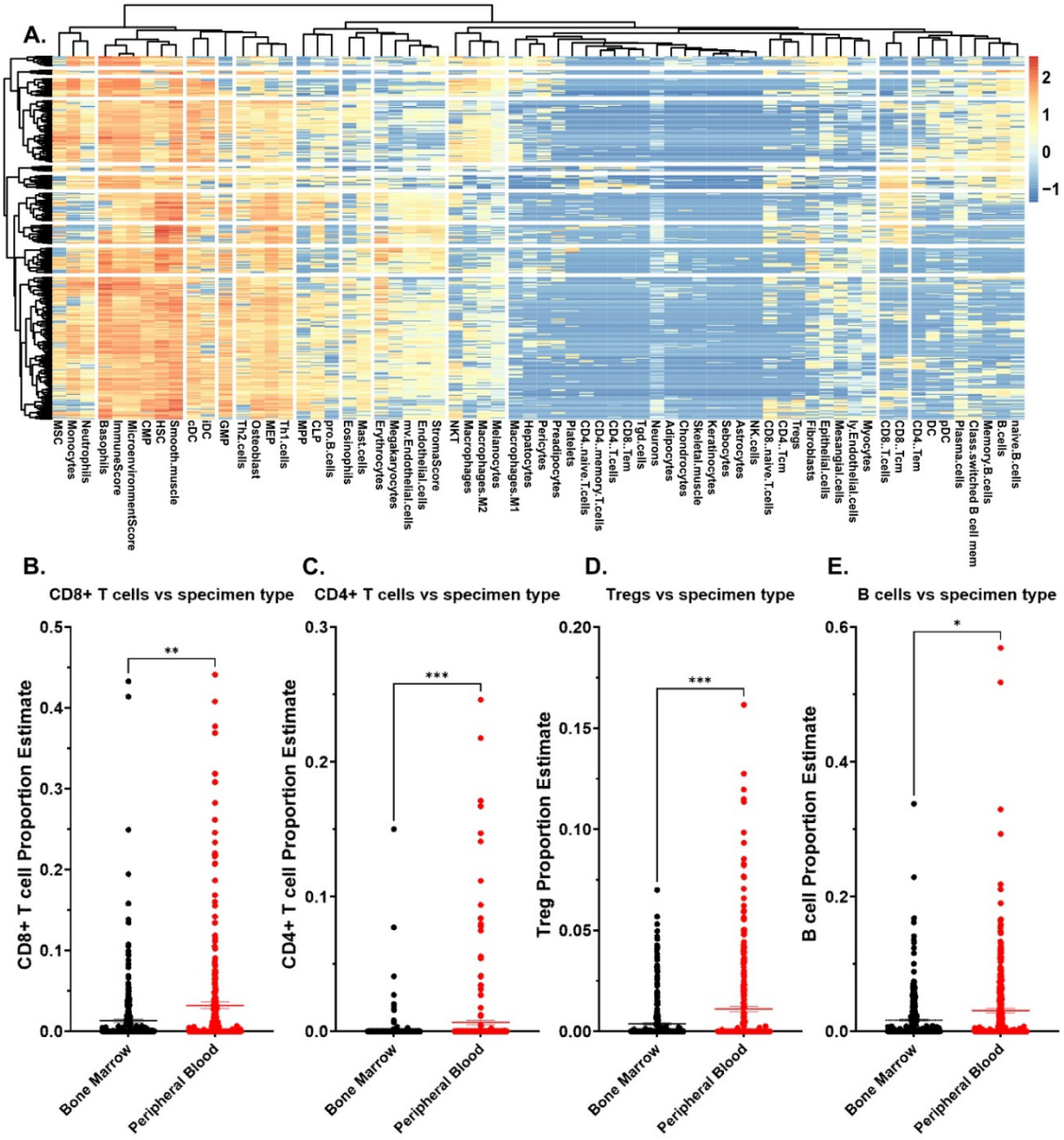

Figure 35 – a.) Heatmap representing log2 normalized immune cell proportion estimations calculated by xCell for 362 AML patient sample bone marrow aspirates. b-e.) Comparisons of the xCell determined cell type proportions between peripheral blood and bone marrow aspirates against b.) CD8+ T cells, c.) CD4+ T cells, d.) Tregs, and e.) B cells. Significance determined by Mann-Whitney T test.

To investigate potential connections with patient features, we performed hierarchical clustering of patients and cell types identified 2 clusters of AML patients with significantly increased proportions of T cell subtypes of multiple lineages (Figure 36a). Further characterization of the clinical and mutational background of these patients (clusters 5 and 8) found that these were enriched in *de novo* or transformed AMLs and absent in relapsed samples (Figure 36b) and had increased IDH2, RUNX1, and TP53 mutations (Figure 36c). Interestingly cluster 11, which clusters with group 5 and 8, also has strong T cell signatures but almost exclusively in CD8 lineages and is characterized by significantly enriched for DNMT3a mutations. Further, cluster 9, which had the highest proportion of neutrophils and eosinophils were significantly enriched in transformed AMLs and almost exclusively TP53 mutated. Finally, we looked at WBC count at specimen acquisition between the different clusters and found that T cell high clusters 5, 8, and 11 and significantly decreased WBC counts (Figure 36d).

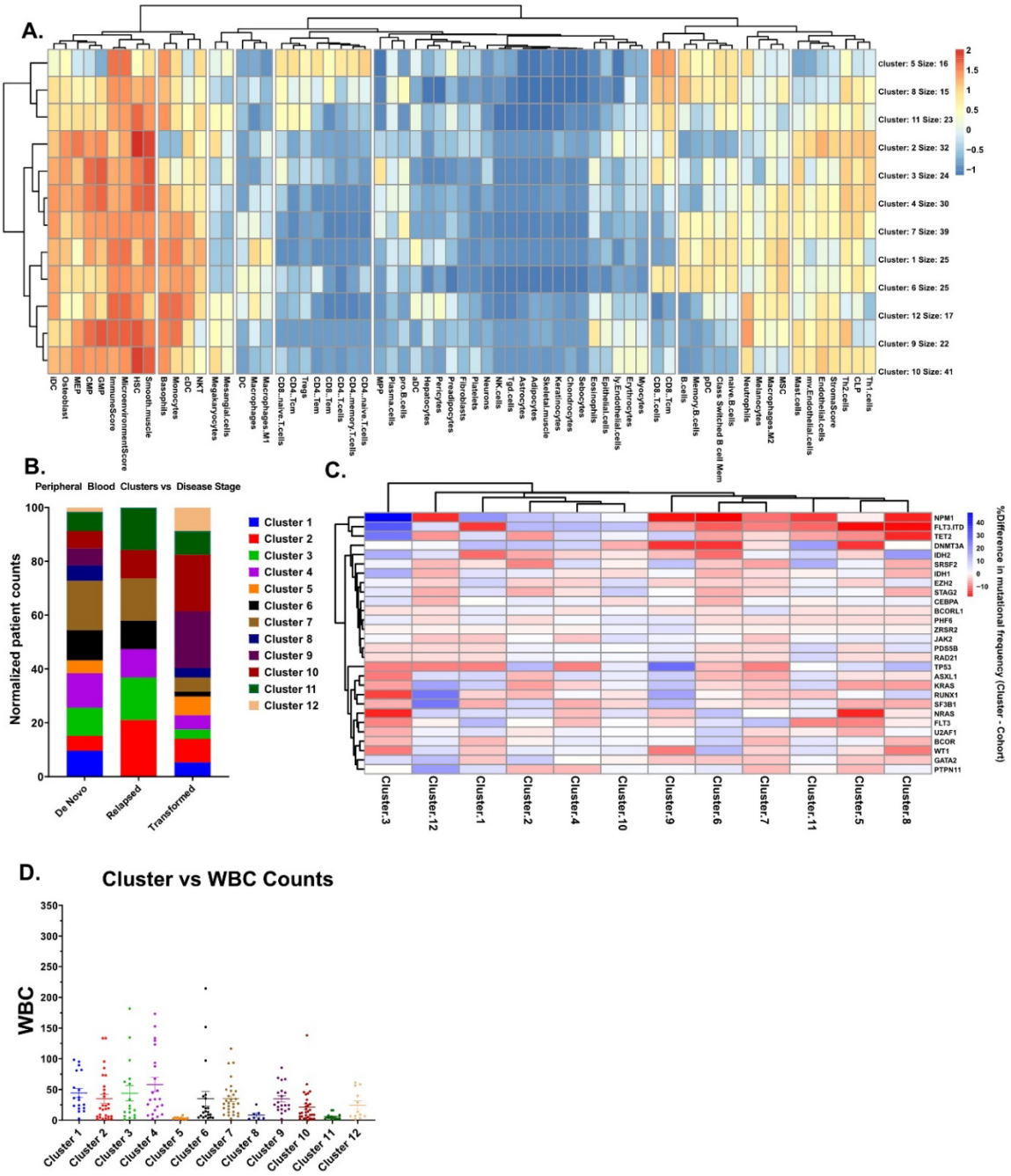

Figure 36 – a.) Peripheral blood cell type proportions calculated in Fig 30a were clustered into 12 groups using K means. Right axis denotes cluster ID and the number of patient samples which make up the cluster. b.) Breakdown of disease status (De novo, relapsed, or transformed) vs. cluster ID. Patient sample counts were normalized to a respective percent. c.) Relative frequency of mutations vs cohort frequency of mutations for each cluster. Heatmap denotes intensity of the difference (Blue = increased frequency in cluster, white = no change, red = decreased frequency relative to entire cohort). d.) White blood cell counts at specimen acquisition for each sample vs cluster ID.

Immune cell co-occurrence identifies leukemic differentiation state as potential marker of immune activation

We next asked which cell types co-occurred together most frequently to investigate any potential contributing cell types to immune suppressive regulatory T cells (Tregs), which have been shown to be correlated with a worse prognosis in AML(193,208). We calculated spearman correlation matrices for all cell types in AML patient peripheral blood (Figure 37a) and bone marrow (Figure 37b) specimens. As expected, cell types from similar lineages (e.g central memory $CD8^+$ T cells and effector $CD8^+$ T cells) correlated very highly. Interestingly, we observed significant positive correlations between Tregs and basophils or monocytes but significant negative correlations between multiple progenitor cell types (CMP, GMP, HSC) in both bone marrow and peripheral blood specimens (Figure 37c). Next, we correlated patient outcomes by cell type proportions, stratified by specimen type, to ask whether any cell types associated with worse survival. We found significant differences in cell types which correlated with survival by specimen type. We find that Treg signatures significantly correlate with worse survival in bone marrow aspirates whereas T_H2 T cell and macrophage signatures correlate with worse survival in peripheral blood specimens (Figure 37d, e).

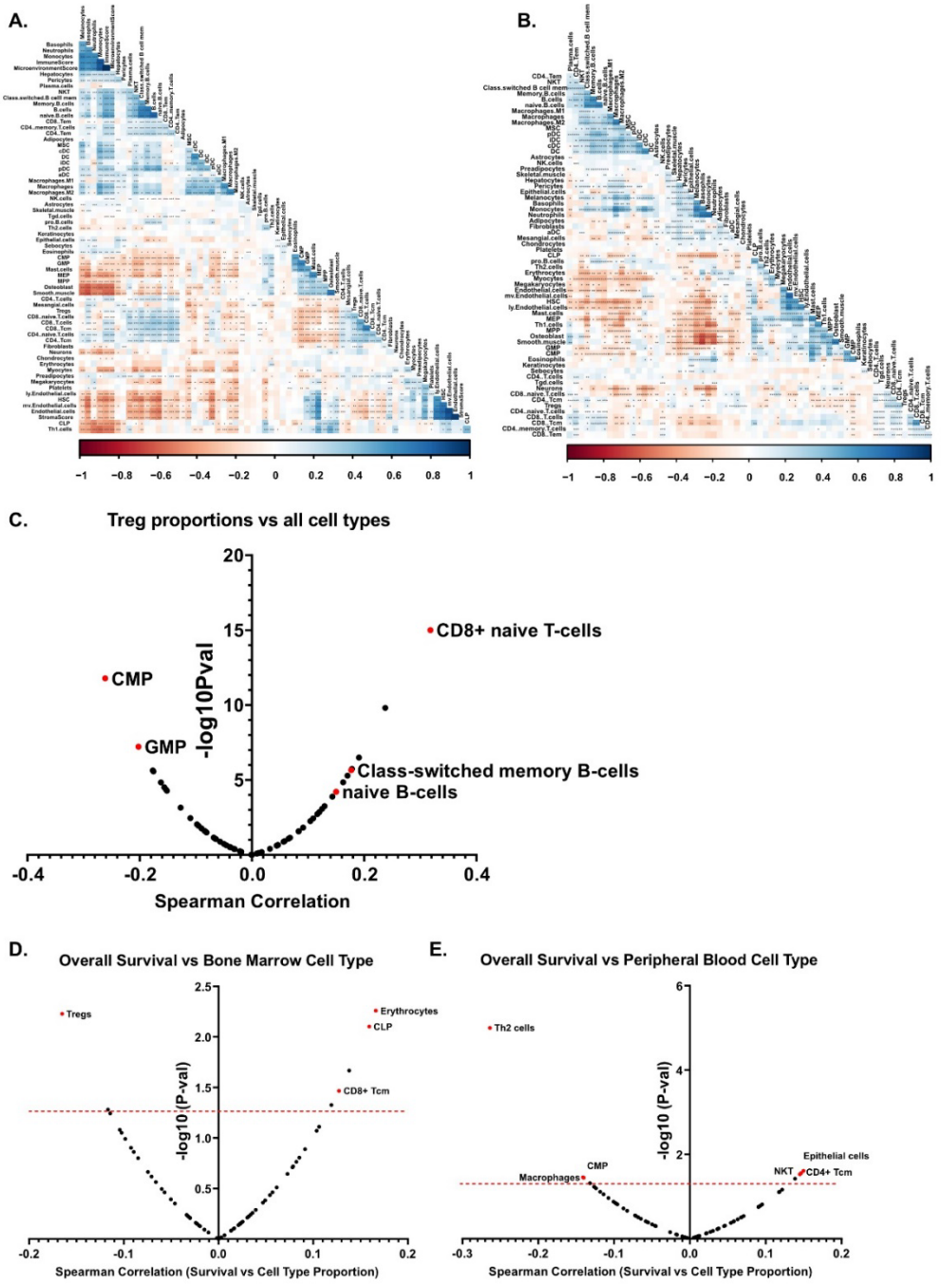

Figure 37 – a-b.) Spearman correlation matrices were generated between all cell type estimations determined by xCell from a.) Peripheral blood and b.) Bone marrow aspirates. Color scaling denotes the magnitude of significance with red indicating that the cell type pair very negatively associate whereas blue indicates very strong positive associations. Significance of the spearman correlations is denoted in each square with asterisks

Immune cell signatures predictive of small-molecule and immunotherapy responses

We next determined cell types correlations with small-molecule responses *ex vivo* in AML patient samples. We restricted correlations to only include inhibitors with greater than 20 unique patient responses. This cutoff yielded 314 unique inhibitor monotherapy or combination therapies (Figure 38a). We and others previously described BETi and venetoclax or palbociclib as having opposing responses in monocytic AMLs, whereby BETi sensitivity is highest in monocytic AMLs(229) whereas venetoclax(142,143) and palbociclib(229) are most sensitive in undifferentiated AMLs. We were able to again find these patterns of response as both venetoclax and palbociclib positively correlated (ie had the highest AUC and was more resistant) with monocytes whereas the BETi OTX-015 strongly negatively correlated with monocytes, thus validating this approach. We identified many novel correlations between inhibitor responses and different cell types. Here, we can focus on responses tethered to a single cell type. As proof of principle, we focused on inhibitors which are more efficacious in samples with high proportions of Tregs. The top three inhibitors with increased effectiveness in Treg high samples– NVPAEW-541, BMS-754807, and metformin, target insulin signaling pathways via inhibition or downregulation of the IGF-1 receptor (Figure 38b). Several studies have demonstrated that activation of IGF-1R induces Tregs(230) and that insulin resistance correlates with decreased Tregs(231). Our *in silico* data suggests that this is a targetable axis in AML patients and that its enhanced efficacy may be driven by targeting Tregs. Additionally, we can instead focus on the responses of a single drug globally. In this case, we focused on the FDA approved hypomethylating agent (HMA) azacytidine (Figure 38c). Here we find that azayctidine resistance correlates with increased proportions of adipocytes, monocytes, and neutrophils whereas Th1 cells and MPP cells correlate with sensitivity.

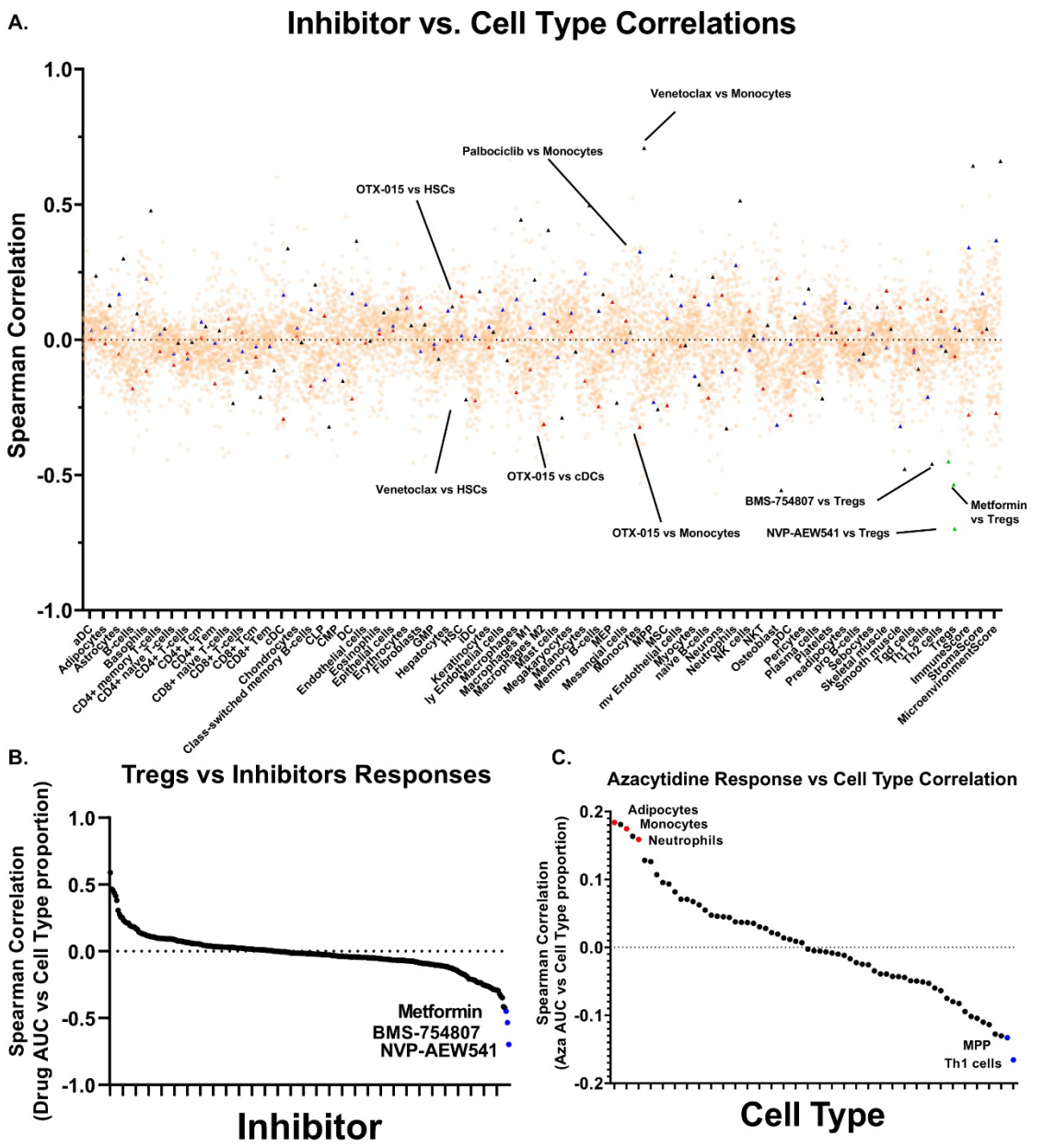

***Figure 38* – a.)** Scatter plot showing all inhibitor correlations vs all cell types. Inhibitor correlations were calculated using *ex vivo* area under the curve values derived from Tyner *et al*. 2018 and restricted to inhibitors with at least 20 unique patient samples. Red triangles denote BETi OTX-015 responses and highlight monocyte and cDC correlations. Black triangles denote BCL2i venetoclax and highlights monocytes and HSCs. Blue triangles denote palbociclib correlations and highlights monocytes. Green triangles denote Treg correlations and highlight IGF-1Ri NVP-AEW541, BMS-754807, and metformin. **b.)** Focused plot of all inhibitor AUC correlations vs. Tregs only. **c.)** Focused plot of all cell types vs HMA azacytidine, highlighting strongly positive correlations in red and negative correlations in blue.

Monocyte high patient samples have decreased ex vivo responses to ICB therapy and higher Tex signatures

We next asked whether any cell type signatures predicted *ex vivo* immune checkpoint response. Lamble and Kosaka *et al*.(195) recently evaluated the efficacy of ICB therapy in 49 bone marrow aspirate samples within the Beat AML database. Of those, 18 had dysfunctional T cells – as determined by reduced proliferative capacity and cytokine secretions. Of these samples with dysfunctional T cells, 9 were rescuable with *ex vivo* treatment with anti-PD1 blockade, and 6 were refractory. We first asked whether any xCell predicted cell types significantly differed between these two groups and found that monocytes were significantly higher in aPD1 refractory samples (Figure 39a). We found this particularly interesting as Van Galen *et al*.(232) had previously noted that monocytic AMLs had immunosuppressive features. ICB therapy is thought to specifically re-invigorate progenitor exhausted T cells (TPEx) and retain the highest anti-tumor activity(100,125). Conversely, exhausted CD8 T cells (Tex), which terminally differentiate from TPEx, have reduced effector function and anti-tumor activity. Additionally, patients with higher TEx/TPex ratios are resistant to ICB therapy(233,234). Thus, given our previous data suggesting that monocytes/monocytic AMLs correlate with *ex vivo* anti-PD1 resistance and that anti-PD1 resistance has been linked to increased proportions of exhausted $CD8^+$ T cells, we utilized Kallisto, a program for quantifying abundances of transcripts from bulk RNA-seq data, and generated a custom T cell exhaustion signature using previously deposited sequencing data(86,87,93) to investigate whether Tex signature correlate with higher proportions of monocytes or monocytic differentiation programs (Figure 39b). We next asked which cell types correlated with our Tex score, excluding CD8+ T cells, and indeed found that monocytes significantly positively correlated whereas undifferentiated myeloid cells such as HSCs, GMPs, and CMPS negatively correlated (Figure 39c).

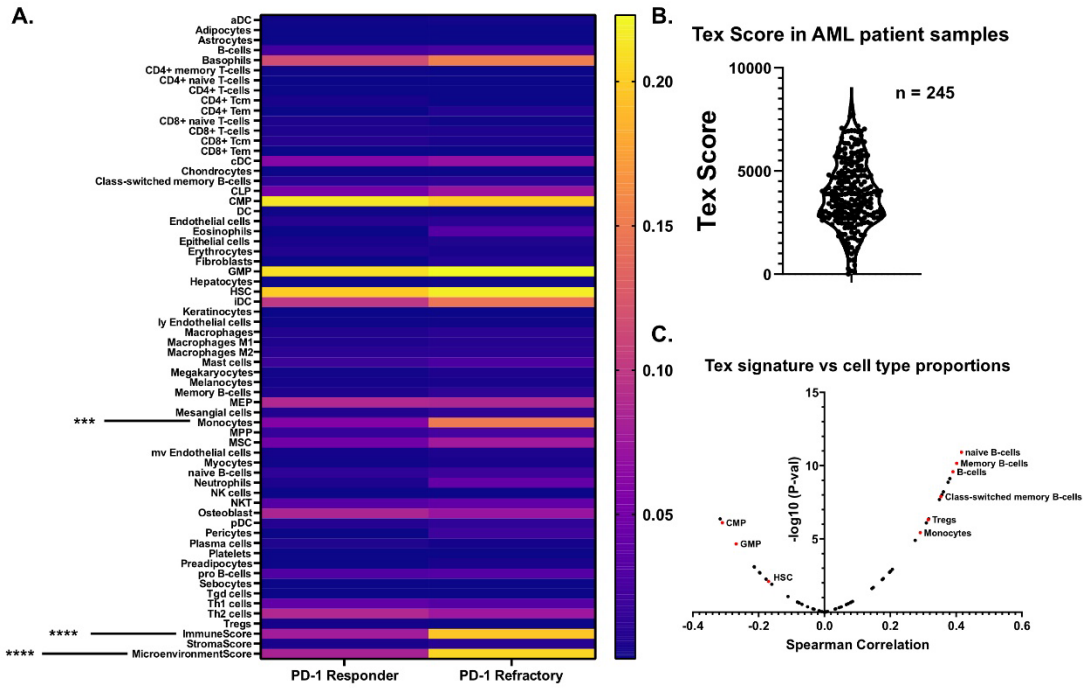

***Figure 39* – a.)** Heatmap which displays the aggregate cell proportion estimate vs. aPD1 *ex vivo* response for samples described by Lamble and Kosaka *et al*. 2019. Significance was calculated for all cell types via 2-way anova (n = 9 PD-1 Responder, n = 6 PD-1 refractory). **b.)** Distribution of Tex scores from peripheral blood samples within the Beat AML database. Briefly, the Tex score was generated by creating a signature based on previous sequencing data on exhausted T cells from Jadhav *et al*. and Man *et al*. **c.)** Volcano plot showing the spearman correlations between the generated Tex score and all other cell types from xCell.

Discussion

The contributions of non-leukemia cells towards drug responses and survival is an actively growing field but has many remaining questions. Here we attempt to address and describe the immune microenvironment of AML to better understand underlying mechanisms driven by the leukemia microenvironment. Utilizing *in silico* approaches we describe the microenvironment of ~600 AML patient bone marrow and peripheral blood aspirates. We validated these approaches using available clinical flow cytometry where available and found that, on average, xCell deconvolution accurately predicted cell type proportion. Our data identified TP53 and IDH2 mutated AMLs as potentially being more immunologically active with dramatically increased proportions of naïve and effector CD8+ T cells. Additionally, we find that these clusters of CD8+ T cell high patients are only present in *de novo* and transformed AMLs and lost during relapse which warrants further investigation. We further correlated 314 small-molecule inhibitors with cell type proportions and identified numerous novel interactions. As proof of principle, we focused on responses potentially tethered to Tregs and find that insulin growth factor receptor signaling as a potentially rationale therapeutic strategy in patients with high Tregs. Additionally, we were able to validate these approaches by investigating correlations between BETi, venetoclax, and palbociclib with monocytes, whose responses have been described by us and others as tethered to monocytic differentiation(142,143,229). Finally, we described the potential connection between monocytes/monocytic differentiated AMLs in predicting *ex vivo* ICB response. We show that monocyte signatures are significantly increased in AML samples with dysfunctional T cells that are refractory to ICB therapy. We further test this connection by generating a signature of exhausted T cells, which are known to drive ICB therapy resistance, and find that they indeed correlate significantly with monocyte signatures. Further studies will focus on

biological validation of novel inhibitor cell type correlations, as well as incorporation of deposited CyTOF data from Lamble and Kosaka *et al*. to further validate the accuracy of xCell predictions.

Methods

Deconvolution of RNA-seq data

Cell type deconvolution was performed using the "raw enrichment analyses" from xCell webtool on previously deposited raw data(20). Inhibitor responses and other related patient data is publicly available in the Beat AML database (http://www.vizome.org/). Clinical flow calls used to compare xCell proportions were also derived from the Beat AML registry.

Heatmaps

Heatmaps were generated by log2 normalizing cell proportion estimations for 309 AML patient sample peripheral blood aspirates. Cell types are grouped by Euclidean distance and patient samples by correlation. The R package "Pheatmap" was used to generate all heatmaps. Clustering of cell types vs specimen or cell types vs mutations was performed using the kmeans method and designating 12 unique clusters.

Correlation Matrices

Spearman correlation matrices and associated p values were calculated using the R package "corrplot" and correlated all cell type proportions against each other. Matrices were separated based on specimen type (bone marrow or peripheral blood).

Inhibitor Correlations with cell types

Inhibitor-cell type correlations were generated for all inhibitors in the Beat AML database with at least 20 unique patient samples. Details on the drug viability assay can be found in Tyner *et al*. 2018(20). This resulted in 314 unique inhibitor monotherapies or combination therapies. Spearman correlations were then generated for all samples comparing inhibitor area's under the curve (AUCs) vs xCell cell type proportions.

Anti-PD1 therapy vs cell type proportions

Ex vivo aPD1 responses were determined based on Lamble and Kosaka *et al*.(195), which identified 6 aPD1 resistant and 9 aPD1 responding samples. Significance for all cell types between aPD1 refractory and responder was calculated using 2-way anova and denoted on the corresponding heatmap.

Terminally exhausted T cell score

The terminally exhausted T cell score was determined using Kallisto to generate transcripts per million. An enrichment signature was then generated using deposited sequencing data from Jadhav *et al.(125)* and Man *et al.(87)* and calculated for all AML peripheral blood samples.

Chapter 5

Summary and Future Directions

Summary of BETi resistance project

In total, I found that BET inhibitor resistance is determined by leukemic differentiation state wherein undifferentiated AMLs are intrinsically resistant while monocytic AMLs are intrinsically sensitive. This is due to increased histone acetylation at BETi target sites which is promoted by hematopoietic transcription factors and aryl hydrocarbon receptor signaling that are naturally highly expressed in more differentiated leukemias. These pathways both act by recruiting the histone acetylating machinery to BRD4 binding sites and are preferentially upregulated in monocytic AMLs. Further, I showed that BETi-mediated inhibition of leukemic differentiation programs selects for less differentiated subclones which supports the notion that BETi resistance can develop as a consequence changed tumor maturation state.

BRD4 dependence along the hematopoietic differentiation lineage

One remaining question, besides the discovery of other inhibitors that may be paired with BETi to combat tumor maturation-driven resistance as we discovered with BCL2i and CDK4/6i, is whether BRD4 dependence changes during hematopoiesis. It stands to reason that, if the function of these hematopoietic transcription factors relies on BRD4-mediated transcription, that BRD4 dependence increases the further differentiated the cell is. Understanding these basic biological mechanisms may provide further insight into the epigenetic changes which occur during the highly coordinated process of both normal and malignant myelopoiesis. Additionally, this may reveal novel therapeutic vulnerabilities. Testing this experimentally would be difficult as BRD4 null embryos are

not viable as are any BRD4 KOs during early development. However, I believe there are a few different approaches one could take to address this. The first that comes to mind is to do conditional KOs of BRD4 restricted to either the common myeloid progenitor (CMP) cells or hematopoietic stem cells (HSCs). The myxovirus resistance-1 (MX1)-Cre system is polyinosinic:polycytidylic acid (polyIC) inducible and has been well established in studies of clonal hematopoiesis of HSCs and other early myeloid progenitor cells(235), transplantation models(236), and more (lineage tracing models reviewed(237)). One could cross this mouse with an established $BRD4^{flox/flox}$(48) and transplant the resulting post-polyIC induced c-kit/CD34+ HSCs into wild-type mice (containing a reporter of some kind – as an example the BRD4 KO could be CD45.1+ and the WT CD45.2+) to differentiate from transplanted cells) and evaluate hematopoietic differentiation skewing. To further investigate this axis, I could make mixed transplantation models where I isolate different $MX\text{-}1^{Cre}/BRD4^{flox}$ hematopoietic cells (HSCs, CMPs, MPPs, monocytes, etc.) and mix with WT cells before re-implanting. As an example, I could sort out CMPs from WT bone marrow aspirates and re-implant with BRD4 KO CMPs and evaluate the impact of individual cell types of hematopoietic differentiation. I could also implant BRD4 KO CMPs without removing non-BRD4 KO CMPs which would allow me to evaluate the competitiveness of BRD4 KO cells vs WT cells both in the cells themselves but also generation of their differentiated progeny. In this particular scenario, I would expect that deletion of BRD4 would significantly reduce the generation of monocytic lineages, as determined by reduced CD45.1+/CD11b+/Ly-6c+/Ly-6g- cells relative to CD45.2+ monocytes, but have limited impact on other differentiated myeloid cells (basophils, eosinophils, etc.).

A BET-ter way to target BRD4 to prevent unwanted toxicity

Clinically, BETi are still understudied. As of writing, only a single Phase I clinical trial is currently recruiting to investigate the efficacy of a new BET inhibitor, PLX51107, in combination with FDA approved hypomethylating agent Azacitidine. However, there are no criteria for selection based on specific diagnosis/differentiation state, which I show predicts BETi response *ex vivo* and in AML patients. Based on these findings, I would propose a more focused clinical trial which recruits patients refractory to venetoclax and other lines of therapy as a consequence of monocytic differentiation as candidates for BETi therapy. This could be easily incorporated with current immunophenotyping diagnostics.

An additional avenue of exploration could be into the development of more targeted BETi therapies. Clinically, BETi, like many other targeted therapies, have had issues with side effects and overt toxicity(77,82), no doubt due to BRD4 being a required transcriptional regulator for many normal processes, as previously described. I do not believe that the PROTAC degraders will overcome unwanted toxicity as the issue at hand, in my mind, is inhibiting BRD4 in the *right* cells, not degrading (ARV-825) vs blocking binding (JQ1, OTX-015, CPI-0610, PLX51107). One potential approach to circumvent these issues would be to create an antibody drug conjugate to target specific monocytic leukemia cells. In figure 11, I identify numerous suitable candidate surface markers which mark malignant and BETi sensitive cells – such as CSF1R, VCAN, and LILRs. These antibody-drug conjugate approaches are actually already used in the treatment of certain AMLs. Gemtuzumab ozogamicin (Mylotarg) is an FDA approved CD33 recognizing antibody conjugated to a cytotoxic agent from the calichemicin family and is used in some cases of CD33+ AMLs(238-241). Conjugation of any of the blocking BETi (JQ1, OTX-015, CPI-0610) already described or the newer generation of BD1 vs BD2 specific BETi with antibodies recognizing specific monocytic AML surface markers may allow for lower effective doses, leading to less off-target activity. These would then

of course be combined with inhibitors more efficacious in undifferentiated AMLs such as BCL2i and CDK4/6i. These focused combinatorial approaches may be more effective in preventing tumor maturation escape and have increased tolerability in patients. Experimentally these novel inhibitors could be validated using the NSG-SGM3 mice (Jackson labs: #013062), which have been established as the optimal humanized mouse model for AML patient xenografts due to their superior engraftment in the bone marrow and reduced rejection rates(242,243). To start, I would generate xenograft models from patient bone marrow aspirates which were determined to have high expression of CSF1R or VCAN by RNA-seq within the Beat AML biorepository. I would then compare the efficacy of the novel agents vs classical BETi at low and high doses. I would assess tumor burden reduction in bulk via white blood cell counts throughout treatment, but also evaluate the phenotype of the circulating tumor cells in the blood via flow cytometry. I would expect that the targeted therapies would be more efficacious at lower doses and have lower mortality over older generation BETi (JQ1, etc.). Another route one could take with this model is to create xenografts of venetoclax refractory/acquired resistant patients and evaluate the efficacy of BETi, VCAN or CSF1R-BETi conjugate, or either combined with venetoclax. I would expect that, should the model be successful in mimicking venetoclax resistance post-transplantation, the targeted BETi would be superior in rescuing venetoclax resistance. I would also expect that combined inhibition would more effectively eliminate both monocytic AML cells (VCAN/CSF1R-BETi) and primitive AMLs (venetoclax).

Summary of T cell exhaustion project

In a novel spontaneous GEMM mouse model of AML, I showed the pre-clinical efficacy of BETi in combination with anti-PD1 in reducing tumor burden and priming immune responses. *In vivo* treatment with BETi generated $CD8^+$ T cells with a more stem-like

state that subsequently proliferated in response to ICB therapy. We further showed that AML patient samples with dysfunctional T cells were able to be rescued with *ex vivo* treatment with BETi. Further studies will seek to understand the complexities of mutational background on responsiveness to BETi + anti-PD1 in patient samples. We were able to rescue 3/5 AML patient samples, all with unique mutational backgrounds, who were refractory to anti-PD1 and TCR stimulation. We concluded with an analysis of the chromatin landscape of *in vivo* JQ1 treated $CD8^+$ T cells via s3-ATAC-seq which preliminary analyses point towards potentially reprogramming TEx cells.

The role of BET inhibition in T cell differentiation – Differentiation block or epigenetic reprogramming?

It is unclear how these mutational backgrounds influence T cell exhaustion and responses to BETi therapy in the context of T cell rescue. These works also suggest a novel role for BRD4 in regulation of T cell differentiation in response to different types of antigen exposure. It is unsurprising that BRD4 acts as a co-factor to regulate T cell differentiation, as has also been shown to be the case of myeloid differentiation, but it is unclear how this potentially changes in response to chronic vs. acute antigen exposures. Mechanistic understanding of how this occurs may provide valuable insights into basic immunological responses that govern memory formation.

One particular aspect of this proposed mechanism of BRD4 regulation of T cell differentiation that remains unanswered is whether BET inhibition directly reprograms exhausted T cells (i.e converts TEx back into functional TPEx T cells or related cell state) or prevents terminally differentiation from occurring (ie prevents transition from TPEx into TEx). It is possible that BET inhibition decreases activity of TCR-activated transcription factors which promote T cell exhaustion (e.g *Batf, Tox, Irf4,* etc.), thus preventing further differentiation of TPEx into TEx, and that the increased pool of TPEx T

cells arises entirely from new clones generated in response to ICB therapy. Alternatively, it is also possible that inhibition of the TCR-activated transcription factors reverses the exhaustion programs directly and allows for dedifferentiation of TEx back into functional TPEx T cells. It has been proposed recently that TEx cells are unable to be rescued, but these studies have largely focused on the ability of the T cells to regain function after serially transplanting or removing antigen, rather than attempting to reprogram the cells directly via epigenetic perturbation(101-103). Additionally, recent data has also pointed to polyclonality even within the TPEx cell populations. Burger *et al.* demonstrated that tumors generate many neoantigens that lead to T cell activation and, via a competitive mechanism, the suboptimally priming antigens drive a novel TPEx subpopulation denoted by expression of CCR6 that is, paradoxically, refractory to immunotherapy(244). To address the question of whether BETi reprogram or block Tex differentiation requires either a model system which controls for antigen exposure and BETi treatment or extremely deep single-cell ATAC/RNA-seq strategies. For the former, an OT-1 system could be utilized. OT-1 mice are genetically engineered to generate CD8+ T cells with TCRs that are selective for MHC I loaded with OVA peptides(245). Recent work has demonstrated the ability to generate exhausted T cells in vitro using OT-1/chicken ovalbumin antigen (OVA) strategies(246). In this system, exhausted OT-1 T cells are generated by serially pulsing with SIINFEKL (an OVA peptide). Thus I could potentially ask whether BETi reprogram or block differentiation (or both) by subjecting these cells to BETi in addition to SIINFEKL. In one condition I would add BETi at the same time as the first SIINFEKL stimulation. If this condition does not generate exhausted T cells than that would suggest that BETi block differentiation. Additionally, I would have a condition where I add BETi after the T cells have been exhausted via SIINFEKL stimulation. If these cells have less exhausted T cells after culturing than a control with SIINFEKL stimulation but no BETi, then that would suggest that BETi reprogram exhausted T cells.

Another, potentially more complicated, method would be to utilize the chronic LCMV models (Clone 13 or Docile strain) previously discussed(86,87) which generate exhausted T cells. In the same line of thinking as for the OT-1/OVA experiment I could take mice and treat with BETi before LCMV infection (blocking differentiation) and after LCMV induced exhaustion (reprogramming). The timelines are very well established as to when exhaustion should begin but, given my data demonstrating how myeloid cell differentiation is affected by BETi, I would optimally validate *in vitro* first. The aforementioned sequencing strategy I attempted and described the initial results of in chapter 3 but have not been able to adequately answer this question thus far but may with more thorough analyses. In this case I would expect to see a subpopulation of cells which originates from the TEx population and is re-expressing stem programs such as TCF1, EOMES, etc. My early analyses seems to point towards reprogramming Tex directly as evidenced by the increase in *Tcf7* accessibility specifically in Tex cells but more analyses need to be completed before I am confident in saying it is reprogramming and not blocking (or both). However, I do not believe this question needs to be answered to be convinced of the clinical potential of combining BETi and anti-PD1 therapies in AML.

It is clear that there are many facets of the proposed mechanism of BETi-mediated rescue of T cell exhaustion that need to be further investigated, but my data provides a starting point to begin to ask these questions and provides rationale for investigating the potential of other epigenetic modifying small-molecule inhibitors in rescuing ICB therapy refractoriness.

Summary of Functional Immune Landscape Project

This project is still in development, and is designed to be a hypothesis generating tool to be incorporated into the Beat AML database for public use. The goal of this project was

to utilize computational tools which can deconvolute bulk RNA-seq data to estimate cellular composition. Towards this end, we utilized the xCell webtool to estimate cellular proportions of bone marrow and peripheral blood samples within the Beat AML registry and demonstrated how they can be utilized to understand novel AML biologies. First, we described cellular compositions differentiated by specimen type and found that both accurately called cell types compared to available flow phenotyping. Additionally, we identified clusters of patients which had higher proportions of T cells, which may be associated with TP53 and IDH2 mutations. Additionally, these T cell high patients were exclusively in de novo and transformed samples. We further identified cell types which frequently co-occurred together and found that Tregs associate with monocytes and B cells and negatively associate with progenitor cells (CMP, GMP, etc.). We called cell types vs *ex vivo* drug responses and were able to validate previous works by me and others with monocytes correlating negatively (i.e higher monocytes meant higer effectiveness) with BETi and positively with Venetoclax and palbociclib (i.e higher monocytes meant decreased effectiveness). As a proof of principle, we utilized this approach to identify novel inhibitors with enhanced sensitivity in samples with higher proportions of Tregs and found multiple inhibitors of insulin growth factor signaling as a potential targetable axis. Finally, we utilized these same approaches to identify potential cellular contributions to *ex vivo* anti-PD1 therapy resistance based on data generated by Lamble and Kosaka *et al*.(195) and found that monocytes significantly correlated with aPD1 resistance.

Validation of *in silico* findings

The future directions of this project are clear: Biological validation. While the ultimate goal of this project is to incorporate the data into the publicly available Beat AML database (http://www.vizome.org/) as an exploratory tool, additional biological validation

is needed. In my initial analyses I was able to recapitulate my findings with monocytes correlating with BETi response but what remains is validation of any lymphoid cell type correlation. Lymphoid cells make up a much smaller fraction of the bone marrow and peripheral blood biopsies and are thus subject to much higher noise in terms of making proportion estimations. Thus, I would propose validation of the identified Treg biologies. One potential route would be to validate the responses of the IGF-1R inhibitors in confirmed Treg high samples. The inferences I am hoping these data can make are in the identification of inhibitors which may directly influence non-tumor cells, such as my work describing BETi in T cell differentiation. The inference based on these Treg data is that IGF-1R inhibitors may act directly on this cell type in addition to tumor cells. Thus, one pilot study I propose is to culture bone marrow/peripheral blood aspirate samples with and without the IGF-1R inhibitors and evaluate the responses in both tumor and Tregs via flow cytometry. Tregs are known to influence blast behavior via many mechanisms, such as cytokine secretions(247,248), so I would additionally evaluate the cytokines secreted via LegendPlex assays, in these culture experiments. For example, I could focus on known tumor-supportive Treg cytokines such as TNFa and IL-10 and assess whether IGF-1R inhibitors increased or decreased secretion. I would predict that IGF-1R inhibitors would decrease production of IL-10 and TNFa based on previous works discussed in chapter 4.

References

1. Orkin SH. Development of the hematopoietic system. Curr Opin Genet Dev **1996**;6(5):597-602 doi 10.1016/s0959-437x(96)80089-x.
2. Tavian M, Peault B. Embryonic development of the human hematopoietic system. Int J Dev Biol **2005**;49(2-3):243-50 doi 10.1387/ijdb.041957mt.
3. Jagannathan-Bogdan M, Zon LI. Hematopoiesis. Development **2013**;140(12):2463-7 doi 10.1242/dev.083147.
4. Sharma S, Gurudutta G. Epigenetic Regulation of Hematopoietic Stem Cells. Int J Stem Cells **2016**;9(1):36-43 doi 10.15283/ijsc.2016.9.1.36.
5. Sugimura R, Jha DK, Han A, Soria-Valles C, da Rocha EL, Lu YF*, et al.* Haematopoietic stem and progenitor cells from human pluripotent stem cells. Nature **2017**;545(7655):432-8 doi 10.1038/nature22370.
6. Birbrair A, Frenette PS. Niche heterogeneity in the bone marrow. Ann N Y Acad Sci **2016**;1370(1):82-96 doi 10.1111/nyas.13016.
7. Metcalf D. Hematopoietic cytokines. Blood **2008**;111(2):485-91 doi 10.1182/blood-2007-03-079681.
8. Seita J, Weissman IL. Hematopoietic stem cell: self-renewal versus differentiation. Wiley Interdiscip Rev Syst Biol Med **2010**;2(6):640-53 doi 10.1002/wsbm.86.
9. Murphy K, Paul Travers, Mark Walport, and Charles Janeway. Janeway's Immunobiology 9th Edition. **2008**.
10. Ciau-Uitz A, Wang L, Patient R, Liu F. ETS transcription factors in hematopoietic stem cell development. Blood Cells Mol Dis **2013**;51(4):248-55 doi 10.1016/j.bcmd.2013.07.010.
11. Gutierrez-Hartmann A, Duval DL, Bradford AP. ETS transcription factors in endocrine systems. Trends Endocrinol Metab **2007**;18(4):150-8 doi 10.1016/j.tem.2007.03.002.

12. Kastner P, Chan S. PU.1: a crucial and versatile player in hematopoiesis and leukemia. Int J Biochem Cell Biol **2008**;40(1):22-7 doi 10.1016/j.biocel.2007.01.026.

13. Oikawa T, Yamada T, Kihara-Negishi F, Yamamoto H, Kondoh N, Hitomi Y*, et al.* The role of Ets family transcription factor PU.1 in hematopoietic cell differentiation, proliferation and apoptosis. Cell Death Differ **1999**;6(7):599-608 doi 10.1038/sj.cdd.4400534.

14. van Riel B, Rosenbauer F. Epigenetic control of hematopoiesis: the PU.1 chromatin connection. Biol Chem **2014**;395(11):1265-74 doi 10.1515/hsz-2014-0195.

15. Fisher RC, Scott EW. Role of PU.1 in hematopoiesis. Stem Cells **1998**;16(1):25-37 doi 10.1002/stem.160025.

16. Pang WW, Schrier SL, Weissman IL. Age-associated changes in human hematopoietic stem cells. Semin Hematol **2017**;54(1):39-42 doi 10.1053/j.seminhematol.2016.10.004.

17. Dombret H, Gardin C. An update of current treatments for adult acute myeloid leukemia. Blood **2016**;127(1):53-61 doi 10.1182/blood-2015-08-604520.

18. Michel G, Baruchel A, Tabone MD, Nelken B, Leblanc T, Thuret I*, et al.* Induction chemotherapy followed by allogeneic bone marrow transplantation or aggressive consolidation chemotherapy in childhood acute myeloblastic leukemia. A prospective study from the French Society of Pediatric Hematology and Immunology (SHIP). Hematol Cell Ther **1996**;38(2):169-76 doi 10.1007/s00282-996-0169-7.

19. Lagunas-Rangel FA, Chavez-Valencia V, Gomez-Guijosa MA, Cortes-Penagos C. Acute Myeloid Leukemia-Genetic Alterations and Their Clinical Prognosis. Int J Hematol Oncol Stem Cell Res **2017**;11(4):328-39.

20. Tyner JW, Tognon CE, Bottomly D, Wilmot B, Kurtz SE, Savage SL*, et al.* Functional genomic landscape of acute myeloid leukaemia. Nature **2018**;562(7728):526-31 doi 10.1038/s41586-018-0623-z.

21. Arber DA. The 2016 WHO classification of acute myeloid leukemia: What the practicing clinician needs to know. Semin Hematol **2019**;56(2):90-5 doi 10.1053/j.seminhematol.2018.08.002.

22. Thein MS, Ershler WB, Jemal A, Yates JW, Baer MR. Outcome of older patients with acute myeloid leukemia: an analysis of SEER data over 3 decades. Cancer **2013**;119(15):2720-7 doi 10.1002/cncr.28129.

23. Sweeney C, Vyas P. The Graft-Versus-Leukemia Effect in AML. Front Oncol **2019**;9:1217 doi 10.3389/fonc.2019.01217.

24. Hagop M. Kantarjian MD TMKM, Courtney D. DiNardo MD, Mary Alma Welch MMSC, Farhad Ravandi MD. Acute myeloid leukemia: Treatment and research outlook for 2021 and the MD Anderson approach. Cancer **2021**;127(8):1186-207 doi 10.1002/cncr.33477.

25. Zhang J, Gu Y, Chen B. Mechanisms of drug resistance in acute myeloid leukemia. Onco Targets Ther **2019**;12:1937-45 doi 10.2147/OTT.S191621.

26. DiNardo CD, Rausch CR, Benton C, Kadia T, Jain N, Pemmaraju N*, et al.* Clinical experience with the BCL2-inhibitor venetoclax in combination therapy for relapsed and refractory acute myeloid leukemia and related myeloid malignancies. Am J Hematol **2018**;93(3):401-7 doi 10.1002/ajh.25000.

27. DiNardo CD, Jonas BA, Pullarkat V, Thirman MJ, Garcia JS, Wei AH*, et al.* Azacitidine and Venetoclax in Previously Untreated Acute Myeloid Leukemia. N Engl J Med **2020**;383(7):617-29 doi 10.1056/NEJMoa2012971.

28. Perl AE, Martinelli G, Cortes JE, Neubauer A, Berman E, Paolini S*, et al.* Gilteritinib or Chemotherapy for Relapsed or Refractory FLT3-Mutated AML. N Engl J Med **2019**;381(18):1728-40 doi 10.1056/NEJMoa1902688.

29. B.J. Bain LE. FAB Classification of Leukemia. Brenner's Encyclopedia of Genetics (Second Edition) **2013**:5-7 doi 10.1016/B978-0-12-374984-0.00515-5.

30. Vardiman JW, Harris NL, Brunning RD. The World Health Organization (WHO) classification of the myeloid neoplasms. Blood **2002**;100(7):2292-302 doi 10.1182/blood-2002-04-1199.

31. Ghavamzadeh A, Alimoghaddam K, Ghaffari SH, Rostami S, Jahani M, Hosseini R*, et al.* Treatment of acute promyelocytic leukemia with arsenic trioxide without ATRA and/or chemotherapy. Ann Oncol **2006**;17(1):131-4 doi 10.1093/annonc/mdj019.

32. Huang ME, Ye YC, Chen SR, Chai JR, Lu JX, Zhoa L*, et al.* Use of all-trans retinoic acid in the treatment of acute promyelocytic leukemia. Blood **1988**;72(2):567-72.

33. Fenaux P, Wang ZZ, Degos L. Treatment of acute promyelocytic leukemia by retinoids. Curr Top Microbiol Immunol **2007**;313:101-28 doi 10.1007/978-3-540-34594-7_7.

34. Wang F, Liu H, Blanton WP, Belkina A, Lebrasseur NK, Denis GV. Brd2 disruption in mice causes severe obesity without Type 2 diabetes. Biochem J **2009**;425(1):71-83 doi 10.1042/BJ20090928.

35. Wang N, Wu R, Tang D, Kang R. The BET family in immunity and disease. Signal Transduct Target Ther **2021**;6(1):23 doi 10.1038/s41392-020-00384-4.

36. Shang E, Wang X, Wen D, Greenberg DA, Wolgemuth DJ. Double bromodomain-containing gene Brd2 is essential for embryonic development in mouse. Dev Dyn **2009**;238(4):908-17 doi 10.1002/dvdy.21911.

37. Dhalluin C, Carlson JE, Zeng L, He C, Aggarwal AK, Zhou MM. Structure and ligand of a histone acetyltransferase bromodomain. Nature **1999**;399(6735):491-6 doi 10.1038/20974.

38. Zeng L, Zhou MM. Bromodomain: an acetyl-lysine binding domain. FEBS Lett **2002**;513(1):124-8 doi 10.1016/s0014-5793(01)03309-9.

39. Wu SY, Chiang CM. The double bromodomain-containing chromatin adaptor Brd4 and transcriptional regulation. J Biol Chem **2007**;282(18):13141-5 doi 10.1074/jbc.R700001200.

40. Baranello L, Wojtowicz D, Cui K, Devaiah BN, Chung HJ, Chan-Salis KY*, et al.* RNA Polymerase II Regulates Topoisomerase 1 Activity to Favor Efficient Transcription. Cell **2016**;165(2):357-71 doi 10.1016/j.cell.2016.02.036.

41. Zhang P, Wang D, Zhao Y, Ren S, Gao K, Ye Z*, et al.* Intrinsic BET inhibitor resistance in SPOP-mutated prostate cancer is mediated by BET protein stabilization and AKT-mTORC1 activation. Nat Med **2017**;23(9):1055-62 doi 10.1038/nm.4379.

42. Dey A, Nishiyama A, Karpova T, McNally J, Ozato K. Brd4 marks select genes on mitotic chromatin and directs postmitotic transcription. Mol Biol Cell **2009**;20(23):4899-909 doi 10.1091/mbc.E09-05-0380.

43. Dey A, Chitsaz F, Abbasi A, Misteli T, Ozato K. The double bromodomain protein Brd4 binds to acetylated chromatin during interphase and mitosis. Proc Natl Acad Sci U S A **2003**;100(15):8758-63 doi 10.1073/pnas.1433065100.

44. Dey A, Ellenberg J, Farina A, Coleman AE, Maruyama T, Sciortino S*, et al.* A bromodomain protein, MCAP, associates with mitotic chromosomes and affects G(2)-to-M transition. Mol Cell Biol **2000**;20(17):6537-49 doi 10.1128/MCB.20.17.6537-6549.2000.

45. Liu W, Stein P, Cheng X, Yang W, Shao NY, Morrisey EE*, et al.* BRD4 regulates Nanog expression in mouse embryonic stem cells and preimplantation embryos. Cell Death Differ **2014**;21(12):1950-60 doi 10.1038/cdd.2014.124.

46. Wu T, Pinto HB, Kamikawa YF, Donohoe ME. The BET family member BRD4 interacts with OCT4 and regulates pluripotency gene expression. Stem Cell Reports **2015**;4(3):390-403 doi 10.1016/j.stemcr.2015.01.012.

47. Najafova Z, Tirado-Magallanes R, Subramaniam M, Hossan T, Schmidt G, Nagarajan S*, et al.* BRD4 localization to lineage-specific enhancers is associated with a distinct transcription factor repertoire. Nucleic Acids Res **2017**;45(1):127-41 doi 10.1093/nar/gkw826.

48. Lee JE, Park YK, Park S, Jang Y, Waring N, Dey A*, et al.* Brd4 binds to active enhancers to control cell identity gene induction in adipogenesis and myogenesis. Nat Commun **2017**;8(1):2217 doi 10.1038/s41467-017-02403-5.

49. Sabari BR, Dall'Agnese A, Boija A, Klein IA, Coffey EL, Shrinivas K*, et al.* Coactivator condensation at super-enhancers links phase separation and gene control. Science **2018**;361(6400) doi 10.1126/science.aar3958.

50. Tasdemir N, Banito A, Roe JS, Alonso-Curbelo D, Camiolo M, Tschaharganeh DF*, et al.* BRD4 Connects Enhancer Remodeling to Senescence Immune Surveillance. Cancer Discov **2016**;6(6):612-29 doi 10.1158/2159-8290.CD-16-0217.

51. Donati B, Lorenzini E, Ciarrocchi A. BRD4 and Cancer: going beyond transcriptional regulation. Mol Cancer **2018**;17(1):164 doi 10.1186/s12943-018-0915-9.

52. Liu W, Ma Q, Wong K, Li W, Ohgi K, Zhang J*, et al.* Brd4 and JMJD6-associated anti-pause enhancers in regulation of transcriptional pause release. Cell **2013**;155(7):1581-95 doi 10.1016/j.cell.2013.10.056.

53. Lamonica JM, Deng W, Kadauke S, Campbell AE, Gamsjaeger R, Wang H*, et al.* Bromodomain protein Brd3 associates with acetylated GATA1 to promote its chromatin

occupancy at erythroid target genes. Proc Natl Acad Sci U S A **2011**;108(22):E159-68 doi 10.1073/pnas.1102140108.

54. Maruyama T, Farina A, Dey A, Cheong J, Bermudez VP, Tamura T*, et al.* A Mammalian bromodomain protein, brd4, interacts with replication factor C and inhibits progression to S phase. Mol Cell Biol **2002**;22(18):6509-20 doi 10.1128/MCB.22.18.6509-6520.2002.

55. Moriniere J, Rousseaux S, Steuerwald U, Soler-Lopez M, Curtet S, Vitte AL*, et al.* Cooperative binding of two acetylation marks on a histone tail by a single bromodomain. Nature **2009**;461(7264):664-8 doi 10.1038/nature08397.

56. Filippakopoulos P, Picaud S, Mangos M, Keates T, Lambert JP, Barsyte-Lovejoy D*, et al.* Histone recognition and large-scale structural analysis of the human bromodomain family. Cell **2012**;149(1):214-31 doi 10.1016/j.cell.2012.02.013.

57. Gamsjaeger R, Webb SR, Lamonica JM, Billin A, Blobel GA, Mackay JP. Structural basis and specificity of acetylated transcription factor GATA1 recognition by BET family bromodomain protein Brd3. Mol Cell Biol **2011**;31(13):2632-40 doi 10.1128/MCB.05413-11.

58. Miller TC, Simon B, Rybin V, Grotsch H, Curtet S, Khochbin S*, et al.* A bromodomain-DNA interaction facilitates acetylation-dependent bivalent nucleosome recognition by the BET protein BRDT. Nat Commun **2016**;7:13855 doi 10.1038/ncomms13855.

59. Uppal S, Gegonne A, Chen Q, Thompson PS, Cheng D, Mu J*, et al.* The Bromodomain Protein 4 Contributes to the Regulation of Alternative Splicing. Cell Rep **2019**;29(8):2450-60 e5 doi 10.1016/j.celrep.2019.10.066.

60. Devaiah BN, Case-Borden C, Gegonne A, Hsu CH, Chen Q, Meerzaman D*, et al.* BRD4 is a histone acetyltransferase that evicts nucleosomes from chromatin. Nat Struct Mol Biol **2016**;23(6):540-8 doi 10.1038/nsmb.3228.

61. Devaiah BN, Lewis BA, Cherman N, Hewitt MC, Albrecht BK, Robey PG*, et al.* BRD4 is an atypical kinase that phosphorylates serine2 of the RNA polymerase II carboxy-terminal domain. Proc Natl Acad Sci U S A **2012**;109(18):6927-32 doi 10.1073/pnas.1120422109.

62. French CA. Demystified molecular pathology of NUT midline carcinomas. J Clin Pathol **2010**;63(6):492-6 doi 10.1136/jcp.2007.052902.

63. French CA, Miyoshi I, Kubonishi I, Grier HE, Perez-Atayde AR, Fletcher JA. BRD4-NUT fusion oncogene: a novel mechanism in aggressive carcinoma. Cancer Res **2003**;63(2):304-7.

64. Wang R, Liu W, Helfer CM, Bradner JE, Hornick JL, Janicki SM*, et al.* Activation of SOX2 expression by BRD4-NUT oncogenic fusion drives neoplastic transformation in NUT midline carcinoma. Cancer Res **2014**;74(12):3332-43 doi 10.1158/0008-5472.CAN-13-2658.

65. Costa FA, Amano MT, Asprino PF, Pavlick DC, Masotti C, Testagrossa L*, et al.* Revealing the BRD4-NOTCH3 fusion: A novel hill in the cancer landscape. Lung Cancer **2021**;154:146-50 doi 10.1016/j.lungcan.2021.02.016.

66. Dang CV. MYC on the path to cancer. Cell **2012**;149(1):22-35 doi 10.1016/j.cell.2012.03.003.

67. Delmore JE, Issa GC, Lemieux ME, Rahl PB, Shi J, Jacobs HM*, et al.* BET bromodomain inhibition as a therapeutic strategy to target c-Myc. Cell **2011**;146(6):904-17 doi 10.1016/j.cell.2011.08.017.

68. Roe JS, Vakoc CR. The Essential Transcriptional Function of BRD4 in Acute Myeloid Leukemia. Cold Spring Harb Symp Quant Biol **2016**;81:61-6 doi 10.1101/sqb.2016.81.031039.

69. Filippakopoulos P, Qi J, Picaud S, Shen Y, Smith WB, Fedorov O*, et al.* Selective inhibition of BET bromodomains. Nature **2010**;468(7327):1067-73 doi 10.1038/nature09504.

70. Albrecht BK, Gehling VS, Hewitt MC, Vaswani RG, Cote A, Leblanc Y*, et al.* Identification of a Benzoisoxazoloazepine Inhibitor (CPI-0610) of the Bromodomain and Extra-Terminal (BET) Family as a Candidate for Human Clinical Trials. J Med Chem **2016**;59(4):1330-9 doi 10.1021/acs.jmedchem.5b01882.

71. Shi X, Liu C, Liu B, Chen J, Wu X, Gong W. JQ1: a novel potential therapeutic target. Pharmazie **2018**;73(9):491-3 doi 10.1691/ph.2018.8480.

72. Dawson MA, Prinjha RK, Dittmann A, Giotopoulos G, Bantscheff M, Chan WI*, et al.* Inhibition of BET recruitment to chromatin as an effective treatment for MLL-fusion leukaemia. Nature **2011**;478(7370):529-33 doi 10.1038/nature10509.

73. Dawson MA, Gudgin EJ, Horton SJ, Giotopoulos G, Meduri E, Robson S*, et al.* Recurrent mutations, including NPM1c, activate a BRD4-dependent core transcriptional program in acute myeloid leukemia. Leukemia **2014**;28(2):311-20 doi 10.1038/leu.2013.338.

74. Zuber J, Shi J, Wang E, Rappaport AR, Herrmann H, Sison EA*, et al.* RNAi screen identifies Brd4 as a therapeutic target in acute myeloid leukaemia. Nature **2011**;478(7370):524-8 doi 10.1038/nature10334.

75. Mertz JA, Conery AR, Bryant BM, Sandy P, Balasubramanian S, Mele DA*, et al.* Targeting MYC dependence in cancer by inhibiting BET bromodomains. Proc Natl Acad Sci U S A **2011**;108(40):16669-74 doi 10.1073/pnas.1108190108.

76. Coude MM, Braun T, Berrou J, Dupont M, Bertrand S, Masse A*, et al.* BET inhibitor OTX015 targets BRD2 and BRD4 and decreases c-MYC in acute leukemia cells. Oncotarget **2015**;6(19):17698-712 doi 10.18632/oncotarget.4131.

77. Braun T, Gardin C. Investigational BET bromodomain protein inhibitors in early stage clinical trials for acute myelogenous leukemia (AML). Expert Opin Investig Drugs **2017**;26(7):803-11 doi 10.1080/13543784.2017.1335711.

78. Piya S, Mu H, Bhattacharya S, Lorenzi PL, Davis RE, McQueen T*, et al.* BETP degradation simultaneously targets acute myelogenous leukemia stem cells and the microenvironment. J Clin Invest **2019**;129(5):1878-94 doi 10.1172/JCI120654.

79. Yang CY, Qin C, Bai L, Wang S. Small-molecule PROTAC degraders of the Bromodomain and Extra Terminal (BET) proteins - A review. Drug Discov Today Technol **2019**;31:43-51 doi 10.1016/j.ddtec.2019.04.001.

80. Ocana A, Pandiella A. Proteolysis targeting chimeras (PROTACs) in cancer therapy. J Exp Clin Cancer Res **2020**;39(1):189 doi 10.1186/s13046-020-01672-1.

81. Gilan O, Rioja I, Knezevic K, Bell MJ, Yeung MM, Harker NR*, et al.* Selective targeting of BD1 and BD2 of the BET proteins in cancer and immunoinflammation. Science **2020**;368(6489):387-94 doi 10.1126/science.aaz8455.

82. Berthon C, Raffoux E, Thomas X, Vey N, Gomez-Roca C, Yee K*, et al.* Bromodomain inhibitor OTX015 in patients with acute leukaemia: a dose-escalation, phase 1 study. Lancet Haematol **2016**;3(4):e186-95 doi 10.1016/S2352-3026(15)00247-1.

83. Starr TK, Jameson SC, Hogquist KA. Positive and negative selection of T cells. Annu Rev Immunol **2003**;21:139-76 doi 10.1146/annurev.immunol.21.120601.141107.

84. Hivroz C, Chemin K, Tourret M, Bohineust A. Crosstalk between T lymphocytes and dendritic cells. Crit Rev Immunol **2012**;32(2):139-55 doi 10.1615/critrevimmunol.v32.i2.30.

85. Prlic M, Bevan MJ. Exploring regulatory mechanisms of CD8+ T cell contraction. Proc Natl Acad Sci U S A **2008**;105(43):16689-94 doi 10.1073/pnas.0808997105.

86. Utzschneider DT, Gabriel SS, Chisanga D, Gloury R, Gubser PM, Vasanthakumar A*, et al.* Early precursor T cells establish and propagate T cell exhaustion in chronic infection. Nat Immunol **2020**;21(10):1256-66 doi 10.1038/s41590-020-0760-z.

87. Man K, Gabriel SS, Liao Y, Gloury R, Preston S, Henstridge DC*, et al.* Transcription Factor IRF4 Promotes CD8(+) T Cell Exhaustion and Limits the Development of Memory-like T Cells during Chronic Infection. Immunity **2017**;47(6):1129-41 e5 doi 10.1016/j.immuni.2017.11.021.

88. Chung HK, McDonald B, Kaech SM. The architectural design of CD8+ T cell responses in acute and chronic infection: Parallel structures with divergent fates. J Exp Med **2021**;218(4) doi 10.1084/jem.20201730.

89. Blank CU, Haining WN, Held W, Hogan PG, Kallies A, Lugli E*, et al.* Defining 'T cell exhaustion'. Nat Rev Immunol **2019**;19(11):665-74 doi 10.1038/s41577-019-0221-9.

90. Wang Y, Hu J, Li Y, Xiao M, Wang H, Tian Q*, et al.* The Transcription Factor TCF1 Preserves the Effector Function of Exhausted CD8 T Cells During Chronic Viral Infection. Front Immunol **2019**;10:169 doi 10.3389/fimmu.2019.00169.

91. Chen Z, Ji Z, Ngiow SF, Manne S, Cai Z, Huang AC*, et al.* TCF-1-Centered Transcriptional Network Drives an Effector versus Exhausted CD8 T Cell-Fate Decision. Immunity **2019**;51(5):840-55 e5 doi 10.1016/j.immuni.2019.09.013.

92. Khan O, Giles JR, McDonald S, Manne S, Ngiow SF, Patel KP*, et al.* TOX transcriptionally and epigenetically programs CD8(+) T cell exhaustion. Nature **2019**;571(7764):211-8 doi 10.1038/s41586-019-1325-x.

93. Scott AC, Dundar F, Zumbo P, Chandran SS, Klebanoff CA, Shakiba M*, et al.* TOX is a critical regulator of tumour-specific T cell differentiation. Nature **2019**;571(7764):270-4 doi 10.1038/s41586-019-1324-y.

94. Seo H, Chen J, Gonzalez-Avalos E, Samaniego-Castruita D, Das A, Wang YH*, et al.* TOX and TOX2 transcription factors cooperate with NR4A transcription factors to impose CD8(+) T cell exhaustion. Proc Natl Acad Sci U S A **2019**;116(25):12410-5 doi 10.1073/pnas.1905675116.

95. Scott-Browne JP, Lopez-Moyado IF, Trifari S, Wong V, Chavez L, Rao A*, et al.* Dynamic Changes in Chromatin Accessibility Occur in CD8(+) T Cells Responding to Viral Infection. Immunity **2016**;45(6):1327-40 doi 10.1016/j.immuni.2016.10.028.

96. Dolina JS, Van Braeckel-Budimir N, Thomas GD, Salek-Ardakani S. CD8(+) T Cell Exhaustion in Cancer. Front Immunol **2021**;12:715234 doi 10.3389/fimmu.2021.715234.

97. Escobar G, Mangani D, Anderson AC. T cell factor 1: A master regulator of the T cell response in disease. Sci Immunol **2020**;5(53) doi 10.1126/sciimmunol.abb9726.

98. Leong YA, Chen Y, Ong HS, Wu D, Man K, Deleage C*, et al.* CXCR5(+) follicular cytotoxic T cells control viral infection in B cell follicles. Nat Immunol **2016**;17(10):1187-96 doi 10.1038/ni.3543.

99. Wu T, Ji Y, Moseman EA, Xu HC, Manglani M, Kirby M*, et al.* The TCF1-Bcl6 axis counteracts type I interferon to repress exhaustion and maintain T cell stemness. Sci Immunol **2016**;1(6) doi 10.1126/sciimmunol.aai8593.

100. Im SJ, Hashimoto M, Gerner MY, Lee J, Kissick HT, Burger MC*, et al.* Defining CD8+ T cells that provide the proliferative burst after PD-1 therapy. Nature **2016**;537(7620):417-21 doi 10.1038/nature19330.

101. Abdel-Hakeem MS, Manne S, Beltra JC, Stelekati E, Chen Z, Nzingha K*, et al.* Epigenetic scarring of exhausted T cells hinders memory differentiation upon eliminating chronic antigenic stimulation. Nat Immunol **2021**;22(8):1008-19 doi 10.1038/s41590-021-00975-5.

102. Barber DL, Wherry EJ, Masopust D, Zhu B, Allison JP, Sharpe AH*, et al.* Restoring function in exhausted CD8 T cells during chronic viral infection. Nature **2006**;439(7077):682-7 doi 10.1038/nature04444.

103. Beltra JC, Manne S, Abdel-Hakeem MS, Kurachi M, Giles JR, Chen Z*, et al.* Developmental Relationships of Four Exhausted CD8(+) T Cell Subsets Reveals Underlying Transcriptional and Epigenetic Landscape Control Mechanisms. Immunity **2020**;52(5):825-41 e8 doi 10.1016/j.immuni.2020.04.014.

104. Yao C, Sun HW, Lacey NE, Ji Y, Moseman EA, Shih HY*, et al.* Single-cell RNA-seq reveals TOX as a key regulator of CD8(+) T cell persistence in chronic infection. Nat Immunol **2019**;20(7):890-901 doi 10.1038/s41590-019-0403-4.

105. Philip M, Fairchild L, Sun L, Horste EL, Camara S, Shakiba M*, et al.* Chromatin states define tumour-specific T cell dysfunction and reprogramming. Nature **2017**;545(7655):452-6 doi 10.1038/nature22367.

106. Miller BC, Sen DR, Al Abosy R, Bi K, Virkud YV, LaFleur MW*, et al.* Subsets of exhausted CD8(+) T cells differentially mediate tumor control and respond to checkpoint blockade. Nat Immunol **2019**;20(3):326-36 doi 10.1038/s41590-019-0312-6.

107. Ghoneim HE, Fan Y, Moustaki A, Abdelsamed HA, Dash P, Dogra P*, et al.* De Novo Epigenetic Programs Inhibit PD-1 Blockade-Mediated T Cell Rejuvenation. Cell **2017**;170(1):142-57 e19 doi 10.1016/j.cell.2017.06.007.

108. Liu X, Wang Y, Lu H, Li J, Yan X, Xiao M*, et al.* Genome-wide analysis identifies NR4A1 as a key mediator of T cell dysfunction. Nature **2019**;567(7749):525-9 doi 10.1038/s41586-019-0979-8.

109. Sharma P, Allison JP. The future of immune checkpoint therapy. Science **2015**;348(6230):56-61 doi 10.1126/science.aaa8172.

110. Wei SC, Duffy CR, Allison JP. Fundamental Mechanisms of Immune Checkpoint Blockade Therapy. Cancer Discov **2018**;8(9):1069-86 doi 10.1158/2159-8290.CD-18-0367.

111. Arasanz H, Gato-Canas M, Zuazo M, Ibanez-Vea M, Breckpot K, Kochan G*, et al.* PD1 signal transduction pathways in T cells. Oncotarget **2017**;8(31):51936-45 doi 10.18632/oncotarget.17232.

112. Sanmamed MF, Chen L. Inducible expression of B7-H1 (PD-L1) and its selective role in tumor site immune modulation. Cancer J **2014**;20(4):256-61 doi 10.1097/PPO.0000000000000061.

113. Mandai M, Hamanishi J, Abiko K, Matsumura N, Baba T, Konishi I. Dual Faces of IFNgamma in Cancer Progression: A Role of PD-L1 Induction in the Determination of Pro- and Antitumor Immunity. Clin Cancer Res **2016**;22(10):2329-34 doi 10.1158/1078-0432.CCR-16-0224.

114. Abiko K, Matsumura N, Hamanishi J, Horikawa N, Murakami R, Yamaguchi K*, et al.* IFN-gamma from lymphocytes induces PD-L1 expression and promotes progression of ovarian cancer. Br J Cancer **2015**;112(9):1501-9 doi 10.1038/bjc.2015.101.

115. Sheppard KA, Fitz LJ, Lee JM, Benander C, George JA, Wooters J*, et al.* PD-1 inhibits T-cell receptor induced phosphorylation of the ZAP70/CD3zeta signalosome and downstream signaling to PKCtheta. FEBS Lett **2004**;574(1-3):37-41 doi 10.1016/j.febslet.2004.07.083.

116. Hui E, Cheung J, Zhu J, Su X, Taylor MJ, Wallweber HA*, et al.* T cell costimulatory receptor CD28 is a primary target for PD-1-mediated inhibition. Science **2017**;355(6332):1428-33 doi 10.1126/science.aaf1292.

117. Patsoukis N, Brown J, Petkova V, Liu F, Li L, Boussiotis VA. Selective effects of PD-1 on Akt and Ras pathways regulate molecular components of the cell cycle and inhibit T cell proliferation. Sci Signal **2012**;5(230):ra46 doi 10.1126/scisignal.2002796.

118. Patsoukis N, Sari D, Boussiotis VA. PD-1 inhibits T cell proliferation by upregulating p27 and p15 and suppressing Cdc25A. Cell Cycle **2012**;11(23):4305-9 doi 10.4161/cc.22135.

119. Patsoukis N, Li L, Sari D, Petkova V, Boussiotis VA. PD-1 increases PTEN phosphatase activity while decreasing PTEN protein stability by inhibiting casein kinase 2. Mol Cell Biol **2013**;33(16):3091-8 doi 10.1128/MCB.00319-13.

120. Naramura M, Jang IK, Kole H, Huang F, Haines D, Gu H. c-Cbl and Cbl-b regulate T cell responsiveness by promoting ligand-induced TCR down-modulation. Nat Immunol **2002**;3(12):1192-9 doi 10.1038/ni855.

121. Shamim M, Nanjappa SG, Singh A, Plisch EH, LeBlanc SE, Walent J*, et al.* Cbl-b regulates antigen-induced TCR down-regulation and IFN-gamma production by effector CD8 T cells without affecting functional avidity. J Immunol **2007**;179(11):7233-43 doi 10.4049/jimmunol.179.11.7233.

122. Karwacz K, Bricogne C, MacDonald D, Arce F, Bennett CL, Collins M*, et al.* PD-L1 co-stimulation contributes to ligand-induced T cell receptor down-modulation on CD8+ T cells. EMBO Mol Med **2011**;3(10):581-92 doi 10.1002/emmm.201100165.

123. Carretero-Gonzalez A, Lora D, Ghanem I, Zugazagoitia J, Castellano D, Sepulveda JM*, et al.* Analysis of response rate with ANTI PD1/PD-L1 monoclonal antibodies in advanced solid tumors: a meta-analysis of randomized clinical trials. Oncotarget **2018**;9(9):8706-15 doi 10.18632/oncotarget.24283.

124. Specenier P. Nivolumab in melanoma. Expert Rev Anticancer Ther **2016**;16(12):1247-61 doi 10.1080/14737140.2016.1249856.

125. Jadhav RR, Im SJ, Hu B, Hashimoto M, Li P, Lin JX*, et al.* Epigenetic signature of PD-1+ TCF1+ CD8 T cells that act as resource cells during chronic viral infection and respond to

PD-1 blockade. Proc Natl Acad Sci U S A **2019**;116(28):14113-8 doi 10.1073/pnas.1903520116.

126. Siddiqui I, Schaeuble K, Chennupati V, Fuertes Marraco SA, Calderon-Copete S, Pais Ferreira D*, et al.* Intratumoral Tcf1(+)PD-1(+)CD8(+) T Cells with Stem-like Properties Promote Tumor Control in Response to Vaccination and Checkpoint Blockade Immunotherapy. Immunity **2019**;50(1):195-211 e10 doi 10.1016/j.immuni.2018.12.021.

127. Sade-Feldman M, Yizhak K, Bjorgaard SL, Ray JP, de Boer CG, Jenkins RW*, et al.* Defining T Cell States Associated with Response to Checkpoint Immunotherapy in Melanoma. Cell **2018**;175(4):998-1013 e20 doi 10.1016/j.cell.2018.10.038.

128. Tan J, Yu Z, Huang J, Chen Y, Huang S, Yao D*, et al.* Increased PD-1+Tim-3+ exhausted T cells in bone marrow may influence the clinical outcome of patients with AML. Biomark Res **2020**;8:6 doi 10.1186/s40364-020-0185-8.

129. Brummelman J, Mazza EMC, Alvisi G, Colombo FS, Grilli A, Mikulak J*, et al.* High-dimensional single cell analysis identifies stem-like cytotoxic CD8(+) T cells infiltrating human tumors. J Exp Med **2018**;215(10):2520-35 doi 10.1084/jem.20180684.

130. Wang JC, Xu Y, Huang ZM, Lu XJ. T cell exhaustion in cancer: Mechanisms and clinical implications. J Cell Biochem **2018**;119(6):4279-86 doi 10.1002/jcb.26645.

131. DiNardo CD, Cortes JE. Mutations in AML: prognostic and therapeutic implications. Hematology Am Soc Hematol Educ Program **2016**;2016(1):348-55 doi 10.1182/asheducation-2016.1.348.

132. Kim TK, Gore SD, Zeidan AM. Epigenetic Therapy in Acute Myeloid Leukemia: Current and Future Directions. Semin Hematol **2015**;52(3):172-83 doi 10.1053/j.seminhematol.2015.04.003.

133. Yang Z, Yik JH, Chen R, He N, Jang MK, Ozato K*, et al.* Recruitment of P-TEFb for stimulation of transcriptional elongation by the bromodomain protein Brd4. Mol Cell **2005**;19(4):535-45 doi 10.1016/j.molcel.2005.06.029.

134. Shi J, Vakoc CR. The mechanisms behind the therapeutic activity of BET bromodomain inhibition. Mol Cell **2014**;54(5):728-36 doi 10.1016/j.molcel.2014.05.016.

135. Jang JE, Eom JI, Jeung HK, Cheong JW, Lee JY, Kim JS*, et al.* AMPK-ULK1-Mediated Autophagy Confers Resistance to BET Inhibitor JQ1 in Acute Myeloid Leukemia Stem Cells. Clin Cancer Res **2017**;23(11):2781-94 doi 10.1158/1078-0432.CCR-16-1903.

136. Rathert P, Roth M, Neumann T, Muerdter F, Roe JS, Muhar M*, et al.* Transcriptional plasticity promotes primary and acquired resistance to BET inhibition. Nature **2015**;525(7570):543-7 doi 10.1038/nature14898.

137. Fong CY, Gilan O, Lam EY, Rubin AF, Ftouni S, Tyler D*, et al.* BET inhibitor resistance emerges from leukaemia stem cells. Nature **2015**;525(7570):538-42 doi 10.1038/nature14888.

138. Shu S, Lin CY, He HH, Witwicki RM, Tabassum DP, Roberts JM*, et al.* Response and resistance to BET bromodomain inhibitors in triple-negative breast cancer. Nature **2016**;529(7586):413-7 doi 10.1038/nature16508.

139. Bell CC, Fennell KA, Chan YC, Rambow F, Yeung MM, Vassiliadis D*, et al.* Targeting enhancer switching overcomes non-genetic drug resistance in acute myeloid leukaemia. Nat Commun **2019**;10(1):2723 doi 10.1038/s41467-019-10652-9.

140. Majumder MM, Leppa AM, Hellesoy M, Dowling P, Malyutina A, Kopperud R*, et al.* Multi-parametric single cell evaluation defines distinct drug responses in healthy hematological cells that are retained in corresponding malignant cell types. Haematologica **2019** doi 10.3324/haematol.2019.217414.

141. Kuusanmaki H, Leppa AM, Polonen P, Kontro M, Dufva O, Deb D*, et al.* Phenotype-based drug screening reveals association between venetoclax response and differentiation stage in acute myeloid leukemia. Haematologica **2020**;105(3):708-20 doi 10.3324/haematol.2018.214882.

142. Pei S, Pollyea DA, Gustafson A, Stevens BM, Minhajuddin M, Fu R*, et al.* Monocytic Subclones Confer Resistance to Venetoclax-Based Therapy in Patients with Acute Myeloid Leukemia. Cancer Discov **2020**;10(4):536-51 doi 10.1158/2159-8290.CD-19-0710.

143. Zhang H, Nakauchi, Y, Koehnke, T, Stafford, M, Bottomly, D, Thomas, R, Wilmot, B, McWeeney, SK, Majeti, R & Tyner, JW. Biomarkers predicting venetoclax efficacy and venetoclax combination strategies. Nature Cancer **2020**.

144. McCarthy DJ, Chen Y, Smyth GK. Differential expression analysis of multifactor RNA-Seq experiments with respect to biological variation. Nucleic Acids Res **2012**;40(10):4288-97 doi 10.1093/nar/gks042.

145. Nechiporuk T, Kurtz SE, Nikolova O, Liu T, Jones CL, D'Alessandro A*, et al.* The TP53 Apoptotic Network is a Primary Mediator of Resistance to BCL2 inhibition in AML Cells. Cancer Discov **2019** doi 10.1158/2159-8290.CD-19-0125.

146. Szklarczyk D, Gable AL, Lyon D, Junge A, Wyder S, Huerta-Cepas J*, et al.* STRING v11: protein-protein association networks with increased coverage, supporting functional discovery in genome-wide experimental datasets. Nucleic Acids Res **2019**;47(D1):D607-D13 doi 10.1093/nar/gky1131.

147. Roe JS, Mercan F, Rivera K, Pappin DJ, Vakoc CR. BET Bromodomain Inhibition Suppresses the Function of Hematopoietic Transcription Factors in Acute Myeloid Leukemia. Mol Cell **2015**;58(6):1028-39 doi 10.1016/j.molcel.2015.04.011.

148. Fiskus W, Sharma S, Qi J, Valenta JA, Schaub LJ, Shah B*, et al.* Highly active combination of BRD4 antagonist and histone deacetylase inhibitor against human acute myelogenous leukemia cells. Mol Cancer Ther **2014**;13(5):1142-54 doi 10.1158/1535-7163.MCT-13-0770.

149. Bunaciu RP, MacDonald RJ, Jensen HA, Gao F, Wang X, Johnson L*, et al.* Retinoic acid and 6-formylindolo(3,2-b)carbazole (FICZ) combination therapy reveals putative targets for enhancing response in non-APL AML. Leuk Lymphoma **2019**;60(7):1697-708 doi 10.1080/10428194.2018.1543880.

150. Hestermann EV, Brown M. Agonist and chemopreventative ligands induce differential transcriptional cofactor recruitment by aryl hydrocarbon receptor. Mol Cell Biol **2003**;23(21):7920-5 doi 10.1128/mcb.23.21.7920-7925.2003.

151. Tian Y, Ke S, Chen M, Sheng T. Interactions between the aryl hydrocarbon receptor and P-TEFb. Sequential recruitment of transcription factors and differential phosphorylation of C-terminal domain of RNA polymerase II at cyp1a1 promoter. J Biol Chem **2003**;278(45):44041-8 doi 10.1074/jbc.M306443200.

152. Wang S, Ge K, Roeder RG, Hankinson O. Role of mediator in transcriptional activation by the aryl hydrocarbon receptor. J Biol Chem **2004**;279(14):13593-600 doi 10.1074/jbc.M312274200.

153. Tasseff R, Jensen HA, Congleton J, Dai D, Rogers KV, Sagar A*, et al.* An Effective Model of the Retinoic Acid Induced HL-60 Differentiation Program. Sci Rep **2017**;7(1):14327 doi 10.1038/s41598-017-14523-5.

154. McKeown MR, Corces MR, Eaton ML, Fiore C, Lee E, Lopez JT*, et al.* Superenhancer Analysis Defines Novel Epigenomic Subtypes of Non-APL AML, Including an RARalpha

Dependency Targetable by SY-1425, a Potent and Selective RARalpha Agonist. Cancer Discov **2017**;7(10):1136-53 doi 10.1158/2159-8290.CD-17-0399.

155. Yang X, Solomon S, Fraser LR, Trombino AF, Liu D, Sonenshein GE*, et al.* Constitutive regulation of CYP1B1 by the aryl hydrocarbon receptor (AhR) in pre-malignant and malignant mammary tissue. J Cell Biochem **2008**;104(2):402-17 doi 10.1002/jcb.21630.

156. Chang JT, Chang H, Chen PH, Lin SL, Lin P. Requirement of aryl hydrocarbon receptor overexpression for CYP1B1 up-regulation and cell growth in human lung adenocarcinomas. Clin Cancer Res **2007**;13(1):38-45 doi 10.1158/1078-0432.CCR-06-1166.

157. Mimura J, Ema M, Sogawa K, Fujii-Kuriyama Y. Identification of a novel mechanism of regulation of Ah (dioxin) receptor function. Genes Dev **1999**;13(1):20-5 doi 10.1101/gad.13.1.20.

158. Hahn ME, Allan LL, Sherr DH. Regulation of constitutive and inducible AHR signaling: complex interactions involving the AHR repressor. Biochem Pharmacol **2009**;77(4):485-97 doi 10.1016/j.bcp.2008.09.016.

159. Rojo R, Pridans C, Langlais D, Hume DA. Transcriptional mechanisms that control expression of the macrophage colony-stimulating factor receptor locus. Clin Sci (Lond) **2017**;131(16):2161-82 doi 10.1042/CS20170238.

160. Fontana MF, Baccarella A, Pancholi N, Pufall MA, Herbert DR, Kim CC. JUNB is a key transcriptional modulator of macrophage activation. J Immunol **2015**;194(1):177-86 doi 10.4049/jimmunol.1401595.

161. Platzer B, Richter S, Kneidinger D, Waltenberger D, Woisetschlager M, Strobl H. Aryl hydrocarbon receptor activation inhibits in vitro differentiation of human monocytes

and Langerhans dendritic cells. J Immunol **2009**;183(1):66-74 doi 10.4049/jimmunol.0802997.

162. Lord KA, Abdollahi A, Hoffman-Liebermann B, Liebermann DA. Proto-oncogenes of the fos/jun family of transcription factors are positive regulators of myeloid differentiation. Mol Cell Biol **1993**;13(2):841-51 doi 10.1128/mcb.13.2.841.

163. Steidl U, Rosenbauer F, Verhaak RG, Gu X, Ebralidze A, Otu HH*, et al.* Essential role of Jun family transcription factors in PU.1 knockdown-induced leukemic stem cells. Nat Genet **2006**;38(11):1269-77 doi 10.1038/ng1898.

164. Somervaille TC, Cleary ML. PU.1 and Junb: suppressing the formation of acute myeloid leukemia stem cells. Cancer Cell **2006**;10(6):456-7 doi 10.1016/j.ccr.2006.11.009.

165. Cook WD, McCaw BJ, Herring C, John DL, Foote SJ, Nutt SL*, et al.* PU.1 is a suppressor of myeloid leukemia, inactivated in mice by gene deletion and mutation of its DNA binding domain. Blood **2004**;104(12):3437-44 doi 10.1182/blood-2004-06-2234.

166. Mueller BU, Pabst T, Osato M, Asou N, Johansen LM, Minden MD*, et al.* Heterozygous PU.1 mutations are associated with acute myeloid leukemia. Blood **2002**;100(3):998-1007 doi 10.1182/blood.v100.3.998.

167. Schnittger S, Dicker F, Kern W, Wendland N, Sundermann J, Alpermann T*, et al.* RUNX1 mutations are frequent in de novo AML with noncomplex karyotype and confer an unfavorable prognosis. Blood **2011**;117(8):2348-57 doi 10.1182/blood-2009-11-255976.

168. Lin LI, Chen CY, Lin DT, Tsay W, Tang JL, Yeh YC*, et al.* Characterization of CEBPA mutations in acute myeloid leukemia: most patients with CEBPA mutations have biallelic mutations and show a distinct immunophenotype of the leukemic cells. Clin Cancer Res **2005**;11(4):1372-9 doi 10.1158/1078-0432.CCR-04-1816.

169. McKenzie MD, Ghisi M, Oxley EP, Ngo S, Cimmino L, Esnault C*, et al.* Interconversion between Tumorigenic and Differentiated States in Acute Myeloid Leukemia. Cell Stem Cell **2019**;25(2):258-72 e9 doi 10.1016/j.stem.2019.07.001.

170. Mechta-Grigoriou F, Gerald D, Yaniv M. The mammalian Jun proteins: redundancy and specificity. Oncogene **2001**;20(19):2378-89 doi 10.1038/sj.onc.1204381.

171. Haimovici A, Humbert M, Federzoni EA, Shan-Krauer D, Brunner T, Frese S*, et al.* PU.1 supports TRAIL-induced cell death by inhibiting NF-kappaB-mediated cell survival and inducing DR5 expression. Cell Death Differ **2017**;24(5):866-77 doi 10.1038/cdd.2017.40.

172. Stanley ER, Chitu V. CSF-1 receptor signaling in myeloid cells. Cold Spring Harb Perspect Biol **2014**;6(6) doi 10.1101/cshperspect.a021857.

173. Asplund A, Stillemark-Billton P, Larsson E, Rydberg EK, Moses J, Hulten LM*, et al.* Hypoxic regulation of secreted proteoglycans in macrophages. Glycobiology **2010**;20(1):33-40 doi 10.1093/glycob/cwp139.

174. Wu YJ, La Pierre DP, Wu J, Yee AJ, Yang BB. The interaction of versican with its binding partners. Cell Res **2005**;15(7):483-94 doi 10.1038/sj.cr.7290318.

175. Masuda A, Yasuoka H, Satoh T, Okazaki Y, Yamaguchi Y, Kuwana M. Versican is upregulated in circulating monocytes in patients with systemic sclerosis and amplifies a CCL2-mediated pathogenic loop. Arthritis Res Ther **2013**;15(4):R74 doi 10.1186/ar4251.

176. Hirayasu K, Arase H. Functional and genetic diversity of leukocyte immunoglobulin-like receptor and implication for disease associations. J Hum Genet **2015**;60(11):703-8 doi 10.1038/jhg.2015.64.

177. Lin KH, Rutter JC, Xie A, Pardieu B, Winn ET, Bello RD*, et al.* Using antagonistic pleiotropy to design a chemotherapy-induced evolutionary trap to target drug resistance in cancer. Nat Genet **2020**;52(4):408-17 doi 10.1038/s41588-020-0590-9.

178. Li W, Gupta SK, Han W, Kundson RA, Nelson S, Knutson D*, et al.* Targeting MYC activity in double-hit lymphoma with MYC and BCL2 and/or BCL6 rearrangements with epigenetic bromodomain inhibitors. J Hematol Oncol **2019**;12(1):73 doi 10.1186/s13045-019-0761-2.

179. Ramsey HE, Greenwood D, Zhang S, Childress M, Arrate MP, Gorska AE*, et al.* BET Inhibition Enhances the Antileukemic Activity of Low-dose Venetoclax in Acute Myeloid Leukemia. Clin Cancer Res **2021**;27(2):598-607 doi 10.1158/1078-0432.CCR-20-1346.

180. Zhang S, Zhao Y, Heaster TM, Fischer MA, Stengel KR, Zhou X*, et al.* BET inhibitors reduce cell size and induce reversible cell cycle arrest in AML. J Cell Biochem **2018** doi 10.1002/jcb.28005.

181. Kurtz SE, Eide CA, Kaempf A, Khanna V, Savage SL, Rofelty A*, et al.* Molecularly targeted drug combinations demonstrate selective effectiveness for myeloid- and lymphoid-derived hematologic malignancies. Proc Natl Acad Sci U S A **2017**;114(36):E7554-E63 doi 10.1073/pnas.1703094114.

182. Drusbosky LM, Vidva R, Gera S, Lakshminarayana AV, Shyamasundar VP, Agrawal AK*, et al.* Predicting response to BET inhibitors using computational modeling: A BEAT AML project study. Leuk Res **2019**;77:42-50 doi 10.1016/j.leukres.2018.11.010.

183. Yu X, Wu C, Bhavanasi D, Wang H, Gregory BD, Huang J. Chromatin dynamics during the differentiation of long-term hematopoietic stem cells to multipotent progenitors. Blood Adv **2017**;1(14):887-98 doi 10.1182/bloodadvances.2016003384.

184. Chen S, Yang J, Wei Y, Wei X. Epigenetic regulation of macrophages: from homeostasis maintenance to host defense. Cell Mol Immunol **2020**;17(1):36-49 doi 10.1038/s41423-019-0315-0.

185. Sheng Y, Ju W, Huang Y, Li J, Ozer H, Qiao X*, et al.* Activation of wnt/beta-catenin signaling blocks monocyte-macrophage differentiation through antagonizing PU.1-targeted gene transcription. Leukemia **2016**;30(10):2106-9 doi 10.1038/leu.2016.146.

186. Bunaciu RP, Jensen HA, MacDonald RJ, LaTocha DH, Varner JD, Yen A. 6-Formylindolo(3,2-b)Carbazole (FICZ) Modulates the Signalsome Responsible for RA-Induced Differentiation of HL-60 Myeloblastic Leukemia Cells. PLoS One **2015**;10(8):e0135668 doi 10.1371/journal.pone.0135668.

187. Tzelepis K, Koike-Yusa H, De Braekeleer E, Li Y, Metzakopian E, Dovey OM*, et al.* A CRISPR Dropout Screen Identifies Genetic Vulnerabilities and Therapeutic Targets in Acute Myeloid Leukemia. Cell Rep **2016**;17(4):1193-205 doi 10.1016/j.celrep.2016.09.079.

188. Robinson MD, Oshlack A. A scaling normalization method for differential expression analysis of RNA-seq data. Genome Biol **2010**;11(3):R25 doi 10.1186/gb-2010-11-3-r25.

189. Ross-Innes CS, Stark R, Teschendorff AE, Holmes KA, Ali HR, Dunning MJ*, et al.* Differential oestrogen receptor binding is associated with clinical outcome in breast cancer. Nature **2012**;481(7381):389-93 doi 10.1038/nature10730.

190. Cavalcante RG, Sartor MA. annotatr: genomic regions in context. Bioinformatics **2017**;33(15):2381-3 doi 10.1093/bioinformatics/btx183.

191. He L, Kulesskiy E, Saarela J, Turunen L, Wennerberg K, Aittokallio T*, et al.* Methods for High-throughput Drug Combination Screening and Synergy Scoring. Methods Mol Biol **2018**;1711:351-98 doi 10.1007/978-1-4939-7493-1_17.

192. Yadav B, Wennerberg K, Aittokallio T, Tang J. Searching for Drug Synergy in Complex Dose-Response Landscapes Using an Interaction Potency Model. Comput Struct Biotechnol J **2015**;13:504-13 doi 10.1016/j.csbj.2015.09.001.

193. Szczepanski MJ, Szajnik M, Czystowska M, Mandapathil M, Strauss L, Welsh A*, et al.* Increased frequency and suppression by regulatory T cells in patients with acute myelogenous leukemia. Clin Cancer Res **2009**;15(10):3325-32 doi 10.1158/1078-0432.CCR-08-3010.

194. Wang L, Jia B, Claxton DF, Ehmann WC, Rybka WB, Mineishi S*, et al.* VISTA is highly expressed on MDSCs and mediates an inhibition of T cell response in patients with AML. Oncoimmunology **2018**;7(9):e1469594 doi 10.1080/2162402X.2018.1469594.

195. Lamble AJ, Kosaka Y, Laderas T, Maffit A, Kaempf A, Brady LK*, et al.* Reversible suppression of T cell function in the bone marrow microenvironment of acute myeloid leukemia. Proc Natl Acad Sci U S A **2020**;117(25):14331-41 doi 10.1073/pnas.1916206117.

196. Williams P, Basu S, Garcia-Manero G, Hourigan CS, Oetjen KA, Cortes JE*, et al.* The distribution of T-cell subsets and the expression of immune checkpoint receptors and ligands in patients with newly diagnosed and relapsed acute myeloid leukemia. Cancer **2018** doi 10.1002/cncr.31896.

197. Williams P, Basu S, Garcia-Manero G, Hourigan CS, Oetjen KA, Cortes JE*, et al.* The distribution of T-cell subsets and the expression of immune checkpoint receptors and ligands in patients with newly diagnosed and relapsed acute myeloid leukemia. Cancer **2019**;125(9):1470-81 doi 10.1002/cncr.31896.

198. Noviello M, Manfredi F, Ruggiero E, Perini T, Oliveira G, Cortesi F*, et al.* Bone marrow central memory and memory stem T-cell exhaustion in AML patients relapsing after HSCT. Nat Commun **2019**;10(1):1065 doi 10.1038/s41467-019-08871-1.

199. Zhou Q, Yik JH. The Yin and Yang of P-TEFb regulation: implications for human immunodeficiency virus gene expression and global control of cell growth and differentiation. Microbiol Mol Biol Rev **2006**;70(3):646-59 doi 10.1128/MMBR.00011-06.

200. Itzen F, Greifenberg AK, Bosken CA, Geyer M. Brd4 activates P-TEFb for RNA polymerase II CTD phosphorylation. Nucleic Acids Res **2014**;42(12):7577-90 doi 10.1093/nar/gku449.

201. Valent P, Zuber J. BRD4: a BET(ter) target for the treatment of AML? Cell Cycle **2014**;13(5):689-90 doi 10.4161/cc.27859.

202. Fiskus W, Cai T, DiNardo CD, Kornblau SM, Borthakur G, Kadia TM*, et al.* Superior efficacy of cotreatment with BET protein inhibitor and BCL2 or MCL1 inhibitor against AML blast progenitor cells. Blood Cancer J **2019**;9(2):4 doi 10.1038/s41408-018-0165-5.

203. Hogg SJ, Vervoort SJ, Deswal S, Ott CJ, Li J, Cluse LA*, et al.* BET-Bromodomain Inhibitors Engage the Host Immune System and Regulate Expression of the Immune Checkpoint Ligand PD-L1. Cell Rep **2017**;18(9):2162-74 doi 10.1016/j.celrep.2017.02.011.

204. Zhu H, Bengsch F, Svoronos N, Rutkowski MR, Bitler BG, Allegrezza MJ*, et al.* BET Bromodomain Inhibition Promotes Anti-tumor Immunity by Suppressing PD-L1 Expression. Cell Rep **2016**;16(11):2829-37 doi 10.1016/j.celrep.2016.08.032.

205. Kagoya Y, Nakatsugawa M, Yamashita Y, Ochi T, Guo T, Anczurowski M*, et al.* BET bromodomain inhibition enhances T cell persistence and function in adoptive immunotherapy models. J Clin Invest **2016**;126(9):3479-94 doi 10.1172/JCI86437.

206. Shih AH, Jiang Y, Meydan C, Shank K, Pandey S, Barreyro L*, et al.* Mutational cooperativity linked to combinatorial epigenetic gain of function in acute myeloid leukemia. Cancer Cell **2015**;27(4):502-15 doi 10.1016/j.ccell.2015.03.009.

207. Moshofsky KB, Cho HJ, Wu G, Romine KA, Newman MT, Kosaka Y*, et al.* Acute myeloid leukemia-induced T-cell suppression can be reversed by inhibition of the MAPK pathway. Blood Adv **2019**;3(20):3038-51 doi 10.1182/bloodadvances.2019000574.

208. Shenghui Z, Yixiang H, Jianbo W, Kang Y, Laixi B, Yan Z*, et al.* Elevated frequencies of CD4(+) CD25(+) CD127lo regulatory T cells is associated to poor prognosis in patients with acute myeloid leukemia. Int J Cancer **2011**;129(6):1373-81 doi 10.1002/ijc.25791.

209. Kallies A, Zehn D, Utzschneider DT. Precursor exhausted T cells: key to successful immunotherapy? Nat Rev Immunol **2019** doi 10.1038/s41577-019-0223-7.

210. Mulqueen RM, Pokholok D, O'Connell BL, Thornton CA, Zhang F, O'Roak BJ*, et al.* High-content single-cell combinatorial indexing. Nat Biotechnol **2021**;39(12):1574-80 doi 10.1038/s41587-021-00962-z.

211. Lamble AJ, Lind EF. Targeting the Immune Microenvironment in Acute Myeloid Leukemia: A Focus on T Cell Immunity. Front Oncol **2018**;8:213 doi 10.3389/fonc.2018.00213.

212. Daver N, Garcia-Manero G, Basu S, Boddu PC, Alfayez M, Cortes JE*, et al.* Efficacy, Safety, and Biomarkers of Response to Azacitidine and Nivolumab in Relapsed/Refractory Acute Myeloid Leukemia: A Nonrandomized, Open-Label, Phase II Study. Cancer Discov **2019**;9(3):370-83 doi 10.1158/2159-8290.CD-18-0774.

213. Wherry EJ, Teichgraber V, Becker TC, Masopust D, Kaech SM, Antia R*, et al.* Lineage relationship and protective immunity of memory CD8 T cell subsets. Nat Immunol **2003**;4(3):225-34 doi 10.1038/ni889.

214. Paley MA, Kroy DC, Odorizzi PM, Johnnidis JB, Dolfi DV, Barnett BE*, et al.* Progenitor and terminal subsets of CD8+ T cells cooperate to contain chronic viral infection. Science **2012**;338(6111):1220-5 doi 10.1126/science.1229620.

215. Zajac AJ, Blattman JN, Murali-Krishna K, Sourdive DJ, Suresh M, Altman JD*, et al.* Viral immune evasion due to persistence of activated T cells without effector function. J Exp Med **1998**;188(12):2205-13 doi 10.1084/jem.188.12.2205.

216. Gray SM, Amezquita RA, Guan T, Kleinstein SH, Kaech SM. Polycomb Repressive Complex 2-Mediated Chromatin Repression Guides Effector CD8(+) T Cell Terminal Differentiation and Loss of Multipotency. Immunity **2017**;46(4):596-608 doi 10.1016/j.immuni.2017.03.012.

217. Pace L, Goudot C, Zueva E, Gueguen P, Burgdorf N, Waterfall JJ*, et al.* The epigenetic control of stemness in CD8(+) T cell fate commitment. Science **2018**;359(6372):177-86 doi 10.1126/science.aah6499.

218. Ladle BH, Li KP, Phillips MJ, Pucsek AB, Haile A, Powell JD*, et al.* De novo DNA methylation by DNA methyltransferase 3a controls early effector CD8+ T-cell fate decisions following activation. Proc Natl Acad Sci U S A **2016**;113(38):10631-6 doi 10.1073/pnas.1524490113.

219. Youngblood B, Hale JS, Kissick HT, Ahn E, Xu X, Wieland A*, et al.* Effector CD8 T cells dedifferentiate into long-lived memory cells. Nature **2017**;552(7685):404-9 doi 10.1038/nature25144.

220. Page N, Klimek B, De Roo M, Steinbach K, Soldati H, Lemeille S*, et al.* Expression of the DNA-Binding Factor TOX Promotes the Encephalitogenic Potential of Microbe-Induced Autoreactive CD8(+) T Cells. Immunity **2018**;48(5):937-50 e8 doi 10.1016/j.immuni.2018.04.005.

221. Milner JJ, Toma C, Quon S, Omilusik K, Scharping NE, Dey A*, et al.* Bromodomain protein BRD4 directs and sustains CD8 T cell differentiation during infection. J Exp Med **2021**;218(8) doi 10.1084/jem.20202512.

222. Binder S, Luciano M, Horejs-Hoeck J. The cytokine network in acute myeloid leukemia (AML): A focus on pro- and anti-inflammatory mediators. Cytokine Growth Factor Rev **2018**;43:8-15 doi 10.1016/j.cytogfr.2018.08.004.

223. Sanchez-Correa B, Bergua JM, Campos C, Gayoso I, Arcos MJ, Banas H*, et al.* Cytokine profiles in acute myeloid leukemia patients at diagnosis: survival is inversely correlated with IL-6 and directly correlated with IL-10 levels. Cytokine **2013**;61(3):885-91 doi 10.1016/j.cyto.2012.12.023.

224. Van Etten RA. Aberrant cytokine signaling in leukemia. Oncogene **2007**;26(47):6738-49 doi 10.1038/sj.onc.1210758.

225. Jia B, Zhao C, Rakszawski KL, Claxton DF, Ehmann WC, Rybka WB*, et al.* Eomes(+)T-bet(low) CD8(+) T Cells Are Functionally Impaired and Are Associated with Poor Clinical Outcome in Patients with Acute Myeloid Leukemia. Cancer Res **2019**;79(7):1635-45 doi 10.1158/0008-5472.CAN-18-3107.

226. Sallman DA, McLemore AF, Aldrich AL, Komrokji RS, McGraw KL, Dhawan A*, et al.* TP53 mutations in myelodysplastic syndromes and secondary AML confer an immunosuppressive phenotype. Blood **2020**;136(24):2812-23 doi 10.1182/blood.2020006158.

227. Que Y, Li H, Lin L, Zhu X, Xiao M, Wang Y*, et al.* Study on the Immune Escape Mechanism of Acute Myeloid Leukemia With DNMT3A Mutation. Front Immunol **2021**;12:653030 doi 10.3389/fimmu.2021.653030.

228. Aran D, Hu Z, Butte AJ. xCell: digitally portraying the tissue cellular heterogeneity landscape. Genome Biol **2017**;18(1):220 doi 10.1186/s13059-017-1349-1.

229. Romine KA, Nechiporuk T, Bottomly D, Jeng S, McWeeney SK, Kaempf A*, et al.* Monocytic differentiation and AHR signaling as Primary Nodes of BET Inhibitor Response in Acute Myeloid Leukemia. Cancer Discov **2021** doi 10.1158/2643-3230.BCD-21-0012.

230. Bilbao D, Luciani L, Johannesson B, Piszczek A, Rosenthal N. Insulin-like growth factor-1 stimulates regulatory T cells and suppresses autoimmune disease. EMBO Mol Med **2014**;6(11):1423-35 doi 10.15252/emmm.201303376.

231. Yuan N, Zhang HF, Wei Q, Wang P, Guo WY. Expression of CD4+CD25+Foxp3+ Regulatory T Cells, Interleukin 10 and Transforming Growth Factor beta in Newly Diagnosed Type 2 Diabetic Patients. Exp Clin Endocrinol Diabetes **2018**;126(2):96-101 doi 10.1055/s-0043-113454.

232. van Galen P, Hovestadt V, Wadsworth Ii MH, Hughes TK, Griffin GK, Battaglia S*, et al.* Single-Cell RNA-Seq Reveals AML Hierarchies Relevant to Disease Progression and Immunity. Cell **2019**;176(6):1265-81 e24 doi 10.1016/j.cell.2019.01.031.

233. Alsaab HO, Sau S, Alzhrani R, Tatiparti K, Bhise K, Kashaw SK*, et al.* PD-1 and PD-L1 Checkpoint Signaling Inhibition for Cancer Immunotherapy: Mechanism, Combinations, and Clinical Outcome. Front Pharmacol **2017**;8:561 doi 10.3389/fphar.2017.00561.

234. Jenkins RW, Barbie DA, Flaherty KT. Mechanisms of resistance to immune checkpoint inhibitors. Br J Cancer **2018**;118(1):9-16 doi 10.1038/bjc.2017.434.

235. Loberg MA, Bell RK, Goodwin LO, Eudy E, Miles LA, SanMiguel JM*, et al.* Sequentially inducible mouse models reveal that Npm1 mutation causes malignant transformation of Dnmt3a-mutant clonal hematopoiesis. Leukemia **2019**;33(7):1635-49 doi 10.1038/s41375-018-0368-6.

236. Velasco-Hernandez T, Hyrenius-Wittsten A, Rehn M, Bryder D, Cammenga J. HIF-1alpha can act as a tumor suppressor gene in murine acute myeloid leukemia. Blood **2014**;124(24):3597-607 doi 10.1182/blood-2014-04-567065.

237. Joseph C, Quach JM, Walkley CR, Lane SW, Lo Celso C, Purton LE. Deciphering hematopoietic stem cells in their niches: a critical appraisal of genetic models, lineage tracing, and imaging strategies. Cell Stem Cell **2013**;13(5):520-33 doi 10.1016/j.stem.2013.10.010.

238. Godwin CD, Gale RP, Walter RB. Gemtuzumab ozogamicin in acute myeloid leukemia. Leukemia **2017**;31(9):1855-68 doi 10.1038/leu.2017.187.

239. Walter RB, Medeiros BC, Gardner KM, Orlowski KF, Gallegos L, Scott BL*, et al.* Gemtuzumab ozogamicin in combination with vorinostat and azacitidine in older patients with relapsed or refractory acute myeloid leukemia: a phase I/II study. Haematologica **2014**;99(1):54-9 doi 10.3324/haematol.2013.096545.

240. Cowan AJ, Laszlo GS, Estey EH, Walter RB. Antibody-based therapy of acute myeloid leukemia with gemtuzumab ozogamicin. Front Biosci (Landmark Ed) **2013**;18:1311-34 doi 10.2741/4181.

241. Nabhan C, Tallman MS. Early phase I/II trials with gemtuzumab ozogamicin (Mylotarg) in acute myeloid leukemia. Clin Lymphoma **2002**;2 Suppl 1:S19-23 doi 10.3816/clm.2002.s.004.

242. Her Z, Yong KSM, Paramasivam K, Tan WWS, Chan XY, Tan SY*, et al.* An improved pre-clinical patient-derived liquid xenograft mouse model for acute myeloid leukemia. J Hematol Oncol **2017**;10(1):162 doi 10.1186/s13045-017-0532-x.

243. Shultz LD, Brehm MA, Garcia-Martinez JV, Greiner DL. Humanized mice for immune system investigation: progress, promise and challenges. Nat Rev Immunol **2012**;12(11):786-98 doi 10.1038/nri3311.

244. Burger ML, Cruz AM, Crossland GE, Gaglia G, Ritch CC, Blatt SE*, et al.* Antigen dominance hierarchies shape TCF1(+) progenitor CD8 T cell phenotypes in tumors. Cell **2021**;184(19):4996-5014 e26 doi 10.1016/j.cell.2021.08.020.

245. Clarke SR, Barnden M, Kurts C, Carbone FR, Miller JF, Heath WR. Characterization of the ovalbumin-specific TCR transgenic line OT-I: MHC elements for positive and negative selection. Immunol Cell Biol **2000**;78(2):110-7 doi 10.1046/j.1440-1711.2000.00889.x.

246. Zhao M, Kiernan CH, Stairiker CJ, Hope JL, Leon LG, van Meurs M*, et al.* Rapid in vitro generation of bona fide exhausted CD8+ T cells is accompanied by Tcf7 promotor methylation. PLoS Pathog **2020**;16(6):e1008555 doi 10.1371/journal.ppat.1008555.

247. Xu Y, Mou J, Wang Y, Zhou W, Rao Q, Xing H*, et al.* Regulatory T cells promote the stemness of leukemia stem cells through IL10 cytokine-related signaling pathway. Leukemia **2021** doi 10.1038/s41375-021-01375-2.

248. Wang M, Zhang C, Tian T, Zhang T, Wang R, Han F*, et al.* Increased Regulatory T Cells in Peripheral Blood of Acute Myeloid Leukemia Patients Rely on Tumor Necrosis Factor (TNF)-alpha-TNF Receptor-2 Pathway. Front Immunol **2018**;9:1274 doi 10.3389/fimmu.2018.01274.